MEDRC

MEDRC Series of R & D Reports
MEDRC Project: 03-AS-003

GREENHOUSE – STATE OF THE ART REVIEW AND PERFORMANCE EVALUATION OF DEHUMIDIFIER

Principal Investigator

Yousef H. Zurigat
Mechanical Engineering Department, University of Jordan, Amman, Jordan

The Middle East Desalination Research Center
Muscat
Sultanate of Oman

January 2008

MEDRC Series of R & D Reports
Project: 03-AS-003

Hard copies and CD of this report are available from:

Middle East Desalination Research Center
P.O. Box 21,
Al Khuwair / Muscat
Postal Code 133
Sultanate of Oman
Tel: (968) 24 415 500
Fax: (968) 24 415 541
E-mail: info@medrc.org.om
Web site: www.medrc.org

Project participants

Principal investigator

Prof. Yousef H. Zurigat
Mechanical Engineering Department
University of Jordan, Amman
Jordan

Tel: + 962-6-5355000/22800
Fax: + 962-6-5355488
E-mail: Zurigat@ju.edu.jo

Primary Project Partners

Prof. Taha Aldoss
Mechanical Engineering Department
University of Jordan for Science and Technology, Irbid
Jordan

Tel: 962-(02) 7201000/ext. 22578
Fax: 962-(02) 7201074
E-mail: taldoss@just.edu.jo

Dr. Belal Dawoud

Chair of Technical Thermodynamics
RWTH Aachen University
Schinkel Str. 8, D-52056 Aachen
Germany

Tel: +49 0241 8095390
Fax: +49 0241 8092255
E-mail: dawoud@ltt.rwth-aachen.de

Dr. Georgios Theodoridis
PhilonNet, Engineering Solutions
Kerkiras 140, Kipseli
Athens 11363,
Greece

Tel: +302108217235
Fax: +30 2108217254
E-mail: georgios.theodoridis@philonnet.gr

THE MIDDLE EAST DESALINATION RESEARCH CENTER

An International Institution
Established on December 22, 1996
Hosted by the Sultanate of Oman in Muscat

Mission Objectives of the Center:

1. to conduct, facilitate, promote, co-ordinate and support basic and applied research in the field of water desalination and related technical areas with the aim of discovering and developing methods of water desalination, which are financially and technically feasible

2. to conduct, facilitate, promote, co-ordinate and support training programs so as to develop technical and scientific skills and expertise throughout the region and internationally in the field of water desalination and its applications and related technical areas

3. to conduct, facilitate, promote, co-ordinate and support information exchange, including, but not limited to, electronic networking technology, so as to ensure the dissemination and sharing throughout the region and internationally of technical information concerning water desalination methods and research and related technical areas, and to establish with other states, domestic and other organizations such relations as will foster progress in the development, improvement and use of water desalination and related technical areas in the region and elsewhere

Further information about the Center's activities is available on the web site (www.medrc.org). The following documents are available from the Center and can be sent on request in paper format or diskette. Alternatively, they can be downloaded from the Center web site.

1. Guidelines for the Preparation of Research Proposals
2. Guidelines for the Preparation of Project Reports
3. Annual Requests for Proposals
4. Abstracts of On-going Projects and Summaries of Completed Projects
5. Research Reports
6. MEDRC Program Framework and Profile
7. MENA Universities and Research Institutes Directory
8. Partnership-in-Research Information for the Middle East
9. MEDRC Annual Reports

TABLE OF CONTENTS

Table of contents……iv
List of tables……vi
List of figures……vii
Nomenclature……..ix
Acknowledgements……xii
Executive summary……..xiii

1. Introduction……..1
1.1 Objectives and approach……3

2. Literature review……..4
2.1 Greenhouse……4
2.2 CFD modeling of greenhouse……8
2.3 Evaporator……11
2.4 Condenser……13
2.4.1 Condensation process……..13
2.4.2 Condenser cooling duty……20
2.4.3 Types of condensers……22
2.4.4 Condenser selection and condenser concept development……23

3. Theoretical analysis of possible methods to cool the condenser of seawater Greenhouse……26
3.1 Overview on the possible condenser cooling technique……..26
3.1.1 Air as condenser coolant……27
3.1.2 Water as condenser coolant……29
3.2 Investigating the potential of evaporative cooling……30
3.3 Estimating the condenser cooling load and the equivalent flow rate of deep Seawater……40
3.4 Summary and conclusions……44

4. Mathematical model of greenhouse desalination integrated system……..46
4.1 The proposed system……46
4.2 Modeling……47
4.2.1 Evaporator……47
4.2.2 Condenser……47
4.2.3 The greenhouse……48
4.3 Method of solution……50

5. Performance of condenser: An experimental study……..51
5.1 Experimental setup and procedures……51
5.2 Design of plate channel condenser……53
5.3 Results and discussion……54
5.4 Heat transfer enhancement……..59
5.5 Conclusions……59

6. CFD mathematical model of greenhouse desalination……61
6.1 Greenhouse physical model……61
6.2 Greenhouse CFD mathematical model……...61
6.2.1 The crop resistance model……62
6.2.2 Crop transpiration model……...63
6.2.3 Effective sky temperature……..65
6.2.4 Ventilation/insect-proof screen model……...65
6.2.5 Evaporator resistance model……..66
6.2.6 Hydrodynamics in greenhouse: A simple demonstration……..66
6.3 Summary and conclusions……...69

7. Closure……...70

8. References……..72

LIST OF TABLES

Table 2.1: Performance of seawater greenhouse for three climate conditions……7
Table 2.2: Orders of magnitude for condensation heat transfer coefficients along with others usually found in series with them……..14
Table 2.3: Condensation results for two types of condensers……...19
Table 3.1: Results summary……..43
Table 5.1: Effect of air velocity on water condensate yield……..58
Table 5.2 Effect of fins on water condensate (ml/hr)……59

LIST OF FIGURES

Figure 1.1: Schematics of greenhouse for sea water desalination……...2
Figure 2.1: Hourly rate of water absorbed by the greenhouse air stream at the evaporator assuming 100% saturation……..12
Figure 2.2: Water absorbed by the air stream in a typical greenhouse in the process of evaporative cooling……..13
Figure 2.3: Temperature and partial pressure profiles in the vicinity of a wall on which condensation is occurring with non-condensable gas present……..15
Figure 2.4: Schematic illustration of condensation with non-condensable gas……..... 16
Figure 2.5: Effect of air on condensation heat transfer……..16
Figure 2.6: Greenhouse air stream cooling load for 2 ^{o}C cooling below dew point temperature (Seeb TMY, $\dot{V}_a$=15 m^3/s)……...21
Figure 2.7: Greenhouse air stream total cooling load for 2 ^{o}C cooling below dew point temperature for the first day of each month of the year (Seeb TMY, $\dot{V}_a$=15 m^3/s)……21
Figure 2.8: A schematic of a new condenser module...……...24
Figure 2.9: Schematics of the new condenser…… 24
Figure 2.10: A schematic of the plate channel condenser module……25
Figure 2.11: Direct contact spray condenser using condensate as the coolant…….25
Figure 3.1: A general overview on the possible solutions to remove the heat of condensation to air or water as condenser coolants…….26
Figure 3.2: A schematic of an evaporative condenser……...28
Figure 3.3: Enthalpy–water load–diagram with the states of ambient air as well as of condenser inlet and outlet air……..31
Figure 3.4: Maximum relative humidity of ambient air depending on ambient air temperature and given effective temperature difference…….33
Figure 3.5: Cumulative probability distribution of diurnal relative humidity in Marmul, the Sultanate of Oman (Zurigat et.al., 2003)……...34
Figure 3.6: The two cooling loops of the seawater greenhouse desalination process…...35
Figure 3.7: Effect of the ambient air relative humidity on the rates of the obtainable freshwater condensation and the required seawater evaporation at an ambient air dry-bulb temperature of 25 °C……36
Figure 3.8: Effect of the ambient air relative humidity on the rates of the obtainable freshwater condensation and the required seawater evaporation at an ambient air dry-bulb temperature of 30 °C……37
Figure 3.9: Effect of the ambient air relative humidity on the rates of the obtainable freshwater condensation and the required seawater evaporation at an ambient air dry-bulb temperature of 35 °C…….38
Figure 3.10: Effect of the ambient air relative humidity on the rates of the obtainable freshwater condensation and the required seawater evaporation at an ambient air dry-bulb temperature of 40 °C……..38
Figure 3.11: Effect of the ambient air dry-bulb temperature as well as the ambient air relative humidity on the rate of fresh water production at a condenser inlet air temperature of 25 °C……39

Figure 3.12: Cross section in the original SWGH design (Paton, 2001)……...39
Figure 3.13: A schematic presentation of the recommended hybrid collector in the roof zone of SWGH……40
Figure 3.14: A schematic presentation for the 1st condenser of a SWGH……41
Figure 3.15: Amount of condensate (solid lines) and cooling load (dashed lines) versus condenser outlet temperature……..42
Figure 3.16: Amount of condensate (solid lines) and the required rate of deep seawater flow (dashed lines) for various condenser inlet and outlet temperatures……44
Figure 4.1: Schematics of greenhouse elements……46
Figure 4.2: Greenhouse energy balance……49
Figure 5.1: Experimental setup schematic diagram……...52
Figure 5.2: Transparent condenser housing duct……...52
Figure 5.3: Experimental setup for condenser testing (University of Jordan)……...53
Figure 5.4: Plate channel condenser module……54
Figure 5.5: Plate channel condenser arrangement……54
Figure 5.6: Water condensate production at constant coolant temperature of 15 ^{o}C and constant air velocity of 0.2 m/s……55
Figure 5.7: Water condensate yield at constant coolant temperature of 20^{o}C and constant air velocity of 0.2 m/s……...56
Figure 5.8: Effect of coolant temperature on condensate yield at air inlet conditions of T_{db}=55 ^{o}C, 53% relative humidity at constant air velocity 0.2 m/s……57
Figure 5.9: Effect of coolant temperature on condensate yield at air inlet conditions of T_{db}=44 ^{o}C, 100% relative humidity at constant air velocity 0.2 m/s……..57
Figure 5.10: Variation of water condensate by varying the air speed at constant coolant temperature of 15 ^{o}C……..……57
Figure 5.11: Variation of water condensate for two different air velocities at constant cooling temperature of 25 ^{o}C……..…..58
Figure 5.12: Fin distribution on condenser surface……..….59
Figure 6.1: Schematic of the desalination greenhouse……...…61
Figure 6.2: Schematic of energy balance on plant canopy……....63
Figure 6.3: Photosynthesis mechanism……..…64
Figure 6.4: Variation of wire screen resistance coefficient with free area ratio……....66
Figure 6.5: Variation of wire screen resistance coefficient with free area ratio……67
Figure 6.6: Velocity profile across the greenhouse……...67
Figure 6.7: The grid system……...68
Figure 6.8: Velocity vectors……..68
Figure 6.9: Pressure contours……69

NOMENCLATURE

A	Total area exposed to ambient
c_p	Specific heat
$C_{p,a}$	Specific air at constant pressure
$C_{p,v}$	Specific heats of water vapor and at constant pressure
$C_{p,w}$	Specific heat of liquid water at constant pressure
D_{bs1}	Conduction heat flux density from the surface of pond bottom to soil layer
H_{ai}, H_{ao}	The inlet and outlet enthalpy of air to evaporator
h	Enthalpy
K	Mass transfer coefficient in the humidifier
L_{ac}	Latent flux density between internal air and cover
L_{ae}	Latent flux density between internal and external air
L_{ce}	Latent flux density between cover and external air
L_{wa}	Latent flux density between water surface and internal air
mb	Millibar
M	Molecular weight
M_a	Mass flow rate of air
M_w	Mass flow rate of water
$\dot{m}$	Mass flow rate
$\dot{m}_a$	Mass flow rate of air
$\dot{m}_w$	Rate of water condensation
Nu	Nusselt number
p_s	Saturation pressure
p	Pressure or Equivalent wet fraction of cover surface
Pr	Prandtl number
$\dot{Q}$	Cooling capacity
$\dot{Q}_l$	Latent cooling load
$\dot{Q}_s$	Sensible cooling load
Q_{win}	Heat energy input flux density to water layer
R_{csky}	Thermal radiation flux density between cover and sky
R_{wc}	Thermal radiative flux density between water surface and cover
R_{wsky}	Thermal radiative flux density between water surface and sky
RH_e	Relative humidity of external air
RH_i	Relative humidity of internal air
r	Latent heat of vaporization of water at 0 °C
S	Humidifier surface area per unit volume
S_b	Solar radiation flux density absorbed by the surface of pond bottom
S_{ce}	Solar radiation flux density reflected by external cover surface
S_{ec}	Solar radiation flux density absorbed by cover
S_g	Global solar radiation flux density
S_w	Solar radiation flux density absorbed by water ($W.m^{-2}$)

S_{wc}	Solar radiation flux density reflected from water surface and absorbed by cover
S_{ws}	Solar radiation flux density penetrating water surface
T	Temperature
T_{ai}, T_{ao}	The inlet and outlet temperature of water to condenser or evaporator
T_c	Cover temperature
T_e	External air temperature
T_i	Internal air temperature
T_{s1}	Temperature of soil layer 1
T_{ss}	Subsoil temperature
T_{sky}	Radiative sky temperature
T_w	Water temperature
T_{wset}	Pre-set water temperature for an active GPS
T_{wi}, T_{wo}	The inlet and outlet temperature of water to condenser or evaporator
t	Temperature or time
t_{cf}	Equivalent thickness of condensate water film on cover surface
t_{cfmax}	Maximum thickness of condensate water film on cover surface
U	Overall heat transfer coefficient or heat loss coefficient
V	Volume of the humidifier
V_{ac}	Convective flux density between internal air and cover
V_{ae}	Convective flux density between internal and external air
V_{bw}	Convective flux density between pond bottom and water
V_{ce}	Convective flux density between cover and external air
V_{wa}	Convective flux density between water surface and internal air
$\dot{V}$	Volume flow rate
v	Specific volume
w	Specific humidity
$w_{aa,db}$	Specific humidity of the air at dry bulb temperature
$w^{s}_{s,c,e}$	Specific humidity of saturated air at condenser exit
x	Absolute water load in dry air
y	Air volume fraction

Greek symbols

ρ	Density
ρ_w	Water density
μ	Dynamic viscosity
ϕ	Relative humidity
Δ	Difference operator
φ	Relative humidity
ε_{dry}	Thermal emissivity of dry cover surface
ε_{wet}	Equivalent emissivity of cover surface with condensate water
ε_{cond}	Thermal emissivity of water surface
λ	Thermal conductivity of bulk fluid
τ_{dry}	Thermal transmissivity of dry cover

τ_{wet}	Equivalent thermal transmissivity of cover with condensate water

Subscripts

a	Air
aa	Ambient air
atm	Atmospheric
b	Bulk
db	Dry bulb
dp	Dew point
dsw	Deep seawater
c	Condenser
eff	Effective
f	liquid
g	gas
HT	Heat transfer
i	interface or inlet
l	latent heat
lw	Liquid water
o	Outlet
s	saturation or sensible
sw	Surface seawater
t	total
v	water vapor
w	liquid water
wb	wet bulb
wv	WE bulb
90 %	90% Approach to the wet-bulb temperature

Superscripts

s	Saturation

ACKNOWLEDGEMENTS

The funding provided by the Middle East Desalination Research Center (MEDRC) is highly appreciated. Special thanks go to MEDRC Project Manager: Dr. K. Venkat Reddy for his excellent mentoring of the project, his constructive suggestions and his efforts in editing the final report. Also, the Mechanical Engineering Department at the University of Jordan, Amman, Jordan has facilitated the laboratory for testing the condenser which was built at the workshop of Chair of Technical Thermodynamics, RWTH Aachen University, Aachen, Germany.

EXECUTIVE SUMMARY

Literature review on greenhouse desalination was conducted and the physical processes in this fairly new technology were identified. A mathematical model for greenhouse desalination was developed and the method of solution was identified. The condensation which constitutes the critical process in the greenhouse desalination system was investigated and a simple and inexpensive condenser was developed and tested experimentally. The methods for cooling the condenser were studied and criteria for selection were developed. Also, the computational fluid dynamics (CFD) approach to greenhouse desalination was reviewed and demonstrated on a simple problem of hydrodynamics in the greenhouse.

Based on the work done in this project it was found that the amount of water evaporated at the evaporator is quite significant if it can be condensed back into liquid water. Thus, the potential of greenhouse desalination is seen to rely heavily on the condenser performance. A plate channel type condenser was built and tested. However, the performance of the condenser is highly affected by the presence of non-condensable gas. The condenser developed in this work is shown to perform better than the more conventional and expensive fin-tube bank condenser developed by other investigators.

Based on the condenser cooling water requirements (in the form of deep seawater) calculations show that large amounts of cooling water is required which may render the greenhouse desalination impractical. While this statement represents one aspect of the greenhouse desalination, concrete statement should be based on economic study which is recommended for future work. Also, future work should focus on direct contact condensers as they have much higher condensation rates and are simpler in design. It is also recommended that overall greenhouse system simulations be conducted based on the mathematical models (including CFD model) developed in this work.

1. INTRODUCTION

With the rapid increase in population and agricultural and industrial developments fresh water shortages are becoming high in many parts of the world especially in Middle East and North Africa region countries in which desalination has become the main source of fresh water supply. The desalination technologies most widely used are thermal and reverse osmosis (RO). Recently, technologies based on air humidification-dehumidification in a greenhouse have been proposed and investigated. The greenhouse desalination is one example (Paton and Davies, 1996; Sablani et al., 2002).

Greenhouse desalination creates proper climate to grow valuable crops and at the same time produce fresh water from saline water for irrigating the crops in the greenhouse. Greenhouse recreates the natural hydrological cycle within a controlled environment (Paton, 2001). Thus, the green house serves as an autonomous small-scale desalination plant while serving as a crop growing space. Typical configuration of greenhouse is given in Figure 1.1. The entire front wall of the greenhouse is a seawater evaporator. It consists of a cardboard honeycomb lattice and faces the prevailing wind. Seawater trickles down over this lattice, cooling and humidifying the air passing through into the planting area. This saturated cool air enters the greenhouse. Greenhouse will have a transparent top cover to allow the sunlight to enter the greenhouse required for photosynthesis. Only a small fraction of sunlight is useful for photosynthesis, the so-called photo-synthetically active radiation (PAR). In a normal greenhouse, the remaining sunlight translates into hot growing conditions and large watering requirements. To overcome this problem, the Sea Water Greenhouse (SWGH) uses a double layer of transparent roof film to provide a thermal barrier. Infrared radiation (IR) is substantially blocked between the layers and retained as heat in the roof cavity. The cool air entering the green house is thus further heated by the energy absorbed through the greenhouse envelope or released by the plants. This results in increasing the moisture absorption capacity of the air, which absorbs the vapor generated by the plants by evapotranspiration and that lost by the soil. Further absorption of water vapor is facilitated by the second evaporator mounted at the exit of the greenhouse. This relatively warm and saturated air exiting the green house is cooled below the dew point temperature in the condenser located after the second evaporator to produce fresh water (see Figure 1.1). Condenser uses cool seawater, which may come from the sea or from the first evaporator, whichever is the cooler. The fresh water condensing from the humid air is of virtually zero salinity. The dry air exiting the condenser may still be cool enough to cool the shaded adjacent space or circulated through a parallel greenhouse to form a closed cycle type arrangement. Fan is needed to draw the air through the greenhouse, and pumps are needed to circulate the sea water. Both need external power for operation.

The published results on greenhouse desalination are few in number and do not give details on thermodynamic, heat, and mass transfer modelling in addition to the limited studies of performance. Furthermore, there are problems still unaddressed in these publications. For example, the study of Paton (2001) which focuses on greenhouse desalination, albeit revealed promising performance in terms of water yield, has very briefly reviewed the literature on multiple effect solar stills and humidification-

dehumidification and the thermodynamic model was discussed briefly and no details of the model were given. Paton (2001) has presented a useful and interesting block diagram of the greenhouse components but no detailed modelling of different components has been given. The simulations of Paton (2001) presented in his report covered different types of climate and all showed encouraging potential in terms of water production.

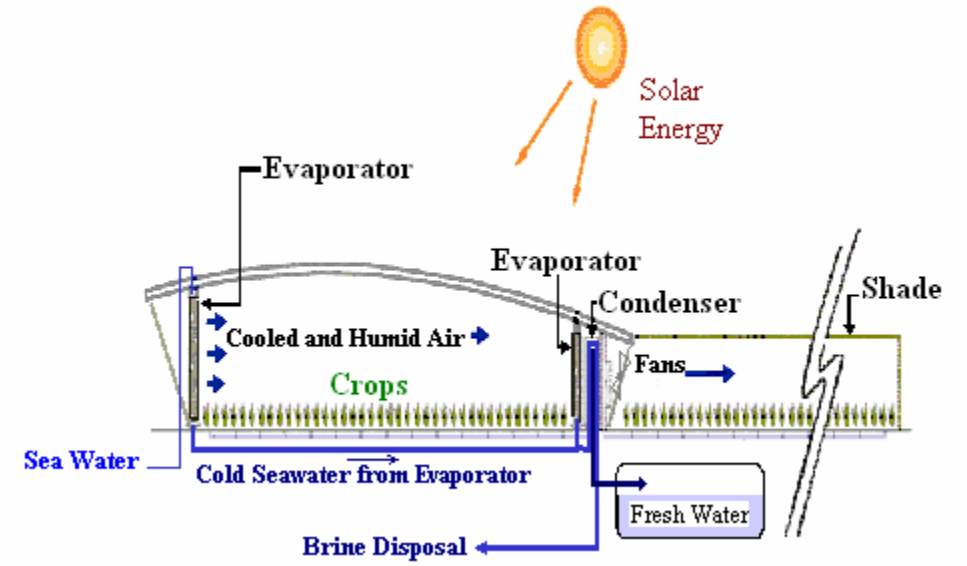

Figure 1.1: Schematics of greenhouse for sea water desalination (Paton, Davies 1996)

To encourage the widespread use of this important technology the contributions of other researchers is vital. Therefore, to make this technology accessible, even for researchers, detailed analysis of different components is essential, especially for the key elements in the greenhouse, i.e., the evaporator, the condenser, the envelope, and the soil and plants. Thus, a rigorous mathematical model describing the basic phenomena occurring in the greenhouse is required to design new greenhouse or evaluate the performance of an existing greenhouse. The basic processes such as heat and mass transfer in soil, plants, and throughout the greenhouse space in addition to the heat transfer through the envelope must be taken into account in the model. The soil constitutes a three-phase medium involving solid, liquid, and water vapor phases. The heat and mass transfer phenomenon in soil is governed by coupled nonlinear partial differential equations representing the moisture content and heat and vapor transfer with the air and plant canopy. Likewise, the heat and mass transfer in plant canopy is governed by the radiative (both solar and long wave) heat transfer with the surroundings and convective heat and mass transfer with the canopy air. Furthermore, evapotranspiration of plants and convective heat and mass transfer between the canopy air and that outside the plant canopy need to be dealt with for proper modeling.

Other problems unaddressed in greenhouse research include the ineffectiveness of the greenhouse in high humidity environments as evaporative cooling is not possible or

highly ineffective to allow for plantation. Possible solutions could be the use of desiccant dehumidification prior to the first evaporator. Liquid and solid desiccants regenerated using solar or waste energy have been developed in the past. The potential of this technique in improving the effectiveness of the greenhouse desalination is yet to be evaluated. Two more problems vital to the design of efficient greenhouse desalination is the cooling water for the green house condenser and the design of the condenser itself. In this respect avenues for economically and technically feasible water cooling should be explored. Water cooling via solar absorption and/or desiccant cooling which may be employed in a hybrid condenser water cooling scheme may prove to be effective. Noting that many regions have hot water springs, the geothermal energy may be utilized as a power supplement for absorption cooling.

1.1 Objectives and approach

The current study focused on conducting a *preliminary study* to assess the state of the art in this relatively new concept of water desalination, the greenhouse concept, and to investigate design improvements of one of its components, the greenhouse condenser. Thus, the present study focuses on conducting a comprehensive literature review covering the physical principles that mathematically describe the greenhouse operation, i.e., thermodynamics and heat and mass transport processes. Also, the condenser which is the vital component of greenhouse desalination is reviewed and a simple condenser is developed and experimentally assessed. Techniques for cooling the condenser coolant (water) are identified and assessed. The outcome of this work should lay the ground for further studies that deal with development of versatile simulation software based on sound mathematical model capable of predicting the performance under a wide parameter space variation. Insight and understanding of the greenhouse physics and proper mathematical modeling are prerequisite for proper design of the greenhouse desalination technology which has the potential in revolutionizing both water desalination and agricultural crop cultivation in regions of the world where fresh water is scarce while saline water is abundant.

The method of approach adopted in this research consists of the following Tasks:

Task 1: Conduct a comprehensive literature review on the physical principles that mathematically describe the greenhouse operation

Task 2: Conduct a literature review on condenser design and build and test a simple condenser for greenhouse desalination system.

Task 3: Produce comprehensive literature review on methods and ways to cool the condenser cooling water and identify the most suitable methods.

Task4: Provide a comprehensive mathematical model assembled from various models of the greenhouse components and identify areas of need of future research work in greenhouse desalination

2. LITERATURE REVIEW

2.1 Greenhouse

The problem of the conventional water distillation plants is being energy-intensive and the requirement for electrical power for operation. The alternative could be through the usage of renewable solar energy using basin-type solar still. However the conventional solar stills are known to have quite low productivity (3 to 5 liters/m^2-day). More efficient multiple-effect stills involve sophisticated design, and are thus more expensive. For more economical system the solar still green-house combination was introduced to minimize the water requirements for small scale greenhouse agriculture (Al Kasabi et al., 1981; Gale and Zeroni, 1984; Hassan et al., 1989).

The microclimate of the greenhouse is of considerable importance for crop growth. Two main climatic scenarios should be considered. The first one is the temperate version, where the temperature in the growing area is *cool and the humidity is high*. This version is suited to crops that are normally difficult or impossible to grow in hot, arid locations. The second scenario is the *tropical version*, where the temperature in the growing area is *warm and the humidity is very high*. Examples of suitable crops include aubergines, cucumbers, melons, pineapples, avocados, and peppers. In the latter version the *airflow is lower* than the temperate version.

To achieve all requirements, namely fresh water production enough for plant growth, and for other usages, and to control the greenhouse microclimate to suit a particular crop Humidification-Dehumidification Desalination Method was proposed (Paton and Davis, 1996; Paton, 2001 and Sablani et al., 2002). The greenhouse humidification-dehumidification integrated system is found to be an economical alternative, having the lowest investment and water cost compared to detached systems of greenhouse and solar thermal desalination systems.

Different operating conditions affect the greenhouse performance. These include the type of the crop itself, being *temperate* or *tropical*, the time of the year, summer time and winter time, location, dimensions and fresh water production requirements, and power consumption (fans and pumps), and crop growth.

Due to the number and complexity of the heat and mass transfer mechanisms included in the greenhouse system integrated with humidification-dehumidification system, one can follow Kindelan (1980) in dividing the system into separate sub-systems in order to allow the analysis of different parts easily. The system can be separated into: the evaporator, the greenhouse and the condenser. The output from the evaporator is the inlet condition for the greenhouse, and that from the greenhouse is the inlet condition for the condenser. The ambient air is the inlet condition for the evaporator. The greenhouse itself is affected by the solar radiation and by the heat transfer of different modes with the surroundings from above. And from below it is affected by the type of the growing plants and the soil bed. Different models have been developed by researchers concerning the analysis of the

greenhouse; Tiwari, et al. (1998), among others. The energy balance equations for different components of the greenhouse system including different layers, a soil layer, a vegetation layer, and air layer and a cover were solved. The thermal radiative, sensible, latent and conductive heat fluxes were modeled in each layer.

An evaporative cooling system for a greenhouse is experimented and modeled by Dilip and Gopal (2002). The system consists of a roof type greenhouse with a cooling pad placed at the inlet to the greenhouse. The air is drawn into the greenhouse via a fan at the other end. The pad is fed continuously with water. The drop in the temperature of the greenhouse is used to measure the effectiveness of the evaporative cooling system.

As mentioned previously the green house is aimed to grow crops. For efficient crop growth the microclimate suiting that particular type of crops needs to be established. Conditions such as light, moisture (in both liquid and vapor form), temperature, and carbon dioxide must be under control. Sunlight is of utmost importance, a rule of thumb is to get the direct sun from 9 am to 3 pm in the winter and about 10 hours of summer sun for year round production. Minimum temperatures must be maintained. The minimum critical temperature depends on the crops themselves. Sustained temperatures above 32-43^{o}C (90ºF to 110ºF) must be avoided. A mechanical backup fan, evaporative cooling, and shading are additional tools for maintaining temperature controlled.

Plants will grow best when the relative humidity is between 45 and 60 percent. Water vapor varies between 1 - 4% of our atmosphere by volume. As the air temperature rises, more water vapor can be held in a given amount of air. And as the air becomes warmer, more moisture must be added to the air to maintain the same relative humidity.

The Vapor Pressure Deficit (VPD) is often used to measure plant/air moisture relationship. Vapor pressure deficit is the difference between saturated air and air at various relative humidities. A VPD range of 8–10 mb has been suggested as an optimum range for different crops. The humidity levels near the dew point needs to be avoided in greenhouses, local water condensation onto plant surfaces promote the growth of disease organisms. Thus all measures must be taken to avoid such an effect. The above greenhouse requirement is essential in order to determine the inside conditions that must be used for the mathematical model of the greenhouse. The boundary conditions for the greenhouse are the incident short-wave irradiance, the downward long-wave radiant flux density, the air temperature, the air humidity, the wind speed, all measured outside the greenhouse. The radiation balance on the crop surface, the surface temperature of crop, and transpiration rate from the crop are the parameters affecting the other boundary conditions. Transmissivity of the greenhouse cover and global heat transfer coefficient can be determined from experimental greenhouse data. Dynamic greenhouse climate models developed by Takakura et al. (1971), Kindelan (1980), and Bot (1983) showed that the accurate simulation of the greenhouse solar interaction requires very complicated and highly detailed models. A simplified solar radiation transmission model can be used instead, which will allow determining the most important factors necessary for greenhouse calculation. A one-dimensional model was developed by Avissar and Mahrer (1982), to simulate the diurnal changes of the greenhouse environment. The model

considered a soil layer, a vegetation layer, an air layer and a cover. The thermal radiative, sensible, latent and conductive heat fluxes were modeled in each layer in terms of its unknown temperature and vapor pressure. Numerical results were verified against an experimental observation of three types of greenhouses. The model proved itself against the experimental findings, providing an accurate determination of the inside air heat transfer coefficient.

To extend the crop production season in order to increase annual productivity, the greenhouse microclimate needs to be controlled. Morris (1956) reported the greenhouse cooling potential by evaporative cooling. Landsberg and White (1979) represented a detailed treatment of the greenhouse evaporative cooling system. Temperature can be lowered by 6-8 ^{o}C with evaporative cooling in greenhouses. Dilip and Gopal (2002) developed a mathematical model to determine the optimization of the cooling parameters of an evaporative cooling (fan and pad type) system. The energy balance equations for different components of the greenhouse system were calculated. The model has been tested against experimental measurements.

Another objective of greenhouse-desalination combination system is the production of the fresh water. Fresh water can be extracted from sea water or brackish water by vaporizing the water, and then condensing this water vapor on a cooler surface. A conventional solar still is a good example where the solar energy is used for evaporation process. Chaibi (2003) reported the benefits of using the greenhouse systems integrated with water desalination. The water desalination system is integrated in a greenhouse roof. By this combined system it is possible to control the greenhouse climate and maximize the water production. However desalination system at the greenhouse roof would affects the photosynthetic active radiation which is very important for the plant growth. Also it is important to introduce a model for the water production as well as the crop water demand. Literature surveys presented by Al-Kasabi et al. (1981), Hassan et al. (1989) and Gale and Zeroni (1984) indicate clearly the principal benefits of the integrated concept. However, as drawbacks are mentioned, high supposed costs and the lack of appropriate analysis tools for the system performance and economy in specific, practical cases.

Due to the complexity of the heat and mass transfer mechanisms included in the greenhouse with integrated desalination in the roof, Chaibi (2003) decided to model different constituents of the system separately. He divided the system into water desalination, total light transmission, crop growth, and greenhouse climate and water balance. The model for water desalination uses a mathematical model similar to those of Oztoker and Selsuk (1971), Sodha et al. (1980), Maalej (1991) and Malik et al. (1996). The model contains equations for the energy balance of the external greenhouse cover, the flowing water layer in the solar still, the light absorber and the insulation layer under the absorber.

The optical performance of the three layers of the desalination roof has been considered when modeled the total light transmission. The desalination roof will affect the greenhouse microclimate affecting the crop growth. The growth rate is a function of climate parameters as the flux of photosynthetic active radiation, the carbon dioxide

concentration of the air, and the greenhouse air temperature. The heat and mass transfer model in the greenhouse are developed for four parts, the crop canopy, the floor, the greenhouse air and the greenhouse envelope. For the model validation, an experiment of small roof module was performed and the results were compared. The simulation is found to give relevant performance estimations of the fresh water production and demand as well as the crop growth under various climate conditions.

Sablani et al. (2003) represented a simulation of an integrated greenhouse-humidification-dehumidification system. The combined effects namely fresh water production and growth of the crop in a greenhouse were considered. The system consists of an evaporator where water vapor extracted from the sea water is carried by the hot and dry outside air stream which cools down as it passes through the evaporator. As the air passes in the greenhouse it will heat up and absorb more water vapor, cooling the greenhouse climate. The saturated air then passes through a condenser where water vapor is condensed thus producing the fresh water. The deep sea water is used as a coolant for the condenser. Commercial software was used for the analysis. The Performance of seawater greenhouse for various climate scenarios was presented.

Sablani, et al. (2002) presented simulation of fresh water production using a humidification and dehumidification seawater greenhouse. A thermodynamic simulation study was performed to investigate the influence of different parameters affecting the greenhouse desalination process. The performance of the seawater greenhouse for various climate conditions was investigated by Paton and Davies (1996). For a greenhouse of 10^4 m^2 area Table 2.1 shows the performance of seawater greenhouse in terms of fresh water production and the power consumption of the fans and pumps per cubic meter of fresh water.

Table 2.1: Performance of seawater greenhouse for three climate conditions (Paton and Davies, 1996)

Climate condition	Total fresh water produced, m^3/year-hectare	Power consumption, kWh/m^3
Temperate	20,370	1.9
Tropical	11,574	1.6
Oasis	23,529	2.3

As part of this work a comprehensive mathematical model will be developed. The model will include all the physical processes governing the greenhouse performance. As a first step, the details of the evaporator model are described in section 2.3. Furthermore, one of the important components of the humidification-dehumidification desalination technique is the condenser. A simple, economical and efficient condenser must be developed in order to increase the system productivity and reduce the cost. This is discussed in section 2.4.

2.2 CFD modeling of greenhouse

Greenhouse microclimate is far from being homogenous. Variations in both space and time of momentum, energy, and mass transfer rates do exist. This is because of the nature of greenhouse physical processes and the intrinsic weather factor as solar flux, wind speed, and air temperature and humidity vary on diurnal and seasonal bases. To resolve greenhouse microenvironment the transport processes must be modeled using CFD technique where the differential equations describing these processes are solved under realistic boundary conditions. With the development of commercial CFD software simulations under wide range of parameter space unattainable experimentally, due to time and cost constraints, have become possible.

Several works have appeared in the literature on using CFD as a modeling tool to study the greenhouse microenvironment. Boulard and Wang (2002) studied the heterogeneity of crop transpiration in a plastic greenhouse. Prediction of crop transpiration distribution is essential for greenhouse water resource management. The greenhouse (22×8 m) was studied using CFD. A solar radiation and a crop heat exchange models have been incorporated into the CFD model. The crop transpiration was modeled by assuming a porous medium with sensible and latent heat exchanges with indoor surroundings. The model was validated using experimental measurements of velocity, temperature and vapor content at two vertical cross sections of the greenhouse. Predictions of transpiration fluxes were made for a mature lettuce crop. The results show strong variations of crop transpiration throughout the greenhouse of up to 30%.

Steady state three-dimensional CFD simulations were carried out by Fatnassi et al. (2003) to study the microenvironment of a large scale 5600 m^2 prototype greenhouse under the climatic conditions of Agadir in south Morocco. The CFD model incorporated non-uniform grid spacing with 316,800 grid points, 120×88×30 for covering a model greenhouse of 40×30×20 m in length, width, and height, respectively. The air flow through the greenhouse was wind-driven with the aid of prevailing windward orientation and roof apertures totaling 224 m^2 in area and covered by insect-proof screens. Also the side walls were equipped with insect-proof screens covered by plastic covers that can be rolled open as desired. Experiments were also conducted and validation of the CFD model was carried out. The side walls screens were let open only on the windward sides (west and east sides) which have total 296 m^2 in area. The air flow through the crop and the screens was modeled as flow through porous media. Predictions of sensible and latent heat transfer between the crop cover and the air shows that the air flows through the crop cover where it is warmed and humidified before escaping through the roof screen apertures. The insect-proof screens were found to result in significant increases in air temperature and humidity inside the greenhouse. Based on the simulations results improvements in greenhouse design were deduced, i.e., increasing the total area of the openings while decreasing the screen mesh size to prevent insects intrusion.

In order to minimize the fan power needed to force the air flow into the greenhouse the greenhouse intake must be oriented perpendicular to the prevailing wind direction. The effect of the variation in wind direction relative to the intake was studied by Davies et al. (2004) using three-dimensional CFD modeling. Their results were expressed in terms of the ratio of the air flow, at any incidence angle θ to that at $\theta = 0^o$ corresponding to flow direction normal to the greenhouse intake area. This ratio was termed the wind-angle acceptance function $f(\theta)$. Values of $f(\theta)$ of 0.8 and 0.6 were found to correspond to θ of 38^o and 52^o, respectively. These values are very close to the theoretically predicted values represented by a cosine function, i.e., $f(\theta) = \cos(\theta)$.

Mistriotis et al. (1997) have studied the influence of the greenhouse geometrical characteristics and in particular its length on the ventilation efficiency, by the aid of a two-scale k-ε turbulence CFD model. After having validated the model by comparing its results to wind-tunnel and full-scale experimental data, they analyzed the wind driven ventilation behavior of a continuous roof ventilator in a twin-span Mediterranean type greenhouse. The outcome of the simulations indicated that greenhouses of this type with length smaller than 50m have higher ventilation rates. They stress however that the results of this study cannot be easily generalized as a lot of different parameters are of great influence (such as local weather conditions, greenhouse orientation, the presence of various types of plants inside the greenhouse, buoyancy effects etc) offering a wide and interesting field for future research.

In the article by Reichrath and Davies (2001), simulation results of the pressure distribution on the external side of a 52 span 167 x 111m commercial Venlo-type glasshouse roof in an external cross-flow are compared with experimental data by Hoxey and Moran (1991). Earlier experimental results on a 7-span glasshouse again by Hoxey and Moran were also used for comparison purposes. The CFD code that was used was the commercial package Fluent 5.3.18 coupled with the standard k-ε turbulence model as well as the renormalisation group (RNG) turbulence model (the latter appearing to give a better agreement with the measurement results). The authors conclude that the CFD predictions are in good agreement with the experimental data and since the pressure distribution around a building is the driving force for the ventilation process inside a naturally ventilated glasshouse, the latter could also be modeled accurately for either smaller or larger glasshouse constructions.

In another study by Bartzanas et al. (2002), numerical simulations by means of the commercial CFD package CFD2000 were conducted in order to analyze the ventilation process in a tunnel greenhouse equipped with an insect-proof screen in the side openings. In particular the influence of the insect-proof screen on airflow and temperature was studied under the effect of different wind directions. The screens on the greenhouse openings and the crop were simulated using the porous media approach. The simulation results indicate that the screen reduced the air velocity inside the green house and in particular inside the crops area by half, increasing thus considerably the temperature levels. Wind direction was also found to affect climatic conditions inside the greenhouse considerably as contrasted airflow and temperature patterns were observed for various wind regimes, especially in greenhouses equipped with insect screens.

Shklyar and Arbel (2004) have designed and developed a numerical solution for the simulation of the 3D internal and external isothermal flows in a full-scale, single-span, pitched-roof greenhouse with continuous vents to either side of the ridge and to each side wall. The turbulence scheme used was the standard k-ε scheme. According to the simulation results, mass fluxes and flow patterns greatly depend on the wind direction and on the opening angles of the windward and leeward vents. In particular, winds perpendicular to the greenhouse ridge have as a result 4-4.9 times greater ventilation rates than winds blowing parallel to the ridge. It was also observed that a change in the wind direction from 0^o to 45^o has a considerably greater influence on the ventilation rate (i.e. 240-340%) than the change of direction from 45^o to 90^o (18%). The results of this study were found to be in good agreement with those of other experiments and observations.

In their study, Lee et al. (2002) developed CFD models in order to investigate the effect of roof vent opening on natural ventilation of fully open-roof multi-span greenhouse. The CFD validity was investigated using the Particle Image Velocimetry data, measured at a large-sized wind tunnel system at National Institute of Rural Engineering in Japan. The discrepancy between simulation and experimental results varied from 33.6% for a wind speed of 3.5m/s to 13.5% for a wind speed 6.3m/s, this error becoming even less than 10% as the number of spans increased over six. The authors conclude that CFD simulation can be a valuable tool for analyzing the internal flow, air temperature, humidity, CO2 concentration or the designs of heating, cooling and ventilation systems in greenhouses.

The aim of another study by Bartzanas et al. (2004) was to numerically determine the effects of different vent arrangements on windward ventilation of a tunnel greenhouse with mature tomato crop using the commercial computational CFD code Fluent v5.3.18. After being validated with tunnel experiment results, the CFD code was applied to investigate the consequences of four different ventilator configurations on the natural ventilation system. For the different configurations, the computed ventilation rates varied from 10 to 58 air recyclings per hour for an outside wind perpendicular to the openings with a speed of 3m/s. Although the mean inside air temperature was very close to the outside air temperature, at several regions of the greenhouse temperatures of 6^oC higher were also computed. According to the authors' final conclusions, highest ventilation rates are not always the best criterion for a ventilation system evaluation. Factors like air velocities in the crop regions, aerodynamic resistances, or air temperature differences could also be of a big importance. For the studied greenhouse configuration, a combination of roof and side openings was estimated as the best solution. In the absence of roof openings, roll-up openings were found to be more efficient than pivoting ones.

Finally, in a study of the virtues of the aerodynamic analysis for the optimization of agricultural buildings' ventilation design, Lee et al. (2003) perform an assessment of the various existing technologies of aerodynamics such as large-sized wind tunnels, particle image velocimetry (PIV) as well as computational fluid dynamics (CFD). The authors acknowledge that CFD has recently become a valuable tool for analyzing natural ventilation systems. They stress however that there is a lack of validation of CFD

numerical results with actual data of airflow, which is mainly due to the difficulties of airflow experimental analysis.

2.3 Evaporator

Cooling the greenhouse inlet air evaporatively may be accomplished in three ways: evaporative media-type, spray (air washer), and direct fogging systems. In practice, in the media-type and the spray cooler systems a wet bulb temperature approach ranging between 80-90% may be achieved while for direct fogging it may reach 98-100%. While the latter system is efficient, it requires de-mineralized water and very high pressure exceeding 10 bar (Zurigat et al., 2004). Therefore, the direct fogging system as a mean of evaporator design is ruled out since sea water is to be used. The spray system (or air washer) is a technically viable option. However, its suitability for handling seawater needs further consideration. Generally media-type evaporator is used for greenhouse application.

A wet-bulb temperature approach of 90% is normally assumed for evaporative media-type cooling. The psychrometric equation (Equation (2.1)) may be used to evaluate the potential of water absorbed by the air entering the greenhouse. Meteorological stations normally report the dry bulb temperature and the relative humidity in addition to other indicators. Using T_{db} and ϕ a number of parameters can be calculated using psychrometrics. That is, the wet-bulb temperature is calculated from the measured T_{db} and ϕ, using the psychrometric equation (Jones, 1994):

$$p_v = p_{ss} - p_{atm}\, A(T_{db} - T_{wb}) \tag{2.1}$$

and

$$p_v = p_{vs}\, \phi \tag{2.2}$$

where

p_v = vapor pressure at T_{db} (kPa)
p_{ss} = saturated vapor pressure at T_{wb} (kPa)
p_{vs} = saturated vapor pressure at T_{db} (kPa)
p_{atm} = local atmospheric pressure (kPa)
T_{db} = dry-bulb temperature (^{o}C)
T_{wb} = wet-bulb temperature (^{o}C)
A = constant having the values: For screen $A = 7.99\text{x}10^{-4}\ \text{C}^{-1}$ and for sling or aspirated (the one used here) $A = 6.66\text{x}10^{-4}\ \text{C}^{-1}$.
ϕ = relative humidity

The saturated vapor pressures p_{ss}, and p_{vs} are calculated at T_{wb} and T_{db}, respectively using:

$$\log P = 30.59051 - 8.2\, \log T + 0.0024804\, T - 3142.31\, T^{-1} \tag{2.3}$$

where T is in K and P in kPa.

Using Equations (2.1) and (2.2), Equation (2.3) is solved numerically for the wet-bulb temperature. Alternatively, the above equations can be solved for the relative humidity given the wet bulb and dry bulb temperature. This is the case experienced in laboratory experiments as the dry bulb and wet bulb temperatures are measured. Based on the above equations the specific humidity, the dew point temperature and the vapor pressure are also calculated. For example, the specific humidity is calculated using:

$$\omega = 0.622 \times \frac{p_v}{p_{atm} - p_v} \tag{2.4}$$

For a typical greenhouse with inlet air velocity of 0.5 m/s and an inlet area of 30 m^2 (Paton, 2004: personal communications), the air flow rate is 15 m^3/s. For given ambient conditions the amount of water vapour absorbed by the air is calculated from Equation (2.4). The Typical Meteorological Year data for Seeb/Sultanate of Oman (Zurigat et al., 2003) were used. Figure 2.1 shows the rate of liquid water absorbed by the air stream in the process of evaporative cooling assuming 100% saturation.

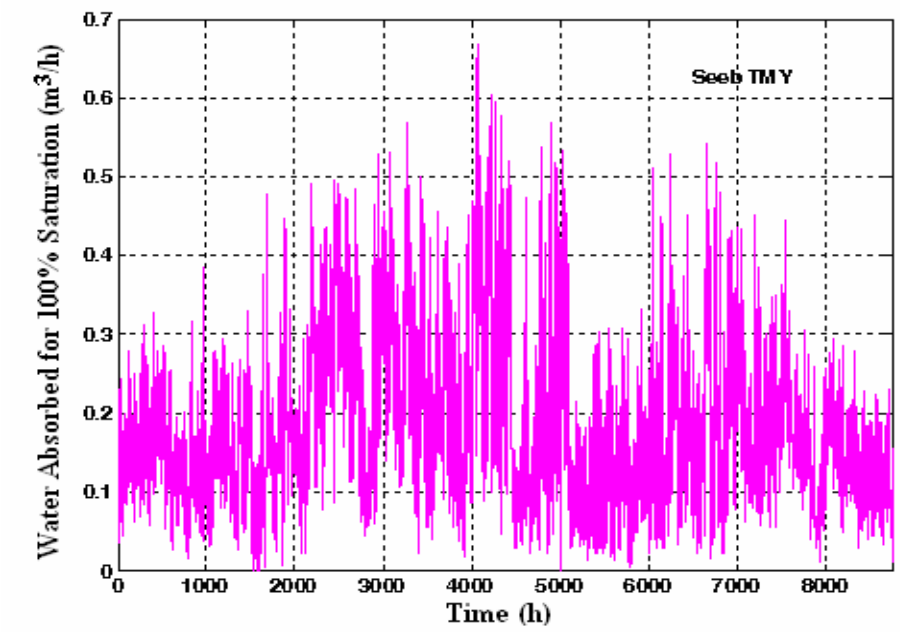

Figure 2.1: Hourly rate of water absorbed by the greenhouse air stream at the evaporator assuming 100% saturation (Seeb TMY, $\dot{V}_a$=15 m^3/s)

Figure 2.2 shows the monthly amount of water absorbed by air that potentially may condense giving an annual total of 1628 m^3/year under the weather conditions of Seeb for 100% and 90% wet bulb temperature approach. Note that the month of August exhibits the lowest water absorbed as it has the highest relative humidity of all months (see Zurigat et al., 2003 and Zurigat et al., 2007). Clearly, the amount of water vapour absorbed is quite sufficient for irrigation if it can be condensed back into liquid water.

This demonstrates the potential of greenhouse desalination technique in providing fresh water for irrigation. The only difficulty in the way is the provision of a condenser capable of condensing the water vapour efficiently into liquid water. This is the critical component of greenhouse desalination that needs thorough analysis; a task undertaken in this work and discussed in section 2.4.

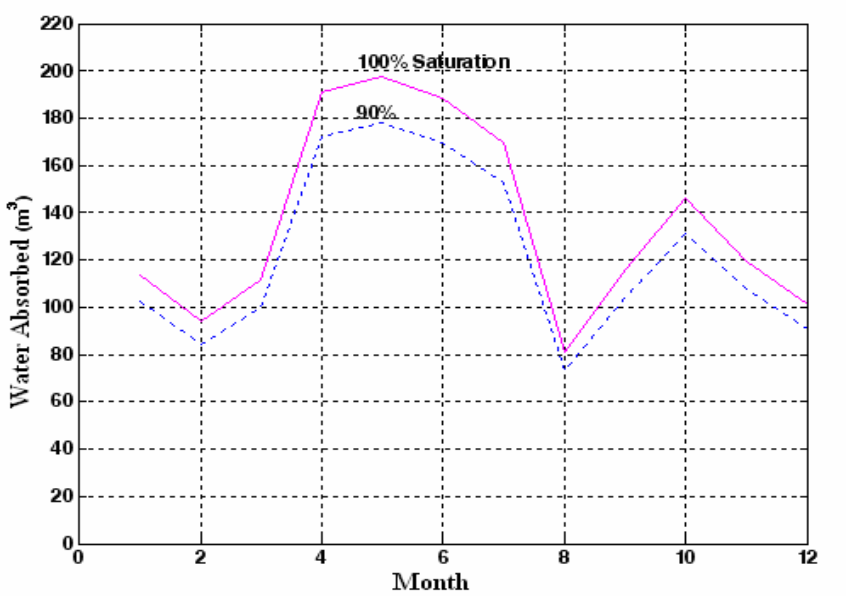

Figure 2.2: Water absorbed by the air stream in a typical greenhouse in the process of evaporative cooling (Seeb TMY, $\dot{V}_a$=15 m^3/s)

2.4 Condenser

2.4.1 Condensation Process

In this section the basic mechanisms involved in condensation process are briefly introduced to shed light onto condensers design and the factors controlling their performance. By definition, condensation is the process by which a vapor phase is cooled to temperatures sufficiently low (below its saturation temperature) to start the nucleation of liquid droplets. Drop nucleation may occur *homogeneously* or *heterogeneously*. The former occurs within the vapor itself while the latter occurs on cooled surfaces. In heterogeneous nucleation two mechanisms are distinguished: the *film-wise* and the *drop-wise* condensation.

Film-wise condensation occurs on surfaces that are easily wetted so a liquid film forms and flows down the surface by gravity. *Drop-wise* condensation occurs on un-wetted surfaces where vapor condenses into droplets which grow in size by further condensation and coalescence with neighboring droplets and roll down the surface leaving clean surface behind for new droplets to form. Table 2.2 shows that drop-wise condensation has condensation heat transfer coefficients ten times higher than their film-wise

counterparts. One is tempted to design condensers based on dropwise condensation heat transfer. However, two problems are encountered: the first one is the maintenance of un-wetted surface which requires specific and frequently expensive materials, surface finish, and promoters while the second problem is the uncertainty in heat transfer coefficient data because of the persistent lack of reliable prediction theory of drop-wise condensation.

Regardless of whether nucleation occurs *homogeneous*ly (within the phase) or *heterogeneous*ly (drop-wise or film-wise) the condensation is an interfacial phenomenon involving interface mass transfer viewed from the kinetic theory as a difference between two quantities; a *rate of arrival* of molecules from the vapor phase region towards the interface and a *rate of departure* of molecules from the condensate surface into the vapor region. Onset of condensation takes place when the rate of arrival exceeds that of departure. The fact that condensation is an interfacial phenomenon makes the presence of non-condensable gas a problem that needs careful attention.

Figure 2.3 shows a wall on which condensation occurs. The vapor condenses on the wall leaving the non-condensable gas to accumulate outside the condensate layer. Thus, two layers are distinguished: the condensate layer on the wall followed by a layer of non-condensable gas (diffusion layer). This layer forms a buffer zone between the free stream mixture of vapor and non-condensable gas and the condensate layer. For vapor in the mixture to condensate on the condensate layer it should diffuse through the non-condensable gas layer, hence the name "diffusion layer". In doing so the partial pressure of the condensing vapor at the interface between the two layers is reduced (see Figure 2.3) and the combined resistance of the condensate layer and diffusion layer reduces the heat transfer rate across the wall.

Table 2.2: Orders of magnitude for condensation heat transfer coefficients along with others usually found in series with them (Chapter 5 in Hetsroni, 1982)

Mode of condensation	α (W/m^2 K)
Typical values for air-free vapors	
Film condensation on surfaces	
Pure steam	6,000-30,000
Gassy steam	600-6,000
Hydrocarbons	1,000-5,000
Dropwise condensation of steam	60,000-300,000
Steam on a cold water jet	200,000-600,000
Steam jet in cold water	$\approx 10^6$
Representative values of heat transfer coefficients often associated with condensing systems	
Tubes	6,000-100,000
Scale in tubes	600-12,000
Water in tubes	2,000-30,000

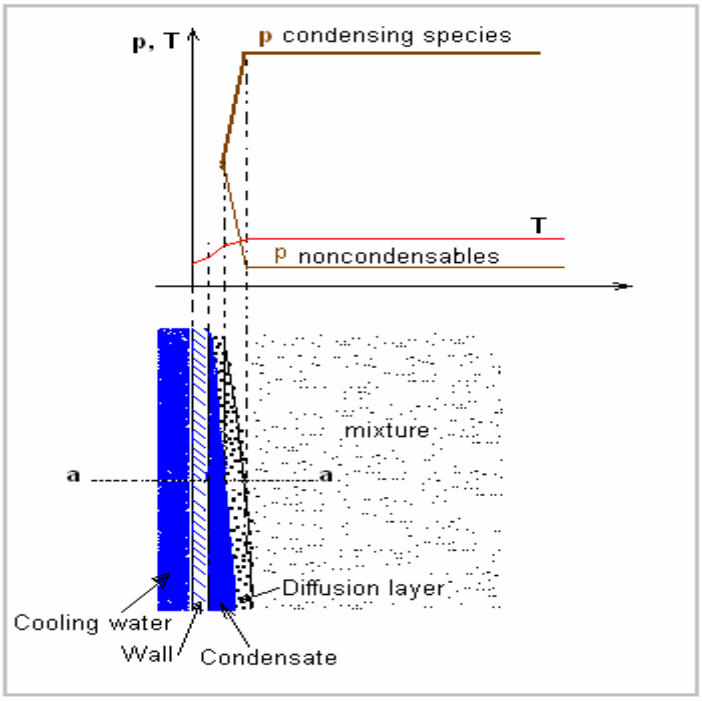

Figure 2.3: Temperature and partial pressure profiles in the vicinity of a wall on which condensation is occurring with non-condensable gas present

Figure 2.4 shows the variations of non-condensable gas concentration and saturation temperature in the boundary layer. The adverse effect of non-condensable gas is seen in Figure 2.5 which shows that as the percentage of air increases the condensation heat transfer coefficient decreases.

The presence of noncondensable gas (NG) leads to a significant reduction in heat transfer during condensation. The effect of NG may be understood by looking at the condensation boundary layer shown in Figure 2.4 which shows a wall at temperature T_w on which a film-wise condensation occurs. The vapour condenses on the wall leaving the noncondensable gas which does not condense and attains its highest concentration x_{ai} at the condensate-mixture interface relative to its concentration in the bulk (free stream) mixture (x_{ab}). The partial pressures of water vapour p_v and NG p_a vary across the condensation boundary layer while their sum is constant and equal to the bulk mixture pressure as shown in Figure 2.4. Accordingly, and because of the presence of NG the saturation temperature of water vapour in the mixture varies; decreases with the increase in noncondensable concentration as the vapour condenses at the condensate film. This causes a reduction in the heat transfer driving temperature difference across the condensate layer. Furthermore, as stated before, the increase in concentration of noncondensable gases at the interface relative to its value at the bulk mixture creates a mass diffusion layer. In this layer the noncondensable gas diffuses away from the interface towards the bulk mixture where the NG concentration is less. Similarly, the vapour diffuses towards the interface due to the presence of vapour concentration gradient across the diffusion boundary layer. Thus, in the presence of NG three resistances occur compared with one for pure vapour.

That is,

1. Thermal resistance across the condensate film (between interface and wall)
2. Forced convective heat transfer resistance between bulk flow and interface
3. Mass transfer resistance to the diffusion of vapour to the interface

In pure vapour case, only the first resistance is present. The net result is a significant decrease in condensation heat transfer coefficient compared with that for pure vapour condensation. Figure 2.5 shows reductions in condensation heat transfer coefficient over 80% occur for just 8% of air in the steam.

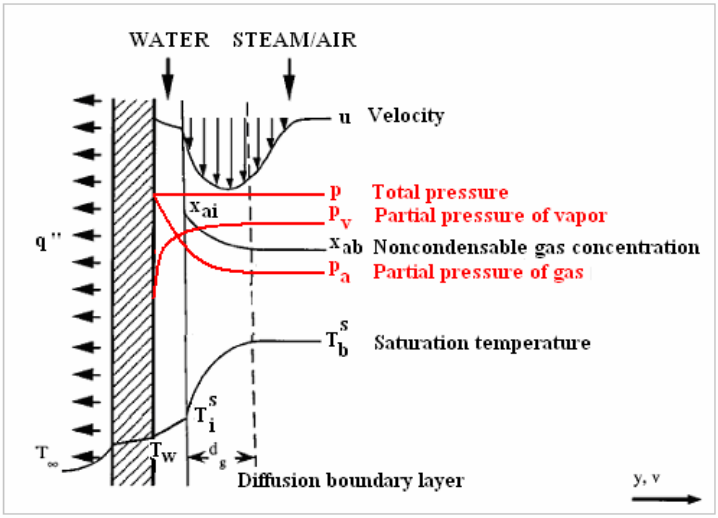

Figure 2.4: Schematic illustration of condensation with non-condensable gas (Peterson, 2000)

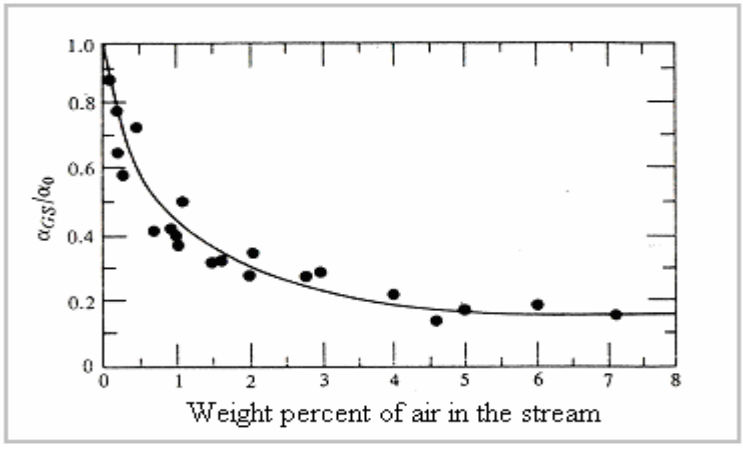

Figure 2.5: Effect of air on condensation heat transfer (Mikheyev, 1977)

The problem of condensation in the presence of non-condensable gases has been studied in the past both experimentally and theoretically and design methods have been developed. Free convection condensation experiments with mixtures of steam and four different gases (air, argon, neon and helium) were conducted by Al-Diwany and Rose (1973). The effect of pressure on condensation of steam-air mixture was investigated by De Vuono (1983) who conducted experiments on condensation by natural convection over a horizontal copper tube of 7.94 cm outside diameter and 1.22 m long under varying pressure. A pressure vessel of 1.52 m outside diameter and 3.35 m long was used for housing the test tube. The total pressure, P_{tot}, in the vessel was varied up to 0.7 MPa. Saturated steam was injected into the vessel and allowed to diffuse to the test tube. The convection condensation heat transfer coefficient was correlated using the following expression:

$$h_c = 1.49\ (\Delta T)^{-1.11}\left(\frac{1-y}{100}\right)^{2.59}(P_{tot})^{0.48} \tag{2.5}$$

where y is the air volume fraction ranging between 0.0 and 0.14 and $\Delta T < 40\,^{o}\mathrm{C}$. Clearly, the effect of pressure is quite significant. However, the scale-up of this result was questionable. Furthermore, for greenhouse condenser the air volume fraction is quite large (over 0.95) which invokes more uncertainties in the application of the above correlation.

Predictions of condensation rates in the presence of a single non-condensable gas species is frequently done using the *diffusion layer* model which expresses the mass transfer coefficient in terms of an equivalent condensation heat transfer coefficient, h_c. The total wall heat flux is then expressed as (Peterson, 2000)

$$q_t = \frac{h_c(T_b^s - T_\infty) + \theta_T^{'} h_s (T_b - T_\infty)}{1 + \dfrac{h_c + \theta_T^{'} h_s}{h_w}} \tag{2.6}$$

Here h_s is the sensible heat transfer coefficient, h_w is the convective (film-wall) heat transfer coefficient, $\theta_T^{'}$ is the so called "modified Eckermann correction" which is a function of the diffusion coefficients of the species, T_∞ is the coolant temperature, T_b is the bulk dry bulb temperature, T_b^s is the bulk saturation temperature evaluated based on the bulk vapor partial pressure. The above expression shows that two resistances control the total heat flux: the parallel resistance with h_s and the series resistance with h_w.

Previous computational studies dealing with condensation in the presence of noncondensable gases have considered two cases: the free convection and the forced convection cases. Using similarity transformation Sparrow and Eckert (1961) and Sparrow and Lin (1964) solved the conservation equations of mass, momentum and energy for laminar film condensation on an isothermal vertical plate. Two dimensionless variables were identified as having the influence on condensation rate. These are the bulk

gas mass fraction and the vapor-gas mixture Schmidt number. The effect of noncondensable gas was found to increase as Sc and *x* increase. These are defined by

$$x=\left(\frac{\rho_f \mu_f}{\rho_g \mu_g}\right)^{1/2} \tag{2.7}$$

$$Sc= \frac{C_p(T_M - T_w)}{h_{fg}\,\mathrm{Pr}_f} \tag{2.8}$$

The mass transfer resistance caused by the accumulation of noncondensables at the vapor-liquid interface is sufficiently quantifiable using the *film* theory. But the theory is insufficient to quantify the effect of fog formation (spontaneous condensation) observed in boundary layer during the experiments of Jurgen and Dietmar (1999) with direct contact condensation of steam-nitrogen mixtures at pressures of 0.2-2 MPa.

In their experimental study of condensation in a vertical cylindrical vessel (3.4m ID and 6.4m high) equipped inside with three water cooled cylinders as condensation surfaces Uchida et al. (1965) found that the heat transfer rate decreases with increasing concentration of noncondensable gas and it depends only on the mass ratio of the participating gases. The molecular weight of the gases and pressure were found to have no effect on heat transfer rate. Condensation heat transfer coefficient was correlated by Uchida et al. (1965) by:

$$h_c = 380\left(\frac{W}{1-W}\right)^{-0.7} \tag{2.9}$$

where *W* is the mass fraction of non-condensable gas. Extrapolation of this result to geometries other than those used in the experiments is not recommended. Contrary to the findings of Uchida et al. (1965), Peterson (2000) stressed the importance of molecular weight of the participating gases. He studied the mass transport in condensation with multi-component non-condensable gases. He noted that when non-condensables consist of mixtures of heavy and light species (low and high mass diffusion coefficients, respectively) the heavy species accumulate preferentially at the condensate-mixture interface which consequently affects the diffusion coefficient. Thus, in multi-component non-condensable mixtures having much different mass diffusion coefficients (hydrogen-nitrogen or helium-nitrogen mixtures) the non-condensable species tend to segregate in the condensation boundary layer. As a result proper predictions of condensation heat transfer coefficient require that an effective mass diffusion coefficient be used instead of the average one. Based on fundamental analysis of mass transport with multiple non-condensable components Peterson (2000) developed an effective diffusion coefficient that may be implemented in simple diffusion layer models. The good news is that he further concluded that for air the use of average diffusion coefficient is valid because oxygen and nitrogen, which constitute the majority of gasses in an air mass, have similar mass diffusion coefficients.

Various methods have been developed for the design of condensers in the presence of non-condensable gas. These are the trial-and-error method of Colburn and his coworkers, and the method of Bell and Ghaly (1973) which is an iterative method and gives results of varying degrees of accuracy depending on the process involved. In this method the value of heat flux $q=U\Delta T$ is calculated by iteratively equating the heat transferred through the condensate, the wall, and the coolant film to the sum of the sensible heat transferred from the non-condensable gas and the latent heat of the vapor transferred by mass diffusion. Two parameters need to be provided as initial guess: the temperature at the interface between the condensate and the gas layer and the corresponding vapor pressure of the condensate. These are iteratively updated until the above mentioned equality is achieved giving the instantaneous heat flux values.

Davies and Paton (2004) described experiments conducted by the authors using two types of condenser with the same surface area of 1.25 m^2. The first type is a *standard tube-and-fin condenser* made of metal and consisted of an array of 76 vertical aluminium fins each measuring 160 mm high by 60 mm wide, at spacing of 2.24 mm giving a total width of 170 mm for each condenser. There were 8 copper tubes passing through the fins each 15 mm in diameter. The second type is called *watermaker condenser* which developed specifically for greenhouse desalination and consists of an array of 70 µm thick polyethylene tubes, 5×5 square array of vertical tubes, each 32 mm in diameter and 500 mm in height, on a pitch of 38 mm between centers. The air flow direction was perpendicular to the axes of the tubes. The results are presented in Table 2.3.

Table 2.3: Condensation results for two types of condensers (Davies and Paton, 2004)

Test	Type of Condenser	Fluid Temperature ^oC				Condensate Flow ml/hour		Coefficient of Mass Transfer (mg/s)/ m^2K
		Air		Water		Observed	Corrected	
		In	Out	In	Out			
1	Tube-and-fin	23.0	17.6	11.8	14.2	187	193	6.0
2	Tube-and-fin	23.0	21.2	14.2	15.6	194	186	6.1
3	Watermaker	25.5	21.4	12.0	14.5	367	363	7.9
4	Watermaker	29.5	27.3	17.2	20.2	457	423	9.7
5	Watermaker	29.6	23.9	16.1	19.2	477	450	11.1

A more sound mathematical treatment of the problem should be based on CFD modeling where details of the flow dynamics, heat, and mass transfer may be resolved. In this respect, the conservation equations of mass, momentum, and energy for the condensate film and the vapor-noncondensable gas boundary layer are solved simultaneously along with the conservation of species for the vapor-gas layer. Proper interface boundary conditions must be supplied and models for turbulence closure selected. In their study of the effect of spontaneous condensation (fog formation) on condensation heat transfer in the presence of noncondensable gases, Jurgen and Dietmar (1999) suggest that three-

dimensional CFD modeling is necessary to predict reliably the effect of spontaneous condensation in condensers. Using steam-nitrogen mixture in their experimental work Jurgen and Dietmar (1999) observed that noncondensable gas accumulates in the coldest region of the condensation system.

Based on this preliminary literature review on condensation it is found that noncondensable gases pose a challenging problem. In this project further work will focus on mixtures of single species noncondensable gas (air) with water vapor, i.e., moist air. This should aid in better understanding of the processes taking place in the greenhouse condenser.

2.4.2 Condenser Cooling Duty

Together with the air dry-bulb temperature and relative humidity, the sensible cooling load $\dot{Q}_s$ is calculated using:

$$\dot{Q}_s = \frac{\dot{V}_a}{v_a} \cdot c_{p,a} \cdot (T_{aa,db} - T_{C,i}) \tag{2.10}$$

where; $T_{aa,db}$ is the dry bulb temperature of the air, $T_{C,e}$ design exit temperature which is slightly less than the dew point temperature. Then the latent cooling load $\dot{Q}_l$ is calculated as follows.

$$\dot{Q}_l = \frac{\dot{V}_a}{v_a} \cdot \begin{Bmatrix} w_{aa,db} \cdot (c_{p,v} \cdot T_{aa,db} + r) - w^s_{c,e} \cdot (c_{p,v} \cdot T_{C,e} + r) \\ -(w_{aa,db} - w^s_{C,e}) \cdot c_{p,w} \cdot T_{C,e} \end{Bmatrix} \tag{2.11}$$

where; $c_{p,v}$: specific heat water vapor at constant pressure, *r*: latent heat of evaporation of water at 0°C, $w^s_{C,e}$: saturated water specific humidity at the exit temperature, $c_{p,w}$: heat capacity of liquid water at constant pressure. The rate of fresh water ($\dot{m}_w$), which will then be condensed from the air within the condenser is then calculated from the following equation:

$$\dot{m}_w = \frac{\dot{V}_a}{v_a} \cdot (w_{aa,db} - w^s_{C,e}) \tag{2.12}$$

The total cooling load $\dot{Q}_t$ is the summation of both the sensible and the latent cooling loads.

$$\dot{Q}_t = \dot{Q}_s + \dot{Q}_l \tag{2.13}$$

The above procedure is applied to ambient air at conditions given by the Seeb TMY (Zurigat et al., 2003) for a greenhouse with typical volumetric flow rate of 15 m^3/s. Figure 2.6 shows the hourly sensible, latent and total cooling loads for the whole year and

Figure 2.7 shows the hourly cooling load for the first day of each month of the year. It should be noted that when the procedure is applied to the greenhouse condenser it yields higher cooling load as the latent cooling load will be much higher than the case presented in Figure 2.6 which was simply a demonstration of the methodology.

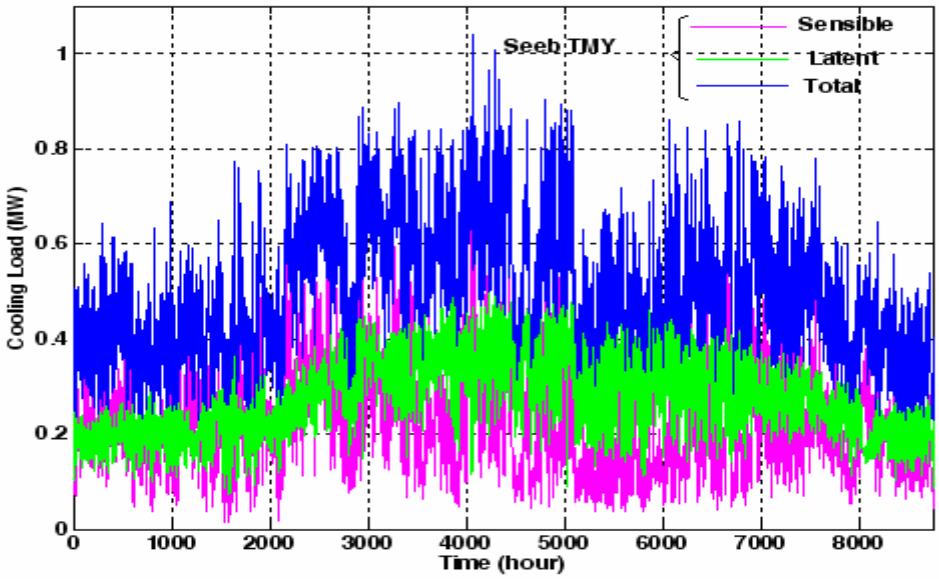

Figure 2.6: Greenhouse air stream cooling load for 2 ^{o}C cooling below dew point temperature (Seeb TMY, $\dot{V}_a$=15 m^3/s)

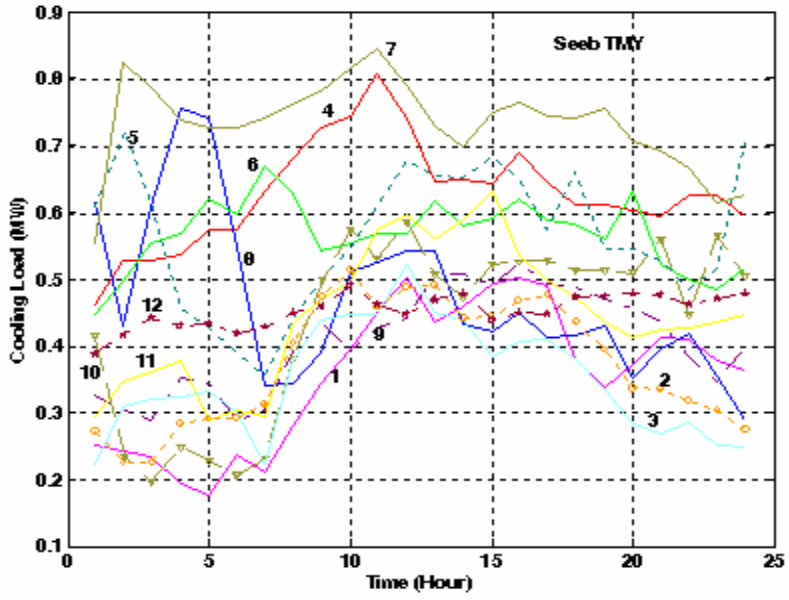

Figure 2.7: Greenhouse air stream total cooling load for 2 ^{o}C cooling below dew point temperature for the first day of each month of the year (Seeb TMY, $\dot{V}_a$=15 m^3/s)

2.4.3 Types of Condensers

Condensing equipment can be classified into a number of generic types as follows:

- ***Tubular Condensers****:* In this type, condensation takes place inside or outside tubes arranged in tube banks. In the process industry, tubular condensers are normally of the conventional shell-and-tube type. The tube bank is mounted inside a cylindrical shell. Condensation may take place in-tube or in the shell depending on the process requirements, i.e., the fouling potential of the cooling liquid, the condensing vapor, the presence of non-condensable gases, and other factors.
- ***Air-cooled Condensers****:* Here, condensation takes place inside finned-tube banks over which air flows by natural or forced convection. Air-cooled condensers are frequently used in gas-turbine power generation plants in areas where cooling water is scarce. For un-finned air-cooled condensers the air side heat transfer resistance is the governing resistance as it is mush higher than the in-tube condensation resistance.
- ***Plate Type Condensers****:* This type includes the plate-and-frame exchanger and the plate-fin (brazed aluminium) exchanger. Plate-type condensers are characterized by relatively high pressure drop and thus they are not suitable for very low-pressure vapors. Also, where the potential for fouling exists they are not a good choice. However, because of their modular construction they, when applicable, are less expensive than other types.
- ***Direct Contact Condensers****:* In this type of condenser, the coolant is brought into direct contact with the condensing vapor. These condensers have extremely large heat transfer rates. They also have simple construction as the need for a heat transfer surface separating the coolant and vapor is eliminated. This often makes direct contact condensers much cheaper for many applications and worth consideration as a first option. In the presence of non-condensable gases it is not clear how low the effectiveness of this type of condensers could reach.

Within the condenser types listed above there are many configurations which make the selection of a condenser for a specific process a difficult task. In some cases, however, the choice is easy. For example, in power plants applications the absence of cooling water narrows down the choice to air-cooled condensers. General guidelines on selection of the type of condenser are available in the literature based on numerous studies and accumulated experience. Selection, design and operation are very delicate and difficult problems in engineering practice. As mentioned previously, one of the major problems encountered is the presence of non-condensable gases which cause a high heat transfer resistance and reduce the condensation rates. Therefore, a common requirement for all types of condensers is that of venting even when a small amount of non-condensable gas is present as it tends to accumulate with time rendering the condenser surface ineffective. It is recommended to locate the venting in the areas where non-condensable gases accumulate.

2.4.4 Condenser Selection and Condenser Concept Development

The condenser in the greenhouse desalination system constitutes the most critical component. For the greenhouse to be cost-effective the condenser has to be effective, simple, cheap, and low in maintenance. Except for the direct contact condensers the above requirements are too stringent conditions to be met by a single condenser type. Therefore, the search for condenser configuration that meets these requirements is justified. A simple condenser is shown in Figure 2.8 which, in principle, has the potential of meeting all the above requirements. It consists of two pipes spaced a certain distance and wrapped with a single sheet of very thin plastic. The top pipe termed the *header pipe* is perforated on its bottom where cold water is sprayed through these perforations. Alternatively, spray nozzles may be fitted instead of perforations to render the condenser convertible to direct contact condenser by merely removing the plastic cover. The bottom pipe is termed the discharge pipe. The sheet vertical ends are wrapped around vertical support rods and glued together forming a channel over which moist air flows. Multiple spray jets of cold water exiting the header pipe through its perforations impinge on the plastic sheets causing them to vibrate. The water flows down the sheets while cooling the surfaces over which water vapor in the moist air flowing outside condenses. The cooling water falling down is discharged through the *discharge pipe* which is a plastic pipe with its upper half cut away forming an open channel inside the assembly. The discharge pipe is inclined towards the outlet (not shown). The condensate flowing down on the outside surface of the module is collected in outside channels or in the bottom of the condenser assembly. This design introduces two favourable features:

1. The vibration results in a reduction in condensate film thickness reducing the condensate thermal resistance. It may also lead to condensation of the form of rivulets leading to higher condensation rates compared with film-wise condensation.
2. Because the non-condensable air constitutes the major part of the moist air the surface compliance is believed to assist in larger mixing outside the condensate layer, thus reducing the adverse effect of non-condensables.

Testing of this condenser in this work has been conducted and showed poor performance (Al-Khalidi, 2006). Hence, it will not be considered further.

The above condenser module may be arranged in different arrangements to construct a large scale condenser. For example, the modules may be grouped in parallel arrangement and spaced a certain distance apart forming channels for the moist air flow. Another arrangement is shown in Figure 2.9 where the moist air may flow along the zigzag channels formed as shown or along the V-channels.

Another condenser type which also has the potential in meeting the above requirements is the plate channel condenser (see Figure 2.10). This condenser has been used in solar desalination based on humidification-dehumidification technique (Müller-Holst, 2001).

Each module of the condenser consists of a plastic channel with dividers designed to create smaller channels and to give structural rigidity. This condenser has been chosen in this work and tested. The results are presented in Section 5. It is worth noting that the condenser module shown in Figure 2.10 may be arranged in a similar manner to that shown in Figure 2.9 forcing the air flow through a maze.

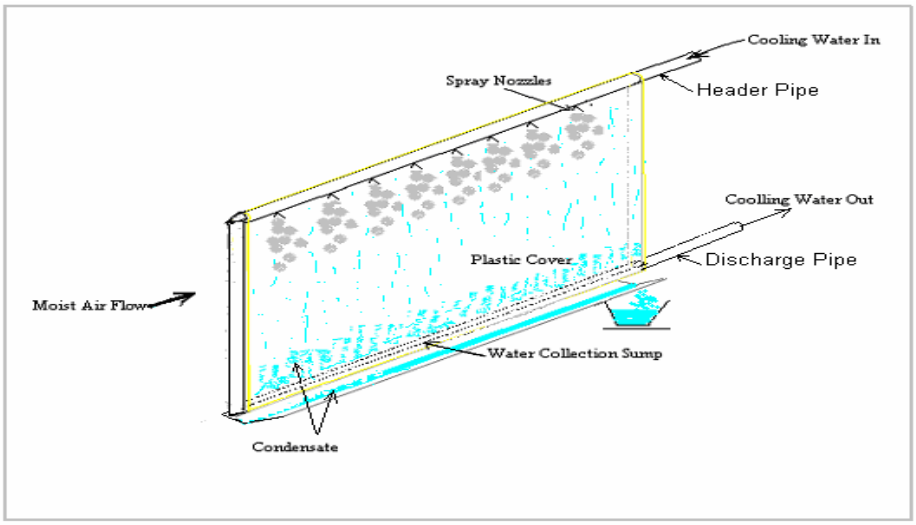

Figure 2.8: A schematic of a new condenser module

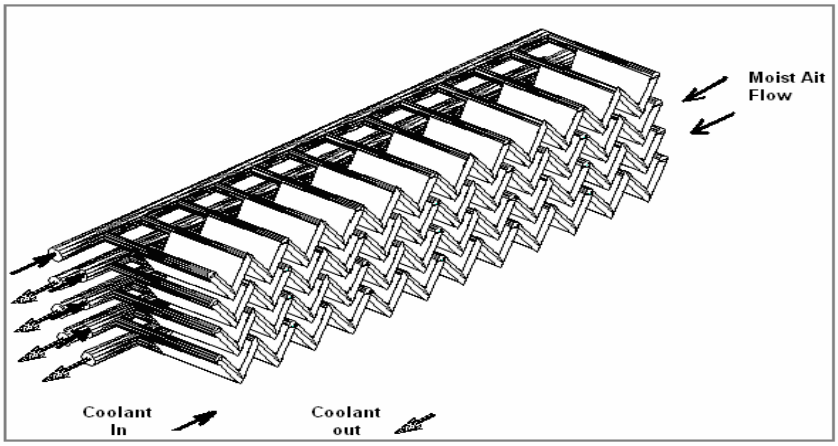

Figure 2.9: Schematics of the new condenser

The third candidate is the *direct contact* condenser which also satisfies the above requirements in the sense that it is simple, inexpensive, and has a very high heat transfer rate per unit volume (see Table 2.2). Furthermore, it is not susceptible to fouling as encountered in tubular or channel condensers. Sub-cooled liquid is sprayed into a vessel through which the condensing vapor is injected. In greenhouse application both the coolant and the condensing vapor are water and thus no separation is required if pure water is used as coolant instead of the seawater. This may be accomplished in the manner shown in Figure 2.11 where sub-cooled water is sprayed co-currently with the moist air.

Condensate is collected at the bottom where a constant level is maintained by gravity withdrawal. A certain volume of the condensate is circulated through a single phase heat exchanger where it is cooled by a coolant (for example, deep cool seawater) to temperatures below the saturation temperature of the vapor phase. This arrangement requires a single phase heat exchanger which is an added cost. However, it can accommodate solar-energy-driven absorption refrigeration that generates chilled water for cooling the circulated condensate. The important design factors in direct contact condensers are the atomization characteristics of the nozzles, i.e., droplet size, distribution, and coalescence, gas flow pattern and nozzle pressure drop.

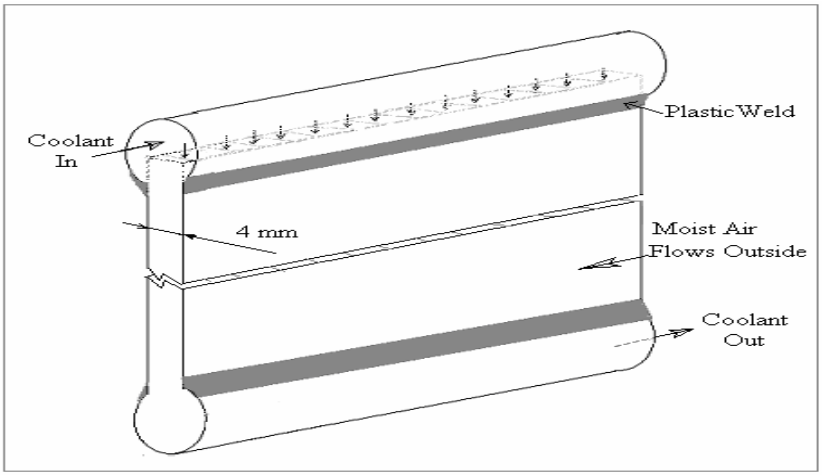

Figure 2.10: A schematic of the plate channel condenser module

This condenser has not been chosen for study in this project. However, it is recommended for future study.

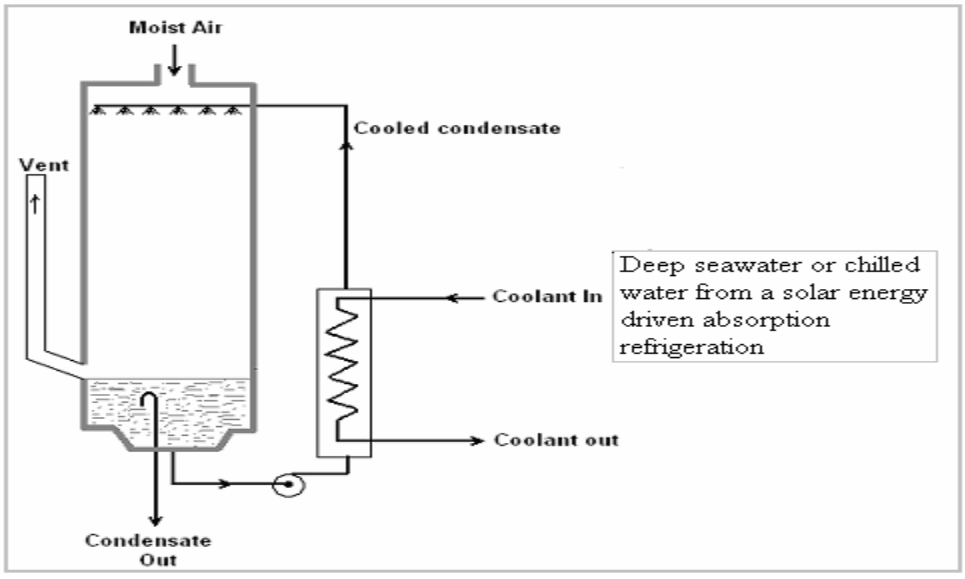

Figure 2.11: Direct contact spray condenser using condensate as the coolant

3. THEORETICAL ANALYSIS OF POSSIBLE METHODS TO COOL THE CONDENSER OF SEAWATER GREENHOUSES

3.1 Overview on the Possible Condenser Cooling Techniques

Dehumidification by cooling the moist (humidified) air is the key to a successful application of the seawater greenhouse (SWGH) desalination. Figure 3.1 is a block diagram presenting a general overview on the possible solutions to remove the heat of condensation from the moist air leaving the second evaporator of the greenhouse in a condenser. Two groups of solutions can be identified which are characterized by the medium which receives the heat of condensation (the condenser coolant). These two mediums are **air** and **water**. The different possibilities for the two coolants related to SWGH are ambient air, cooled air, fresh water, surface or deep seawater. The latter can be directly used as a condenser coolant while the former media may need to be cooled either by evaporative cooling or by a cooling machine.

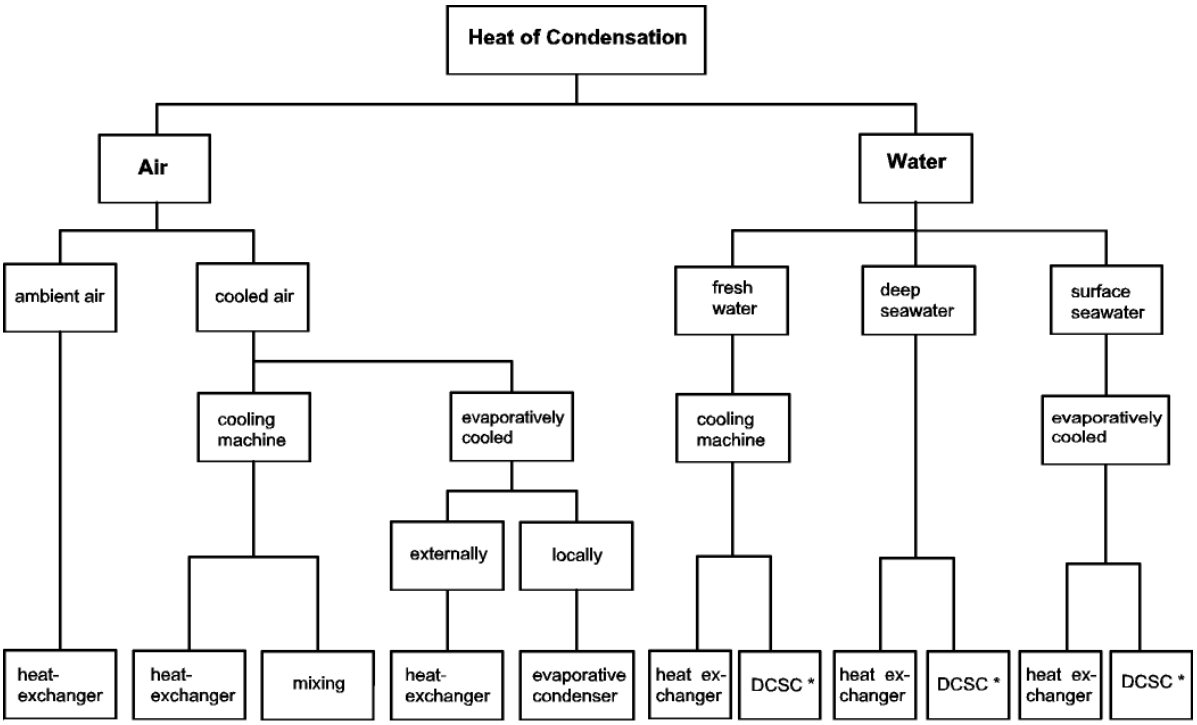

Figure 3.1: A general overview on the possible solutions to remove the heat of condensation to air or water as condenser coolants

Evaporative cooling can be realized externally in a cooling tower or locally in the so-called evaporative condensers. The possible techniques to transfer the heat of condensation to the coolants are listed in the last row of blocks. These techniques include indirect heat transfer utilizing suitable heat exchangers or an evaporatively cooled condenser as well as direct heat transfer. The latter technology includes mixing the moist air stream entering the condenser with a cooled air stream by a cooling machine as well as direct contact spray condensers. These technologies and possibilities will be illustrated and their technical advantages and disadvantages will be discussed in the following sections.

3.1.1 Air as a condenser coolant

Air might be used either as ambient air or as cooled air. In the case of a SWGH (see Figure 1.1), cooling with ambient air makes no sense as the wet air entering the condenser is colder than or at least as warm as the ambient air. Cooled air can be generated either by incorporating a cooling machine or due to evaporative cooling. Applying a cooling machine to cool ambient air, which will then act as a condenser coolant, is certainly a possible technical solution. However, if a cooling machine is to be used, it is much better to generate cold water than cold air since water possesses superior heat transfer characteristics than air. Moreover, pumping a liquid is less energy consuming than pumping a gas and, therefore, the parasitic power requirements will be much lower in case of water as a condenser coolant.

With a cooling machine ambient air can be cooled down below its dew point temperature and then mixed with the wet air entering the condenser of the greenhouse. With this specific solution, both the temperature of the cold air and the ratio of the flow rates of the two air streams have to be regulated to guarantee that the state of the mixed air will always lie in the fog region. The condensate can then be separated with a mist eliminator. This solution requires a microprocessor-based predictive control, which may be an expensive option for a SWGH.

The second possibility to cool the ambient air and use it as a condenser coolant is to apply evaporative cooling. Evaporative cooling can be applied in two different ways depending on the installation site. Air might be evaporatively cooled in an external cooling tower or locally. External cooling towers are used if the space for the heat exchanger is limited and a compact structure is required. Even if air is evaporatively cooled in an external cooling tower, an air to air heat exchanger is required to cool the condenser of the greenhouse. Due to the poor heat transfer characteristics of air, it is preferred to make use of the evaporatively cooled water as a condenser coolant, which is the case in Figure 1.1.

The remaining possibility for air as a coolant is to apply the evaporative cooling concept locally by utilizing the so called evaporative condensers. Evaporatively cooled heat exchangers can achieve higher heat transfer rates than dry heat exchangers (Hasan and Siren, 2003). They have many applications in the fields of air-conditioning, refrigeration

and power plants. Heat transfer takes place between a vapour or a hot fluid flowing inside tubes and air through a water film, which is formed by spraying water (in case of SWGH seawater) onto the outer surface of the heat exchanger tubes. Figure 3.2 depicts the arrangement of such an evaporative condenser.

In the case of a seawater greenhouse, humid air from the second evaporator will enter the evaporative condenser instead of water vapor in Figure (3.2-a). A certain inclination in the condenser tubes has to be considered for the condensate to flow by gravity assistance out of the condenser. Fins on the outer surface of the tubes, over which seawater is sprayed, can enhance the overall heat transfer coefficient substantially (Hasan and Siren, 2003, Leidenfrost and Korenic, 1986, Finlay and Harris, 1984). Moreover, and as depicted in Figure 3.2.a., the same concept can be used to cool down the hot water leaving the condenser of a SWGH in a closed loop. Using this alternative has the potential to simplify the design and reduce the parasitic energy consumption in pumping. The limitations on this technology include, among others, the corrosion, fouling and contamination of the outer surface of the condenser tubes as well as, eventually, the high relative humidity of the ambient air. In the case of a greenhouse, this process of air humidification takes place already in the first and second evaporators. So adding a third humidifier may require a re-evaluation for both energy and water management concepts of the greenhouse.

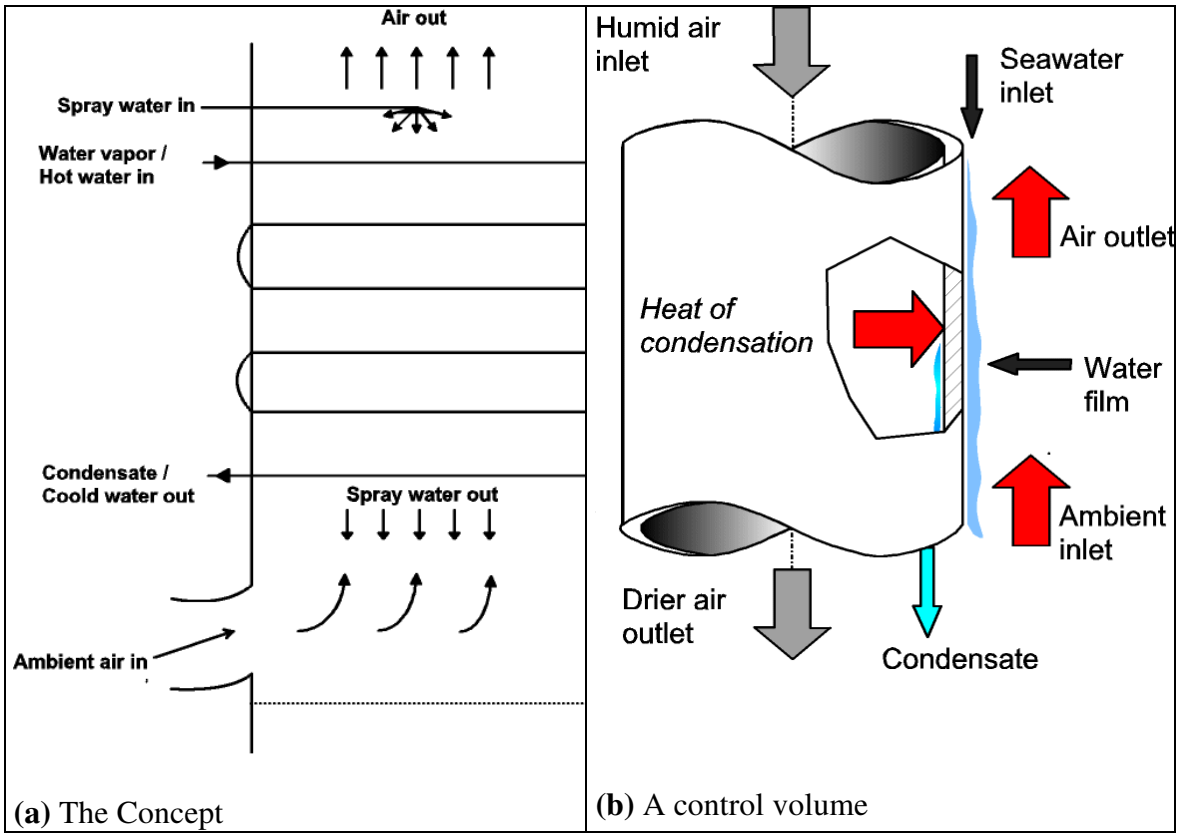

Figure 3.2: A schematic of an evaporative condenser

3.1.2 Water as a condenser coolant

Water as a condenser coolant for greenhouse applications can be ***deep*** or ***surface*** seawater. Deep seawater is cold enough to act as a condenser coolant, while surface seawater may require an evaporative cooler to decrease its temperature to a suitable range so that it may work effectively as a condenser coolant. A serious disadvantage of utilizing seawater is the high content of biological organisms, which can then be deposited on the heat transfer surfaces resulting in performance degradation of the condenser (Heldt and Schnell, 2000). This fouling problem requires a frequent cleaning for the contaminated surfaces, which means higher operating costs.

Also fresh water can be utilized as a coolant for the greenhouse condenser. However, as the greenhouse technology is developed for producing fresh water in remote areas, the utilization of fresh water as a condenser coolant has to be limited to closed loop applications. It has then to be cooled with a vapor compression or a sorption cooling machine. Sorption cooling includes both absorption and adsorption cooling. All types of cooling machines require a driving energy (electricity in case of vapor compression or heat for sorption cooling). In addition, heat must be rejected from these cooling machines, which turns us to the starting point of this work. Moreover, utilizing a cooling machine is associated with relatively high investment and operating costs. Their application seems only reasonable in case of very humid locations and requires the development of an intelligent energy management concept for the whole greenhouse.

There are two methods to transfer the heat of condensation from the humid air leaving the second evaporator of the greenhouse to the cooling water. The first method is to utilize a heat exchanger with humid air on one side and the coolant on the other side. The second methodology applies a direct heat and mass transfer between the humid air and a cooled (in an external heat exchanger) portion of the condensate in a so-called direct contact spray condenser (DCSC) which is illustrated in Figure 2.11. A DCSC is simple, inexpensive, and has a very high heat transfer rate per unit volume (Hetsroni, 1982, Pita and John, 1970). Furthermore, it is not susceptible to fouling as encountered in tubular or channel condensers. A portion of the condensate is sub-cooled in the external heat exchanger and sprayed co-currently with the humid air leaving the second evaporator of the greenhouse. Condensate is collected at the bottom where a constant level is maintained by gravity withdrawal. The coolant of the external heat exchanger can be deep or evaporatively cooled surface seawater or fresh water, which has then to be cooled with a cooling machine. The key design parameters of a DCSC are the atomization characteristics of the nozzles, i.e. droplet size, distribution, and coalescence, gas flow pattern and nozzle pressure drop.

The above discussion suggests that evaporative cooling with surface seawater seems to be the most suitable cooling technology for the greenhouse condenser. The use of deep seawater has to be judged in a case by case study based on a detailed life cycle cost analysis. For the situation, in which evaporative cooling is not an effective solution, which is the case in hot and humid locations, the use of a cooling machine is the

remaining solution. In that case the main problem, which arises, is not only the cooling of the condenser, but it has simply to do with the main function of a greenhouse to create a temperate condition for cultivating crops. The utilization of a rotating adsorption wheel similar to those of desiccant cooling systems to dehumidify the ambient air before it enters the greenhouse may be the solution. However, the temperature of the dehumidified air will increase due to the release of the heat of adsorption of water vapor onto the desiccant material. This increases the complexity of designing and controlling the process and, of course, the system costs. Accordingly, research and development efforts have to concentrate on developing an effective energy management concept for the greenhouse in hot and humid climates. The purpose of this work is to estimate the potentials and limitations of utilizing evaporative cooling for surface seawater as well as of utilizing a cooling machine and deep seawater.

3.2 Investigating the Potential of Evaporative Cooling

The temperature of surface seawater is generally colder than the ambient air temperature. However, the temperature depression of surface seawater below the ambient air varies according to the location as well as the time of the year. It is, therefore, not always possible to apply surface seawater directly for cooling the greenhouse condenser. In combination with evaporative cooling the use of surface seawater can be a sufficient solution in most of the cases.

After the work of Merkel (1925), who developed the basic theory of evaporative cooling, Berliner (1975) has described the basics of calculating and constructing different types of cooling towers. Based mainly on those two works as well as on the following investigations and the development of the Mollier's specific enthalpy-specific humidity diagram for humid air by Baehr (1961), Poppe and Rögener (1991) developed design algorithms for evaporative cooling systems.

The potential of evaporative cooling depends mainly on the relative humidity and the dry bulb temperature of the ambient air. Thus it is important to elaborate the boundary conditions under which evaporative cooling will be a suitable solution. Figure 3.3 depicts schematically the states of ambient air as well as of condenser inlet and outlet air on the specific enthalpy- water load (specific humidity) diagram (Baehr, 1961). It is assumed that the air entering the condenser has the same dry-bulb temperature of the ambient air. In the first evaporative cooler, both ambient air and surface seawater are cooled adiabatically. The change of state of the ambient air takes place on a constant enthalpy line.

The lowest temperature, which can be obtained for both air and water, is the ambient air wet-bulb temperature. A wet-bulb temperature approach of 90% is typical for media type evaporative coolers. The temperature of air and water leaving the evaporative cooler has to be lower than the temperature of air leaving the condenser by a sufficient temperature difference for the heat transfer ΔT_{HT} (Step (1) in Figure 3.3). Figure 3.3 shows also the

change of state of air over the condenser. First the condenser inlet air is cooled down to its dew-point temperature (same water load and φ = 1.0). This change of state (3) takes place without condensation. Any further temperature reduction will result in condensing freshwater from the humid air. The change of state, which is associated by condensing fresh water, is termed as the effective change of state in the condenser and the temperature difference, over which this change of state takes place is defined as the effective temperature difference ΔT_{eff} or (2) in Figure 3.3. This change of state takes place on the saturation line (φ = 1.0). The amount of condensate per kg of dry air flowing into the greenhouse (specific condensate) can be read from the h-x diagram depicted in Figure 3.3 as the difference between the water loads of air entering ($x_{c,i}$) and leaving the condenser ($x_{c,o}$). So the effective temperature difference is directly related to the amount of condensate, which can be gained from the greenhouse process. Assuming the relative humidity of air entering the condenser will remain constant and equal to 0.9, decreasing the temperature of air entering the condenser will result in shifting the condenser inlet state point downwards along the (φ = 0.9) line. This means, in other words, that the water load of air entering the condenser will decrease which results in decreasing the specific condensate. Alternatively, if the ambient air relative humidity increases, by keeping its dry-bulb temperature constant, the state of air leaving the evaporative cooler will move upwards to the right which means that the water load of air leaving the condenser will increase. Accordingly, the specific condensate will also decrease. It is obvious that the obtainable ΔT_{eff} and, hence, the specific condensate depends on the states of both ambient air and the condenser inlet air.

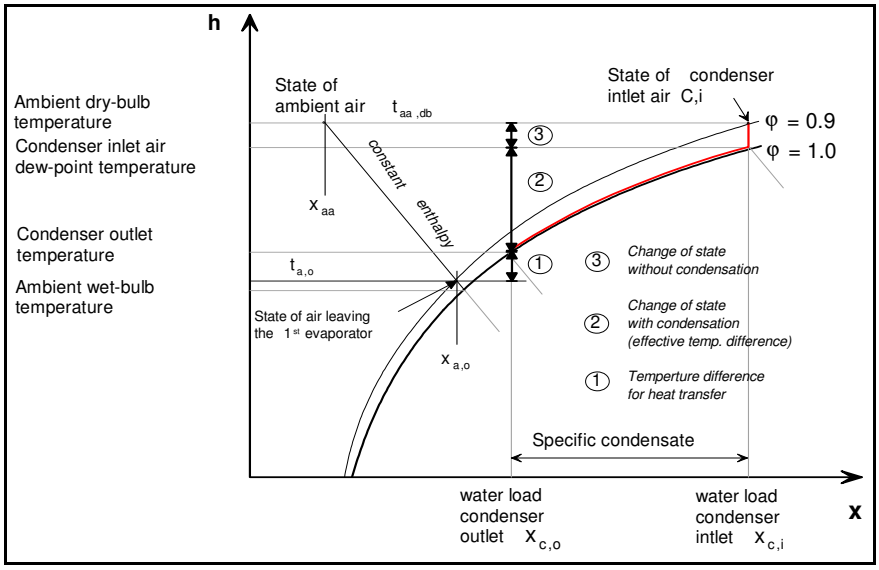

Figure 3.3: Enthalpy–water load–diagram with the states of ambient air as well as of condenser inlet and outlet air

Referring to the effectiveness (also known as the wet-bulb temperature approach) of the adiabatic evaporative cooling process as (ε) the temperature of air exiting the evaporative cooler is then:

$$t_{a,o} = t_{aa,db} - \varepsilon \cdot (t_{aa,db} - t_{aa,wb}) \tag{3.1}$$

An energy balance for the adiabatic evaporative cooler will result in the following expression for the water load of the exiting air ($x_{a,o}$) from the evaporative cooler (Lucas, 2003)

$$x_{a,o} = \frac{c_{p,a}(t_{aa,db} - t_{a,o}) + x_{aa}(c_{p,wv} \cdot t_{aa,db} + r - c_{p,lw} \cdot t_{a,o})}{c_{p,wv} \cdot t_{a,o} + r - c_{p,lw} \cdot t_{a,o}} \tag{3.2}$$

Thus, the state of air at the exit of the evaporative cooler is estimated. The mass flow rate of surface seawater $\dot{m}_{sw}$ which is evaporated and carried out by the air stream in the evaporative cooling process is then given by:

$$\dot{m}_{sw} = \dot{m}_a \cdot (x_{a,o} - x_{aa}) \tag{3.3}$$

Herein $\dot{m}_a$ represents the mass flow rate of dry air entering the greenhouse, which can be estimated according to the relation: $\dot{m}_a = \dot{V}_{aa} / v_{aa}$, where $\dot{V}_{aa}$ stands for the volume flow rate of ambient air into the greenhouse. The specific volume of humid air per kg of dry air (v_{aa}) is described by Lucas (2003) as:

$$v_{aa} = (0.287 + 0.462 \cdot x_{aa}) \cdot \frac{T_{aa}}{p_{atm}} \tag{3.4}$$

The ambient dry-bulb temperature (T_{aa}) is in K and (p_{atm}) is in kPa. The absolute water load, x_{aa} (also known as specific humidity) of air at its dry bulb temperature is, in turn, calculated using Equation (3.5) (Lucas, 2003).

$$x_{aa} = \frac{p_s(T_{aa})}{\frac{p_{atm}}{\varphi} - p_s(T_{aa})} * \frac{M_{wv}}{M_a} \tag{3.5}$$

Herein; the saturation water vapor pressure p_s is evaluated at the ambient air dry-bulb temperature using Equation (3.6) (Wagner and Pruss, 1993), p_{atm}: atmospheric pressure, φ: relative humidity, M_{wv} and M_a are the molar masses of water vapor and air, respectively. In this equation T_{aa} is in K and p_s is in kPa.

$$p_s = 22064 \cdot \exp\left\{\left(-7.76451 \cdot \left(1 - \frac{T_{aa}}{647.14}\right) + 1.45838 \cdot \left(1 - \frac{T_{aa}}{647.14}\right)^{1,5} - 2.7758 \cdot \left(1 - \frac{T_{aa}}{647.14}\right)^3 - 1.23303 \cdot \left(1 - \frac{T_{aa}}{647.14}\right)^6\right) / \left(\frac{T_{aa}}{647.14}\right)\right\} \tag{3.6}$$

Based on the above set of equations, we estimated the effect of the ambient air dry bulb temperature on the maximum allowed ambient air relative humidity to obtain certain values of ΔT_{eff} and presented the results in Figure 3.4. To obtain these results, we assumed that the temperature of air entering the condenser equals the ambient dry-bulb temperature and that its relative humidity is 90 %. Moreover, a temperature difference of 3 K is set for the heat transfer process and a wet-bulb temperature approach of 90 % for the evaporative cooling process is assumed. It can be observed, under the assumptions made here, that in order that an effective temperature difference over zero may be realized, the relative humidity of the ambient air must be lower than 66 % at an ambient dry-bulb temperature of 45 °C. As the ambient dry-bulb temperature decreases below 45 °C the maximum permitted ambient relative humidity decreases, in order that condensation may take place with an evaporatively cooled condenser. This puts the 65 % relative humidity as an upper limit for evaporative cooling to be an effective solution for cooling the condenser at an ambient dry-bulb temperature of 45 °C. The upper curve of Figure 3.4 sets the limit of the relative humidity for the given ambient dry-bulb temperatures provided that the assumed 3 K is enough for the heat transfer process. If the 3 K temperature difference is not enough for the heat transfer process in the condenser; let us say we need rather a temperature difference of 7 K and an effective temperature difference of 5 K then we have to read from the dashed curve, which is labelled with 9 in Figure 3.4. This is because this curve represents a total temperature difference of 12 K (ΔT_{eff} is 9 K and ΔT_{HT} is 3 K as a general assumption for the whole Figure). For this case the upper limit on the ambient relative humidity drops to 33% at an ambient dry-bulb temperature of 45 °C. On the same curve an ambient air relative humidity of 18% can be read as the maximum limit for an ambient air dry-bulb temperature of 30 °C. It is worth here to mention that Figure 3.4 is generally valid everywhere under the assumptions made above.

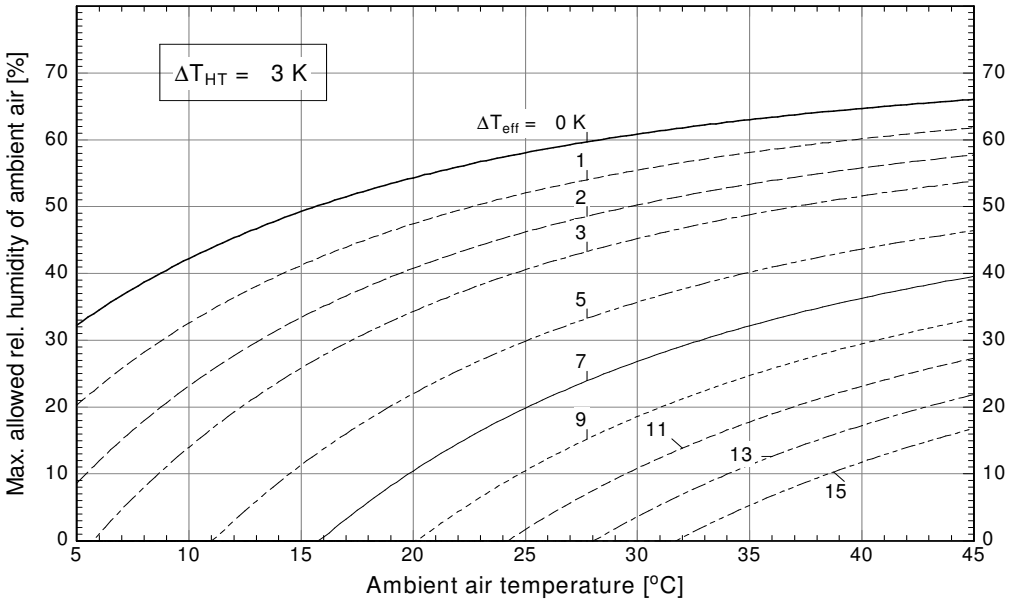

Figure 3.4: Maximum relative humidity of ambient air depending on ambient air temperature and given effective temperature difference

In order to assess the applicability of evaporative cooling as a technology for cooling the condenser of a greenhouse at a certain location, one has to construct the so called cumulative probability distribution curve for the relative humidity for each specific location, which requires a typical meteorological year data (TMY). Figure 3.5 shows such a cumulative probability distribution curve for the relative humidity for the location Marmul in Oman based on the TMY-data of Zurigat et al. (2003). Regarding the application with a greenhouse, only the diurnal data are taken into account. The diagram shows that during approximately 12 % of the daytime in one year the relative humidity is higher than 65 % and hence evaporative cooling is definitely not a viable solution over this period. In 51.5 % of the yearly daytime the relative humidity is higher than 30 %. In other words, over almost 50 % of the daytime an effective temperature difference of at maximum 10 K is possible at an ambient air dry-bulb temperature of 45 °C. This effective temperature difference drops to almost 9 K and 5 K at ambient air dry-bulb temperatures of 40 and 25 °C, respectively.

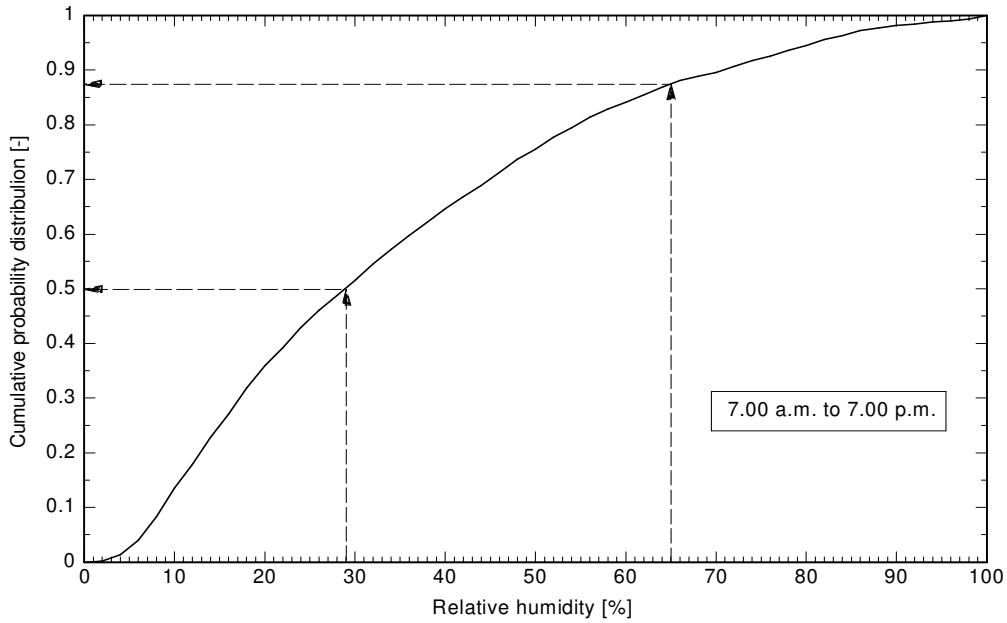

Figure 3.5: Cumulative probability distribution of diurnal relative humidity in Marmul, the Sultanate of Oman (Zurigat et al., **2003)**

To estimate the impact of evaporative cooling on the amount of freshwater condensate from the greenhouse it is advisable to divide the process into two cooling loops (Figure 3.6). The first loop comprises the first and second evaporator as well as the first condenser. The second loop contains only the second condenser and its coolant is deep seawater. The two cooling loops are interconnected by a pipe to compensate for the evaporated seawater in both evaporators and to substitute the disposed brine to reduce the salinity of the water in the first cooling loop. For the calculation of the amount of freshwater condensate that could be gathered from the first condenser as well as the amount of surface seawater, which has to be evaporated in the first evaporator, the following assumptions have been made:

1. A wet-bulb temperature approach of 90 % is assumed to calculate state (B) of air as well as state 7 of seawater leaving the 1st evaporator.
2. Water leaves the 1st evaporator at the same temperature of air at state (B).
3. There is no temperature difference between states 7 and 3 of the cooled seawater.
4. The relative humidity of air leaving the second evaporator and entering the 1st condenser amounts to 90% (State (D)).
5. The temperature difference between air leaving the 1st condenser (State (E)) and the coolant entering it (State (3)) is $\Delta T_{HT} = 5$ K.
6. The volume flow rate of the ambient air entering the greenhouse amounts to 15 m^3/s. This flow rate corresponds to an air speed of 0.2 m/s and a SWGH dimensions of (width, length, height) of (18m, 60m, 4m) (Paton, 2001; Zurigat et al., 2003; Sablani et al., 2003). The air change number amounts then to 0.2 min^{-1}.

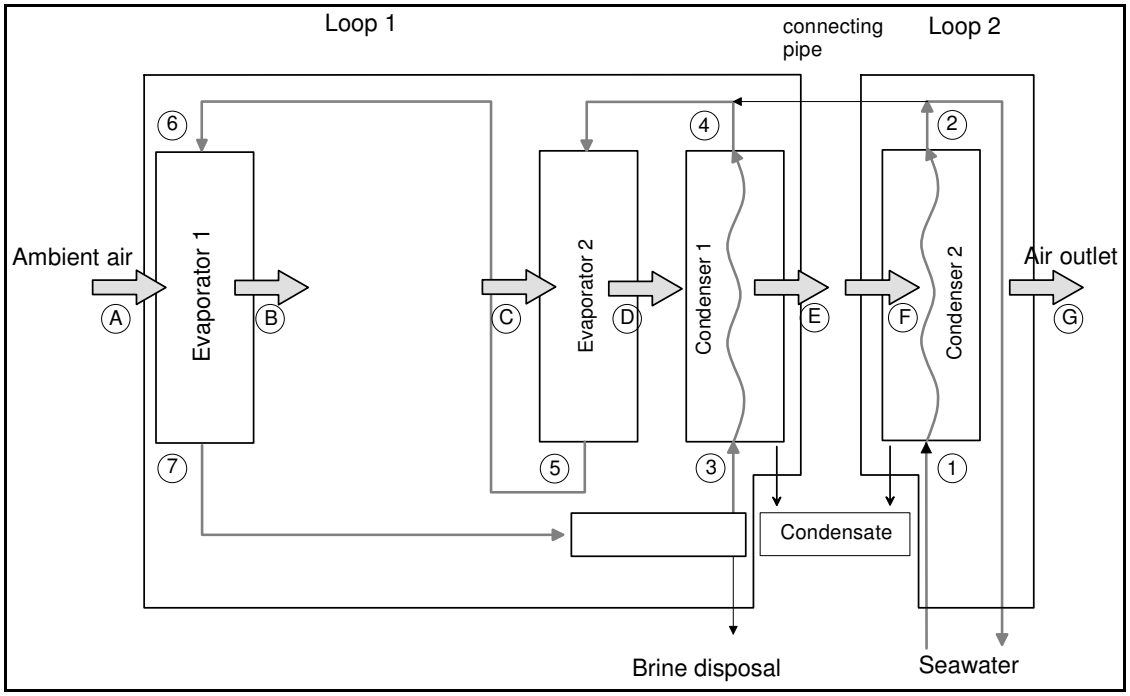

Figure 3.6: The two cooling loops of the seawater greenhouse desalination process

In order to estimate the amount of seawater to be evaporated in the 1st evaporator the set of equations 3.1-3.6 have been applied. The amount of the obtainable freshwater condensate is calculated according to the following equation:

$$\dot{m}_{fw} = \frac{\dot{V}_{aa}}{v_{aa}} \cdot (x_{c,i} - x_{c,o}) \qquad (3.7)$$

Figures 3.7-3.10 present the results of these estimations for ambient dry-bulb temperatures in the range of 25 to 40 °C with a 5°C step. These Figures show the effect of the relative humidity of the ambient air on both the rate of freshwater condensate and the rate of seawater evaporation at different condenser inlet air temperatures. In each

Figure the maximum temperature of air entering the 1st condenser is set equal to the ambient dry-bulb temperature. As the ambient dry-bulb temperature and the wet-bulb temperature approach are fixed for each Figure, the rate of seawater evaporation depends only on the ambient relative humidity.

So at an ambient dry-bulb temperature of 25 °C (Figure 3.7) the rate of seawater evaporation increases almost linearly from 0 to 1160 kg/h as the relative humidity of the ambient air decreases from 100 to 0 %. As the ambient temperature increases (Figures 3.8-3.10) the rate of seawater evaporation increases as the capability of air to be wetted with water vapor increases with its temperature. Most important is the effect of the relative humidity on the rate of freshwater condensate at the different tested ambient temperatures. In Figure 3.7, we can simply observe the limitation on evaporative cooling as a technology for cooling the greenhouse condenser at the ambient dry-bulb temperature of 25 °C. In case the condenser inlet air temperature equals 20 °C the maximum ambient relative humidity, under which a freshwater condensate gain is possible, amounts to 20 %. As the relative humidity decreases below this limit the amount of freshwater condensate increases almost linearly. This relative humidity limit increases to 46 % in case the temperature of air entering the condenser increases to 25 °C (see Figure 3.7).

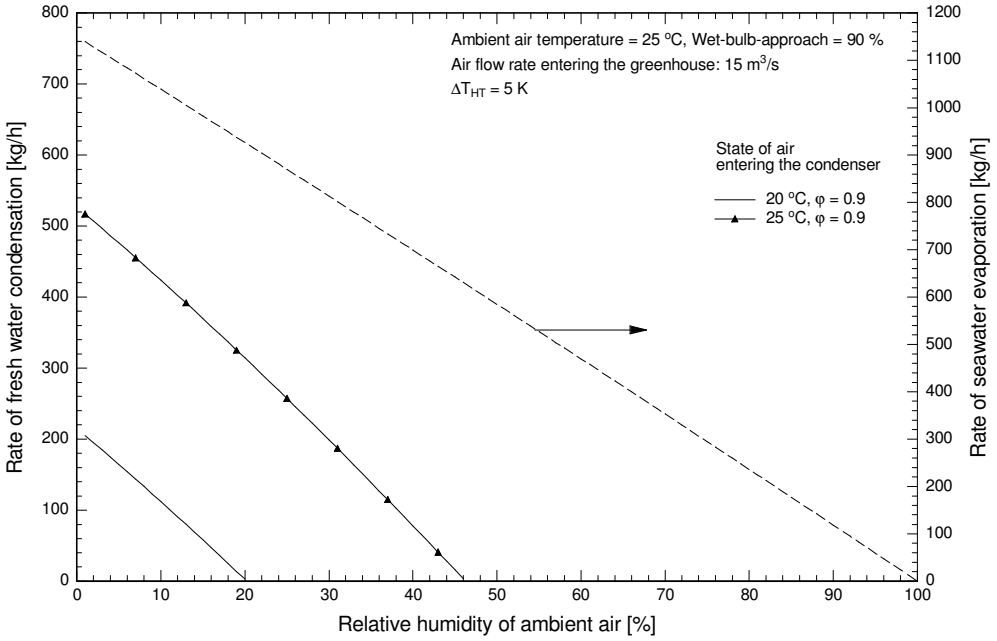

Figure 3.7: Effect of the ambient air relative humidity on the rates of the obtainable freshwater condensation and the required seawater evaporation at an ambient air dry-bulb temperature of 25 °C

In Figure 3.8 the ambient dry-bulb temperature amounts to 30 °C. Under this condition, if the condenser inlet air temperature amounts to 25 °C, the maximum ambient air relative humidity, beyond which fresh water condensation is possible, is 27 %. This limit increases to almost 50 % if the condenser inlet air temperature increases to 30 °C.

Now comparing the curves of the 25 °C condenser inlet air temperatures between Figures 3.7 and 3.8, one can observe that the ambient relative humidity limit decreases from 46 % in Figure 3.7 down to 27 % in Figure 3.8. With the same wet-bulb temperature approach, the obtainable air and water temperatures at the exit of the evaporative cooler decreases as the ambient temperature decreases. As the temperature of the cooling water (states 7 or 3 in Figure 3.6) is the dominant factor in the operation of the condenser, the relative humidity of the ambient air can increase at lower ambient dry-bulb temperatures and freshwater condensation is still possible. Accordingly, the rate of freshwater condensation is higher for lower ambient dry bulb temperatures at the same ambient air relative humidity.

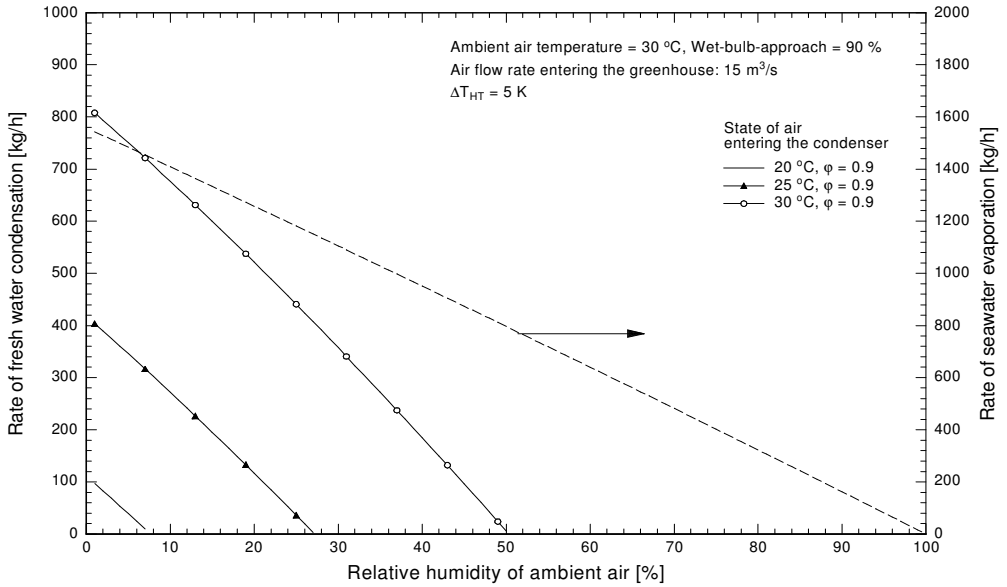

Figure 3.8: Effect of the ambient air relative humidity on the rates of the obtainable freshwater condensation and the required seawater evaporation at an ambient air dry-bulb temperature of 30 °C

In Figures 3.9 and 3.10 the ambient air dry-bulb temperature amounts to 35 and 40 °C. The relative humidity limit, below which fresh water condensation is possible, increases from 32% to 53 % as the condenser inlet air temperature increases from 30 °C to 35 °C, respectively, at an ambient air temperature of 35 °C. Figure 3.10 shows that at an ambient air temperature of 40 °C these limits on the ambient air relative humidity drop to 20 % and 36 %, respectively, as the condenser inlet temperature increases from 30 °C to 35 °C.

Furthermore, it can be observed from Figures 3.7-3.10 that the amount of freshwater condensate increases as the condenser inlet air temperature increases. This could be simply explained with the fact that the higher the air temperature the higher it's specific humidity, at the same value of the relative humidity (90% as per assumption 4 above). Figure 3.11 summarizes the effect of the ambient air dry-bulb temperature as well as its relative humidity on the rate of fresh water production for a condenser inlet air temperature of 25 °C.

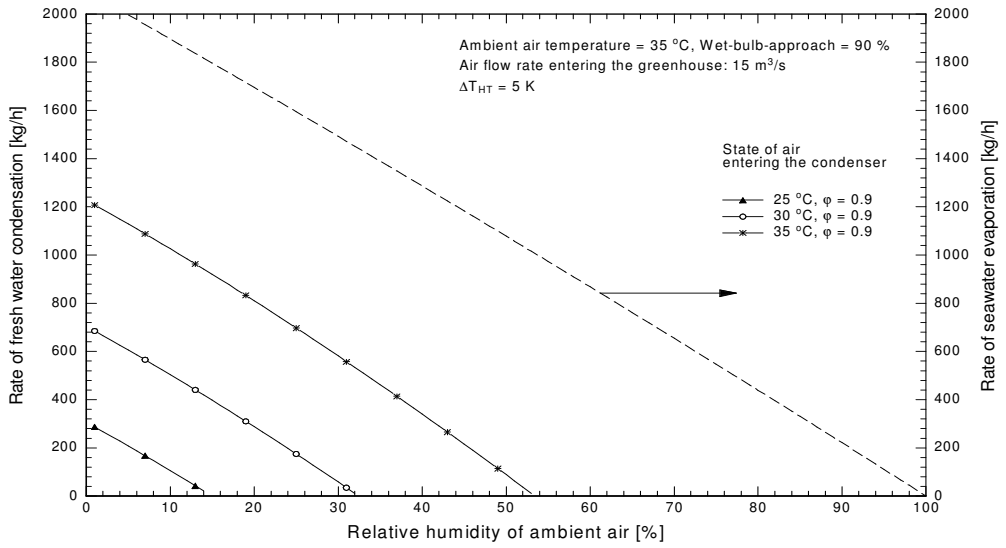

Figure 3.9: Effect of the ambient air relative humidity on the rates of the obtainable freshwater condensation and the required seawater evaporation at an ambient air dry-bulb temperature of 35 °C

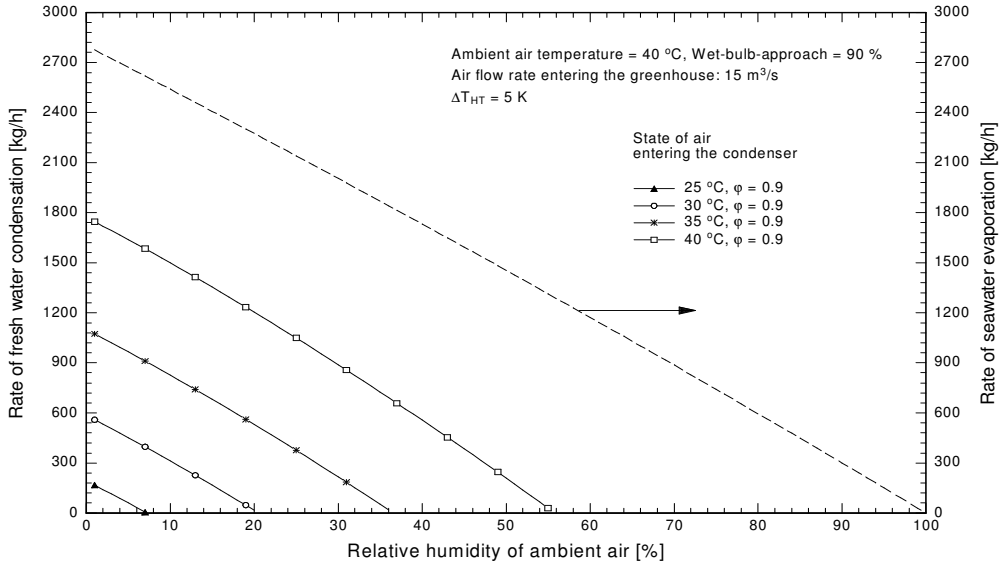

Figure 3.10: Effect of the ambient air relative humidity on the rates of the obtainable freshwater condensation and the required seawater evaporation at an ambient air dry-bulb temperature of 40 °C

It is clear from Figure 3.11 that the freshwater production rate decreases as the ambient air relative humidity increases for each ambient air dry-bulb temperature. As the state of air entering the condenser is fixed, the amount of condensate depends mainly on the temperature of the condenser coolant. The latter depends, for a fixed ambient air relative humidity, on the ambient air dry-bulb temperature ($t_{aa,db}$) and decreases as $t_{aa,db}$ decreases. This explains the enhancement in the fresh water production rate with the decrease in $t_{aa,db}$ at fixed ambient air relative humidities.

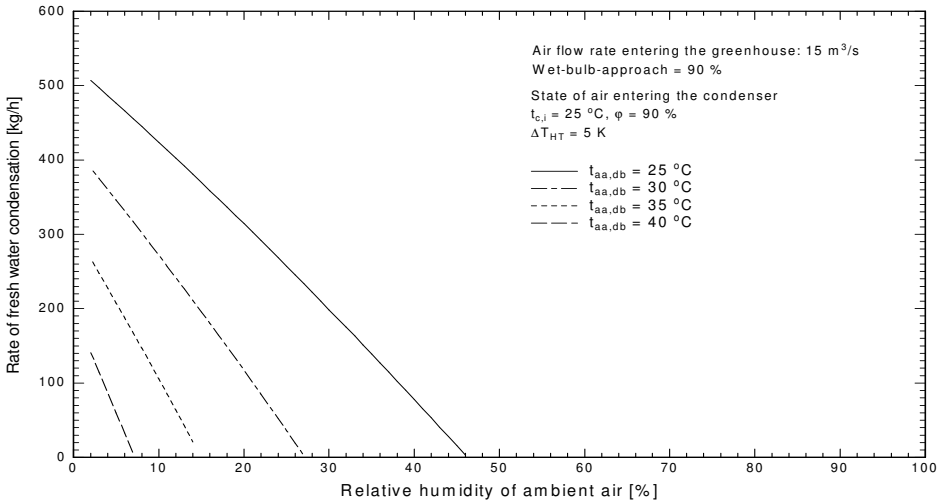

Figure 3.11: Effect of the ambient air dry-bulb temperature as well as the ambient air relative humidity on the rate of fresh water production at a condenser inlet air temperature of 25 °C

Recalling that the purpose of a greenhouse is not only to produce freshwater but also to create a more temperate climate for cultivating the crops, it is highly recommended from the above analysis to enhance the temperature of air as it passes through the 2nd humidifier. This is partially done in Figure 3.6 by introducing a portion of the heated condenser cooling water (state 2) to humidify the air in the 2nd evaporator (state 4 in Figure 3.6). Another possibility is already suggested by Davies and Paton (2004) by introducing heating channels for seawater in the intermediate roof between the planting zone and the roof zone of the greenhouse. The function of these channels is to heat up the seawater and use it to humidify the air leaving the greenhouse canopy in the 2nd evaporator. In the original work of Paton (2001) a circulation of air between the two zones has been suggested as illustrated in Figure 3.12.

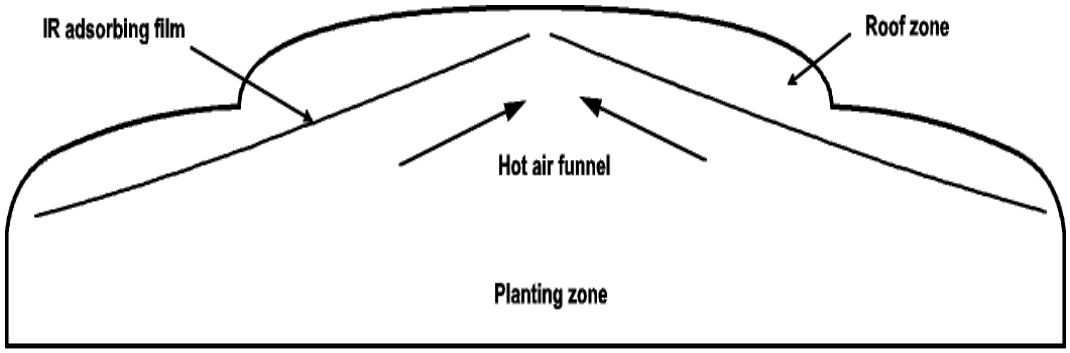

Figure 3.12: Cross section in the original SWGH design (Paton, 2001)

From the thermodynamic point of view heating the air is more effective than heating the water for obtaining higher air temperatures at the exit of an adiabatic humidifier.

Accordingly, it is suggested to seal the roof zone and use it as an air collector to heat up a portion of the greenhouse air flow rate. An extra zone has to be added after the canopy to mix this heated air with the air leaving the planting zone before the mixed air then flows to the 2nd evaporator. Besides, it is recommend to have a hybrid collector (air and water) in the roof zone, as depicted in Figure 3.13. Moreover, the mixing zone itself can be designed as an air or a hybrid collector to further heat up both air streams as well as the seawater stream leaving the greenhouse before entering the 2nd evaporator. These modifications will definitely enhance the thermal performance of the greenhouse and increase its freshwater production. Of course the number of collector elements, size of each element and the construction material must be optimized regarding the parasitic power needed as well as the life time. This will be the subject of a future study by the authors.

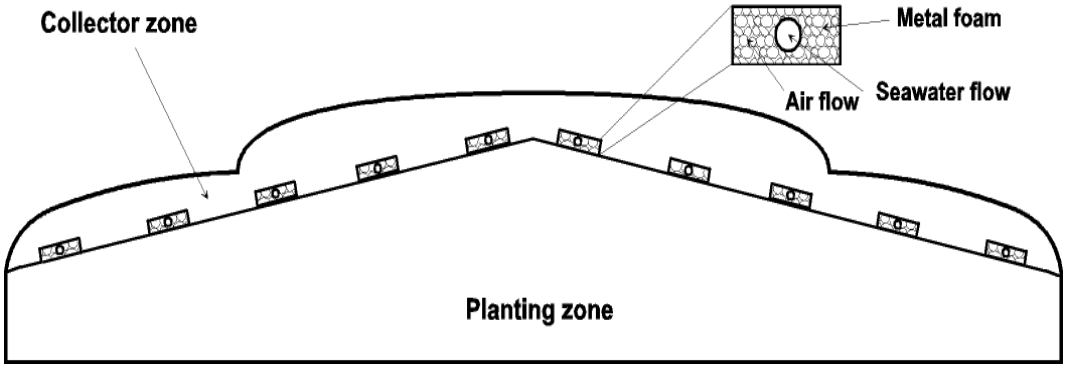

Figure 3.13: A schematic presentation of the recommended hybrid collector in the roof zone of SWGH

However, as seen from the above results, there are restricted limitations on the ambient relative humidity in order to achieve freshwater production with evaporative cooling as a condenser cooling technique. It is, therefore, the purpose of the next section to estimate the required cooling capacities of condenser cooling machines as well as the corresponding flow rates of deep seawater, in case of hot and humid climates.

3.3 Estimating the Condenser Cooling Load and the Equivalent Flow Rate of Deep Seawater

In case there is no cooling potential by evaporative cooling due to hot and humid climates, the application of a cooling machine for the first condenser is one solution. Alternatively, the 1st condenser may be cooled with deep seawater. It is, therefore, the purpose of this section is to estimate the cooling capacity of such a cooling machine and also to estimate the equivalent rate of deep sea water, if it has to be used instead. An energy balance around the 1st condenser which is depicted schematically in Figure 3.14 results in the following equation for the condenser cooling load ($\dot{Q}_c$) (Lucas, 2003).

$$\dot{Q}_c = \frac{\dot{V}_{aa}}{v_{aa}} \cdot [c_{p,a} \cdot (t_{c,i} - t_{c,o}) + x_{c,i} \cdot (c_{p,wv} \cdot t_{c,i} + r) - x_{c,o} \cdot (c_{p,wv} \cdot t_{c,o} + r) - (x_{c,i} - x_{c,o}) \cdot c_{p,lw} \cdot t_{c,o}] \quad (3.8)$$

Herein c_p stands for the specific heat capacity, x for the air specific humidity and t for the temperatures (in °C). The latent heat of vaporization of water at 0 °C is termed as r and taken as 2500 kJ/kg. If this cooling capacity is to be removed by deep seawater, the following expression can be used.

$$\dot{Q}_c = \dot{m}_{dsw} \cdot c_{p,dsw} \cdot (t_{dsw,i} - t_{dsw,o}) \quad (3.9)$$

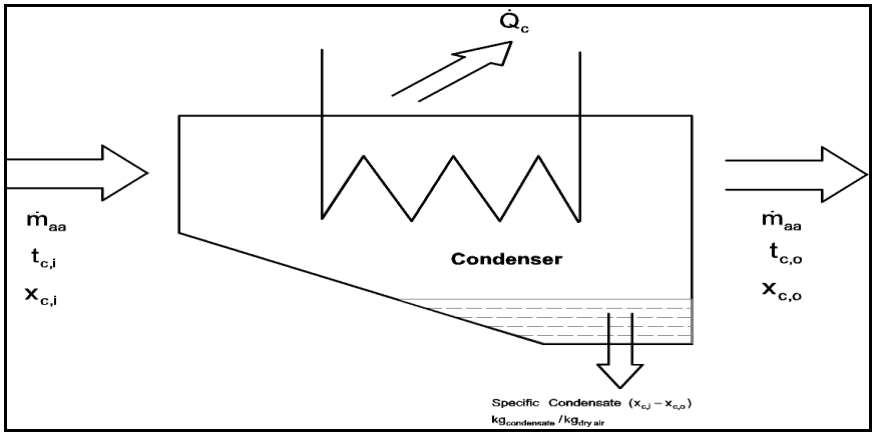

Figure 3.14: A schematic presentation for the 1st condenser of a SWGH

In order to estimate the rate of deep seawater $\dot{m}_{dsw}$, which is required to remove the cooling capacity $\dot{Q}_c$ calculated by equation 3.8, it has been assumed that the specific heat of deep seawater equals that of freshwater (4.186 kJ/(kg.K)). A typical temperature difference of 10 K has been assumed between the inlet and outlet of deep seawater. The density of the ambient air has been assumed constant and amounts to 1.16 kg/m^3 (Lucas, 2003). The rate of ambient air flow into the greenhouse has been fixed to 15 m^3/s (Paton, 2001, Sablani et al, 2003, Davis et al, 2004). Moreover, the relative humidity of the condenser inlet air has been set to 90 %.

Figure 3.15 illustrates the estimated rate of freshwater condensation as well as the cooling load of the required cooling machine at different condenser inlet air temperature as a function of the temperature of air leaving the condenser. The intersection of the rate of condensation lines with the x-axis correspond to the dew-point temperature of air entering the condenser. As the temperature of air leaving the condenser decreases below its dew-point temperature, the rate of condensation starts to increase above zero. It is evident that the cooling load increases with the temperature of air leaving the condenser.

The equivalent values of deep seawater flow rates for the condenser cooling capacities under the assumptions made above are depicted in Figure 3.16 along with the rates of freshwater condensate. In order to cool the condenser inlet air from 35 to 25°C, a cooling capacity of 0.74 MW is required for the cooling machine to produce 0.8 tons/h of freshwater (see here Figure 3.15). To produce the same amount of freshwater by applying deep seawater to cool the 1st condenser, a deep seawater flow rate of 62.5 tons/h is required as can be read from Figure 3.16.

Most cooling machines are accompanied with heat rejection. A vapour compression cooling machine, which has a **c**oefficient **o**f **p**erformance (COP) of 3.5 will produce 3.5 kW cooling capacity for each kW of electrical energy. A simple energy balance shows that this machine has to reject 4.5 kW to the atmosphere, which means a rate of heat rejection of 1.3 kW per kW cooling they offer. The situation is worse with sorption cooling machines. Both adsorption and single-stage absorption cooling machines may reach a COP of 0.6. These machines have the merit of being heat driven, which can be an advantage to utilize solar energy as a driving energy. However, the rate of heat rejection with such machines amounts to 2.3 kW per each kW cooling produced for the given COP of 0.6.

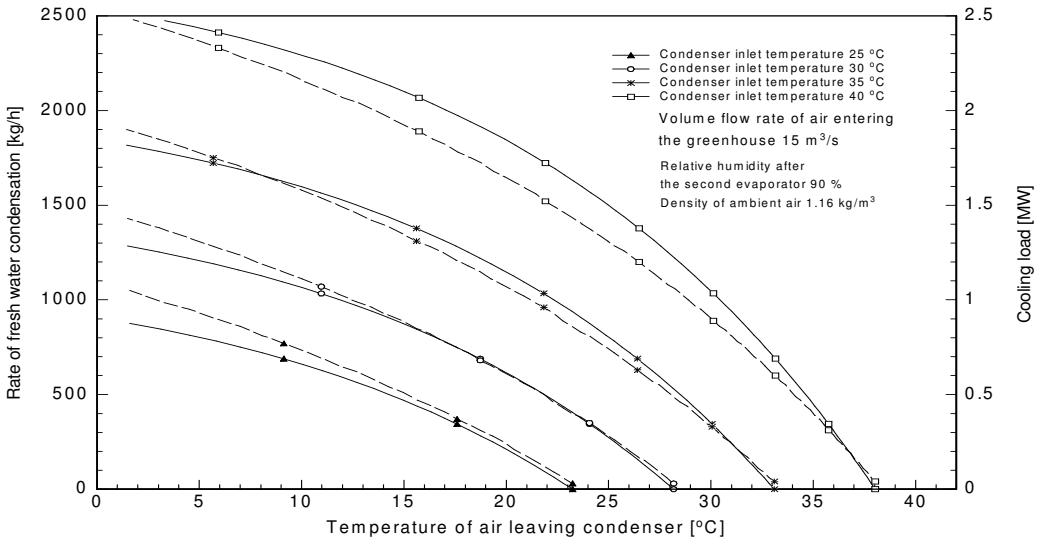

Figure 3.15: Amount of condensate (solid lines) and cooling load (dashed lines) versus condenser outlet temperature

The idea to utilize a cooling machine instead of evaporative cooling was due to the high relative humidity of the ambient air, which means that there is no potential for evaporative cooling. This potential is now highly required to reject the heat of condensation from vapour compression cooling machines and both heats of condensation and sorption from the sorption cooling machines. The above results suggest that the choice of introducing a cooling machine needs a careful life cycle cost analysis for the desalination greenhouse. A summary of the results for the cases considered in this study is given in Table 3.1.

Table 3.1: Results summary

Cooling Medium/Cooling Technique	Result or Conclusion
1. Ambient air/None (as is)	Not possible as the ambient air is warmer or as warm as the moist air entering the condenser
2.Cooled air	Generally, cooling air as a condenser coolant is less efficient than cooling water.
• Cooling machine	Aside from the high investment and operating costs any efficient cooling machine may rather cool water, instead of air which can be used directly to cool the condenser.
• Evaporative cooling (a) External	Additional equipment will be needed (cooling tower) making it an expensive option. Needs fans and blowers. High investment and operating costs.
(b) Evaporative Condenser	Adding a third evaporative cooler increases the complexity of the greenhouse system in addition to the limitation imposed by the ambient air conditions, i.e., relative humidity and temperature.
2. Fresh water/ cooling machine	Used in a closed loop system. Condenser may be of direct or non-direct contact type. A cooling machine is required.
3. Surface seawater/evaporative cooling	The most convenient. Works subject to the conditions that ambient relative humidity be between 54 and 40% for corresponding ambient air dry bulb temperatures between 45 and 25^{o}C. Fouling problems may exist.
4. Deep seawater/None (as is)	Deep seawater flow rates were estimated based on 10K seawater temperature rise across the condenser. As with surface seawater fouling problems may exit.

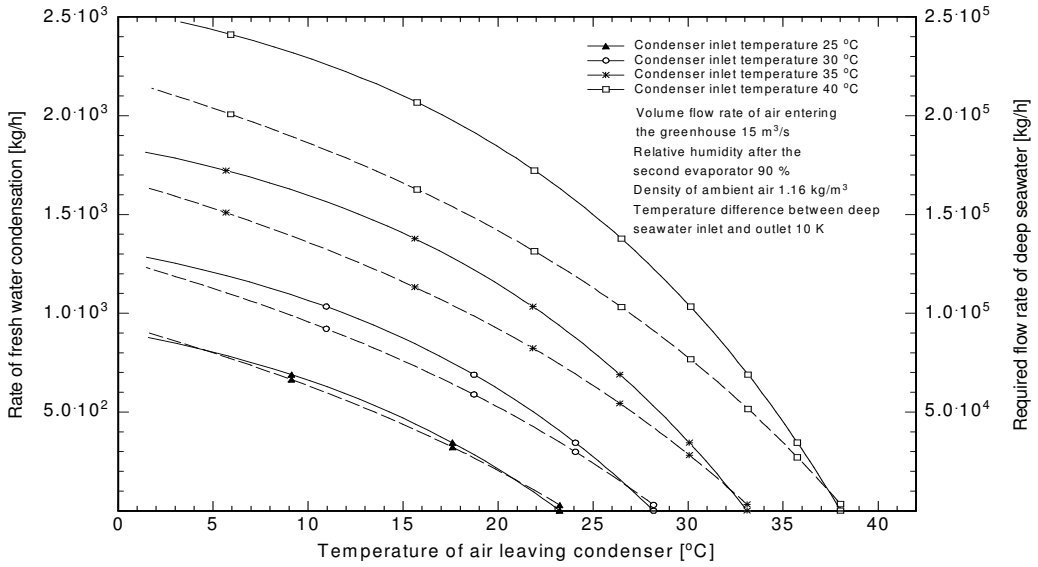

Figure 3.16: Amount of condensate (solid lines) and the required rate of deep seawater flow (dashed lines) for various condenser inlet and outlet temperatures

3.4 Summary and Conclusions

In this section an overview on the possible cooling technologies of the condenser of a seawater greenhouse desalination technique has been given. The possibilities to cool the cooling water of such condenser are to apply evaporative cooling for surface seawater, to make use of a cooling machine, or to utilize deep seawater as a condenser coolant. Applying evaporative cooling reveals that there is a limitation on the relative humidity of the ambient air which depends on the ambient air dry-bulb temperature. Considering a 6 K temperature difference between the moist air and the evaporatively cooled surface seawater, for the heat transfer process in the condenser of a SWGH, the fresh water production starts at ambient air relative humidities below 54 % for an ambient air dry-bulb temperature of 45 °C. This limit on the ambient air relative humidity decreases to 48 % and 40 % for the ambient air dry-bulb temperatures of 35 and 25 °C, respectively, at the same temperature difference for the condenser heat transfer process. These limits have been obtained by assuming that the moist air entering the condenser attains a relative humidity of 90 % and a temperature, which equals the ambient air dry-bulb temperature. Besides, a 90 % wet-bulb approach has been assumed for the evaporative cooling process. A measure to permit applying evaporative cooling for a wider range of ambient relative humidities is to increase the temperature of air entering the condenser. A modification on SWGH design in order to realize this option has been recommended. The roof zone of the greenhouse has to be sealed and an air collector or a hybrid (air-water) collector has to be integrated into it. After the canopy, an additional zone has to be constructed for mixing the so heated air in the roof zone with the air leaving the planting zone. The heated seawater in such a hybrid collector will then be used to humidify the mixed air before entering the 1st condenser. Moreover, the mixing zone can be designed

as a hybrid collector in order to further enhance the freshwater production rate of SWGHs.

In case deep seawater is used to cool the 1st condenser both the cooling capacities of cooling machines and the rate of deep seawater flow have been estimated for different condenser inlet and outlet temperatures. A cooling capacity in the order of 1 MW is required for an air flow rate of 15 m^3/s entering the SWGH. A deep seawater flow rate of about 100 tons/h will be sufficient to remove the same cooling capacity, despite the fouling problem, which will be encountered. Both cooling capacity and the corresponding deep seawater flow rate are directly proportional to the air volume flow rate. A life-cycle cost analysis seems a must in the last two cases. Moreover, alternative solutions for hot and humid climates have to be worked out with, for example, applying rotating desiccant wheels or liquid desiccant systems to dehumidify the entering air to the greenhouse. The heat of sorption, which has then to be removed, can be utilized to heat the air stream before it flows into the 2nd evaporator. These ideas are in phase with our recommendation to apply an air or a hybrid collector in the roof zone; namely to increase the temperature of air entering the condenser to enhance the freshwater production of seawater greenhouses.

4. MATHEMATICAL MODEL OF GREENHOUSE DESALINATION INTEGRATED SYSTEM

4.1. The Proposed System

An open air, open water desalination-greenhouse integrated system is considered for modeling. Solar energy and deep cold sea water are used as the driving force for the system. The system consists of the following main modules, Figure 4.1.

1. The main evaporator
2. The greenhouse
3. The secondary evaporator
4. The condenser

Atmospheric air is drawn through the evaporator (1), comes out saturated at T2 (the first humidification process). As the air passes the greenhouse it will be heated to a higher temperature due to solar heating effect. This will increase its water carrying capability. Passing this air into the secondary evaporator will allow the air to be saturated with more water (the second humidification process). The water contents of the air then will be extracted in the following condenser (the dehumidification process). The condensate will be collected at the bottom of the condenser as fresh water.

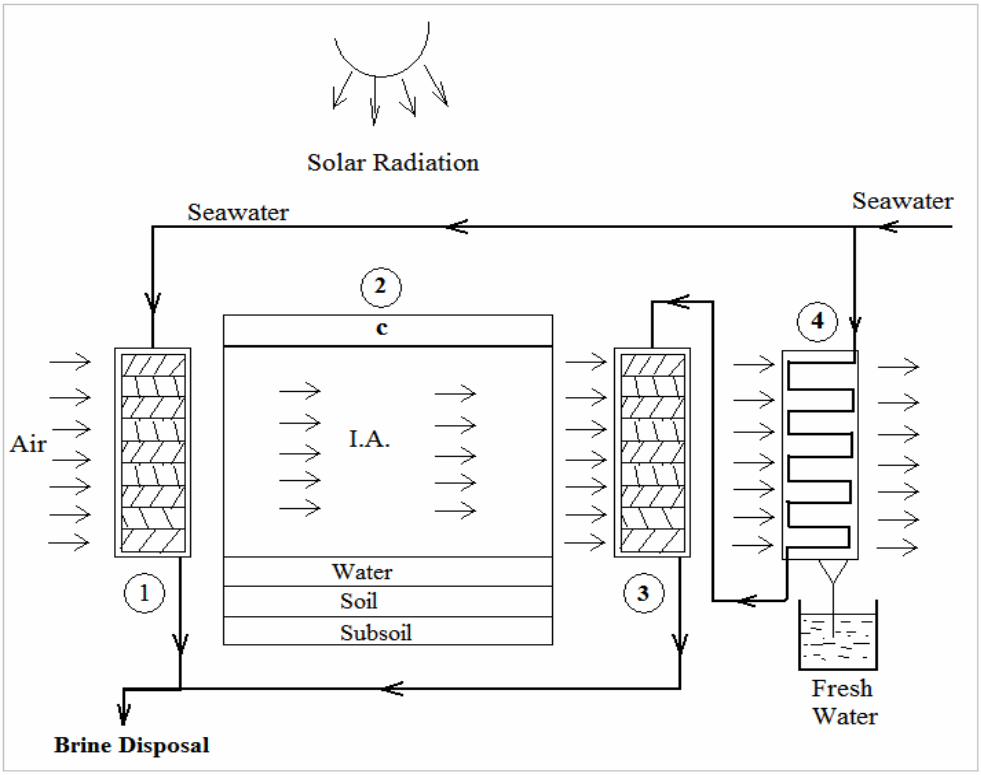

Figure 4.1: Schematics of greenhouse elements

4.2 Modeling

1. The evaporators will be treated as a cooling tower
2. The condenser will be treated as an air/water heat exchanger
3. The greenhouse will be treated as an air open / water open solar still system

4.2.1 Evaporators

$$M_w C_{pw}(T_{wi}-T_{wo}) - 0.5U_{loss} A_{cond} [0.5(T_{ai} + T_{ao})-T_{amb}] = M_a(H_{ao} - H_{ai}) \quad (4.1)$$

$$M_a(H_{ao}-H_{ai}) = KSV [\{(H_{wi}-H_{a2})-(H_{wo} - H_{a1})\}/Ln\{(H_{wi} - H_{a2})/(H_{wo} - H_{a1})\}] \quad (4.2)$$

4.2.2 Condenser

$$M_w C_{pw} (T_{wo} - T_{wi}) + 0.5 U_{loss} A_{evp} [0.5 (T_{a1} + T_{a2}) - T_{amb}] = M_a (H_{a2} - H_{a1}) \quad (4.3)$$

$$M_w C_{pw}(T_{wo}-T_{wi})=U_{cond} A_{cond} [\{(T_{ai}-T_{wo})-(T_{ao}-T_{wi})\}/ln\{(T_{ai}-T_{wo})/(T_{ao}-T_{wi})\}] \quad (4.4)$$

where
T_{wi}, T_{wo} the inlet and outlet temperature of water to condenser or evaporator
T_{ai}, T_{ao} the inlet and outlet temperature of water to condenser or evaporator
H_{ai}, H_{ao} the inlet and outlet enthalpy of air to evaporator
M_w mass flow rate of water
M_a mass flow rate of air
U heat loss coefficient
A total area exposed to ambient
K mass transfer coefficient in the humidifier
V volume of the humidifier
S humidifier surface area per unit volume

The enthalpy and humidity of the saturated air can be calculated using the correlations of Stoeckers and Jones (1982)

$$H = 0.0058 T^3 - 0.497 T^2 + 19.87 T - 207.61 \quad (4.5)$$

$$W = 2.19 \times 10^{-6} T^3 - 1.85 \times 10^{-4} T^2 + 7.06 \times 10^{-3} T - 0.077 \quad (4.6)$$

H in J/kg, and W in kgH_2O/kg-dry air, and T in C^o.

Assuming a humidifier as a typical cooling tower with wooden slats packing, the mass transfer coefficient, Nawayseh et al. (1997), can be calculated using the following correlations:
Natural draft $1 < M_w / M_a < 8$

$$K S V / L = 1.19 (M_w / M_a)^{-0.66} \quad (4.7)$$

Forced draft $0.1 < M_w / M_a < 2$

$$K\ S\ V / L = 0.52\ (M_w / M_a)^{-0.16} \quad (4.8)$$

To utilize the latent heat of the condensation of water to maximum, the condenser surface area must be very large. The non-condensable air effect is the most affecting the condenser heat transfer coefficient. Following Bell and Ghaly (1973), h_c, the condenser heat transfer coefficient can be related to h_a, the convection heat transfer coefficient of the humid air as follows:

$$h_c = h_a / z \quad (4.9)$$

z is the condensation factor equal to sensible load divided by total heat load in the condenser

$$z = C_{pa}\ dT/dH \quad (4.10)$$

at water side, the heat transfer coefficient can be calculated from the following correlation, Holman,

$$Nu_w = 0.023\ Re^{0.8}\ Pr^{0.3} \quad (4.11)$$

And the condensate rate = $W_{ai} - W_{ao}$

4.2.3 The Greenhouse

Following Zhu et al. (1998), the green house can be assumed to consist of the following layers (see Figure 4.2):

1. the far sky
2. the near external air
3. the transparent cover
4. the internal air
5. the water bed simulating the vegetation layer
6. soil layer
7. deep soil layer

The greenhouse will receive a saturated air from the outlet of the evaporator; the air will exchange heat and mass inside the greenhouse, and will be heated due to solar radiation effects, leaving it capable of absorbing more humidity at outlet from the greenhouse. To maximise the desalination production this air can be passed through an additional evaporator downstream.

Calculating the heat and mass balance for each of the above layers of the greenhouse enough equations will be formulated that will enable solving for all the variables involved. What is most important is the climate condition inside the greenhouse, the air temperature and humidity.

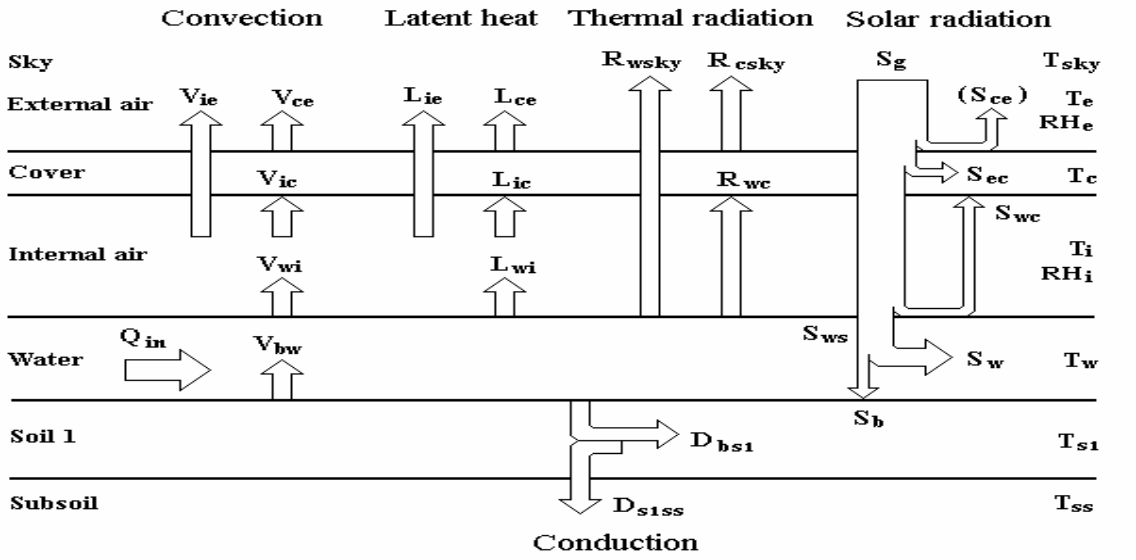

Figure 4.2: Greenhouse energy balance

Top Cover Layer:

$$M_c \, dT_c/dt = S_{es} + V_{ac} - V_{ce} + L_{ac} - L_{ce} + R_{wc} - R_{csky} \quad (4.12)$$

Internal Air Layer:

$$M_a \, dT_w/dt = V_{wa} - V_{ac} + L_{wa} - L_{ac} - L_{ae} - V_{ae} + Q_{ain} - Q_{aout} \quad (4.13)$$

Water Layer:

$$M_w \, dT_w/dt = S_w + V_{bw} - V_{wa} - L_{wa} - R_{wc} - R_{wsky} + Q_{win} \quad (4.14)$$

Soil Layer:

$$V_{bw} + D_{bs1} = S_b \quad (4.15)$$

where

S is the solar radiation flux
V is the convective heat flux
L is the latent heat flux
D is the conductive heat flux

The impact of water condensation on the lower side of the cover must be considered. The cover can be partially wet or completely wet. Pieters et al. (1996), introduces P-parameter which represents the fraction surface wetting. The radiation properties of the surface depend on two parameters, the thermal transmissivity, τ, and thermal emmissivity, ε.

Thus,

$$\tau_{wet} = (1 - P)\,\tau_{dry} \quad (4.16)$$

$$\varepsilon_{wet} = (1 - P)\,\varepsilon_{dry} + P\,\varepsilon_{cond} \quad (4.17)$$

where the subscript, (wet) means for the wet surface, (dry) for the dry surface with no condensate, and (cond) for the condensate itself and $P = th_f / th_{fmax}$ = the film thickness to maximum film thickness ratio

The following boundary conditions are used to solve the above differential equations.

1. global and diffuse solar radiation flux densities
2. external air temperature and relative humidity
3. wind speed
4. subsoil temperature, which can be assumed constant

The output from the above system of equation will be the following.

1. the cover temperature
2. the internal air temperature
3. the internal air relative humidity
4. the soil temperature
5. the water temperature in case of passive system, i.e. zero heat energy input flux, Q_w
6. or, the heat input flux density in case of active system, i.e. a non-zero Q_w

4.3 Method of Solution

The system can be solved in segregation way, i.e. assuming the temperature of the sea water entering the evaporator and that out of the condenser, knowing the inlet ambient air temperature and humidity ratio that enters the main evaporator, calculate the air properties out from the evaporator. Consider this as inlet to greenhouse, plus knowing the other boundary conditions about the greenhouse, solve for all variables inside the greenhouse, plus the properties of the air at the exit section from the greenhouse. The air properties out from the greenhouse is the inlet conditions to the second evaporator, and with the same sea water temperature out from the condenser, the equations governing the second evaporator are solved for the properties of air exiting the second evaporator. The properties of air entering the condenser becomes known, knowing also the properties of the fed sea water, the equations of the condenser are solved for the properties out from the condenser, sea water temperature out from the condenser, and the amount of the fresh distilled water out of the condenser.

The above procedure is repeated until reaching the convergence where variables are not varying any more within certain tolerances. Then the procedure is repeated for another time step, and so on.

The model developed in this section is not tested and simulation studies are not carried using this model since it is not in the project scope.

5. PERFORMANCE OF CONDENSER: AN EXPERIMENTAL STUDY

5.1 Experimental Setup and Procedures

One major problem vital to the design of efficient greenhouse desalination is the design of the condenser which constitutes the heart of the greenhouse desalination system. For greenhouse desalination to be practical it has to be economical which dictates a simple and inexpensive condenser design. The condenser has to deal with moist air where the non-condensable gas (the air) constitutes the major portion of the flowing medium. The presence of non-condensable gases considerably reduces the heat transfer coefficient.

The experimental setup designed to test different types of condensers is shown in Figures 5.1-5.3. The test section is made from transparent Plexi glass box. The first part of the test section is the calming section where the flow becomes uniform before entering the condenser box where the condenser modules are mounted. The second part is the condenser box where the condenser modules are fitted to the condenser frame. At the bottom of the condenser box a corrugated channel is located to collect the water condensate from individual condenser modules. Flow resistance baffles are installed underneath the condenser to prevent flow by-pass, i.e., force the air to pass through the channels between the condenser modules.

The experimental set up shown in Figure 5.1 consists of an air conditioning unit which provides the moist air at the desired conditions, water-to-water heat which supplies cooling water at the required constant temperature and a test section that houses the condenser modules. The test section is equipped with condensate collection trays, one for each module. The air conditioning unit shown consists of a pre-heater, a humidification section, a refrigeration coil and a re-heater. The unit controls the air flow rate, humidity and temperature.

The water-to-water heat pump consists of a refrigeration cycle connected to two brazed plate heat exchangers one on the hot side and the other on the cold side. These two heat exchangers are connected to two 1 m^3 water tanks from which the constant-temperature coolant (water) is obtained either from the hot side or from the cold side or by mixing both.

Based on the working conditions of greenhouse condenser the parameters affecting the condensation process along with their range were selected. These are: air inlet temperature range (30-50ºC), air inlet humidity range (50%-100%), air inlet velocity range (0.2-0.4m/s), cooling water temperature range (15-30ºC), and cooling water flow rate range 2-5 l/min.

Calibration of sensors such as air flow meter, water flow meter and other available devices was carried out. Although the air conditioning unit has an orifice flow meter the air volume flow rate was measured by measuring the local air velocity at the exit from the

test section using a pitot tube and integrating the velocity profile. The repeatability of the measurements was tested via two experiments at two different days at the same conditions.

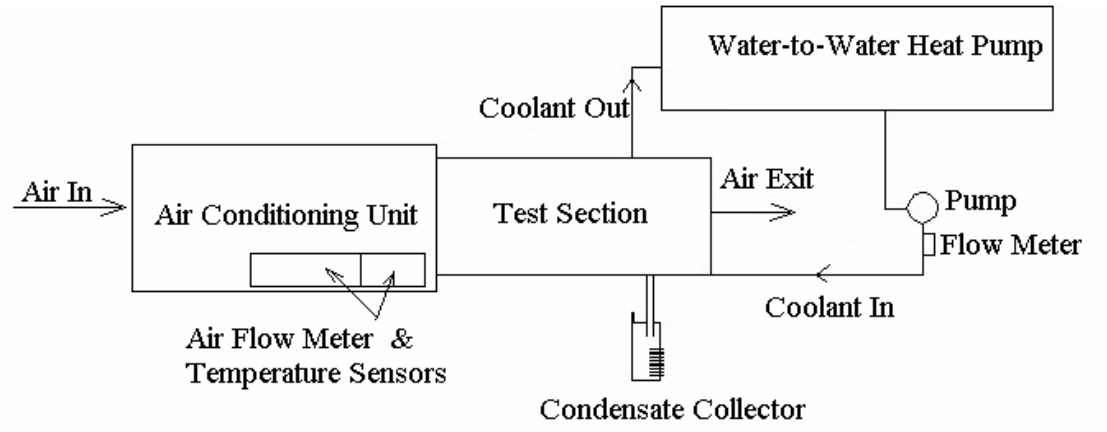

Figure 5.1: Experimental setup schematic diagram

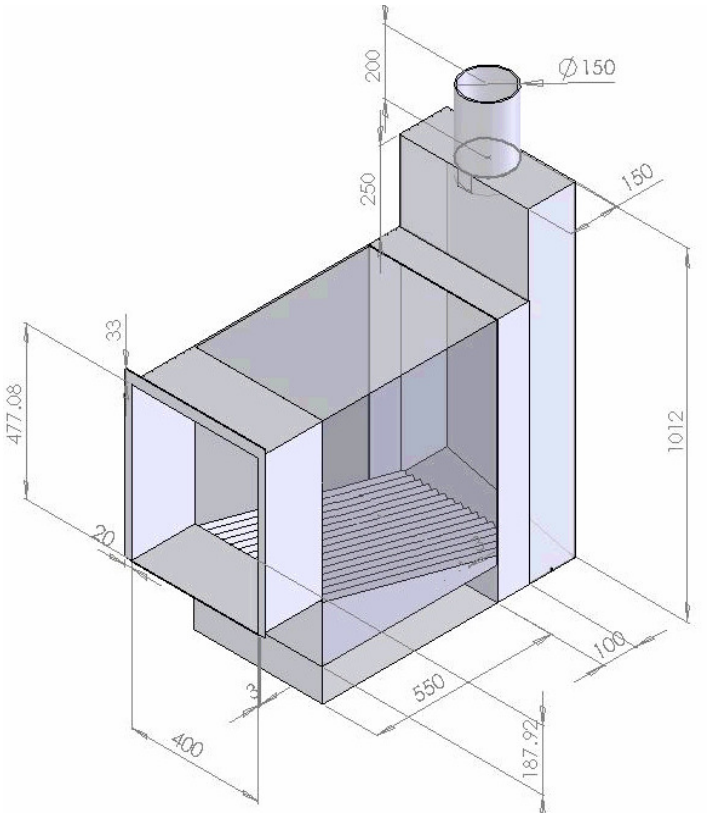

Figure 5.2: Transparent condenser housing duct

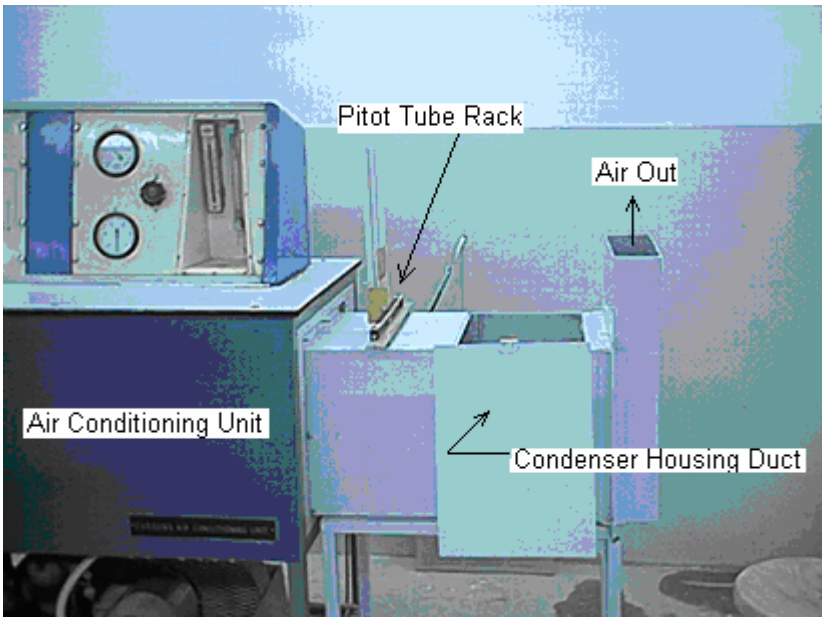

Figure 5.3: Experimental setup for condenser testing (University of Jordan)

The experimental procedure consists of the following steps:

1. The air conditioning unit is switched on and the air condition is controlled at the set condition, i.e., dry bulb temperature, relative humidity and flow rate.
2. Once the readings in step 1 above are stabilized the coolant pump and the coolant cooling unit are turned on. The water flow rate is regulated to achieve the desired coolant temperature.

Parametric study includes the variation of the coolant temperature and flow rate, the variation of the moist air temperature, relative humidity, and flow rate.

5.2 Design of Plate Channel Condenser

The plate channel condenser was made of plastic. Figures 5.4 and 5.5 show the dimensions of the condenser unit manufactured at the workshop of the Chair of Technical Thermodynamics, Aachen University, Germany. The condensation process occurs on the outer side surface of the channel with coolant flowing vertically inside small passages. The plate channel is connected to a header and a return pipe made from aluminium slotted to accommodate the plate channel. Coolant flow visualization using dye was carried out and showed uniform flow distribution among the small vertical channels of the unit.

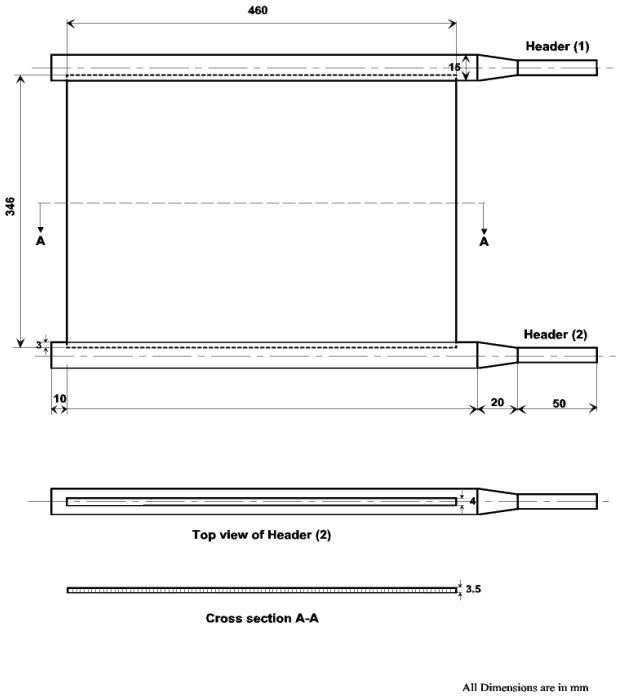

Figure 5.4: Plate channel condenser module

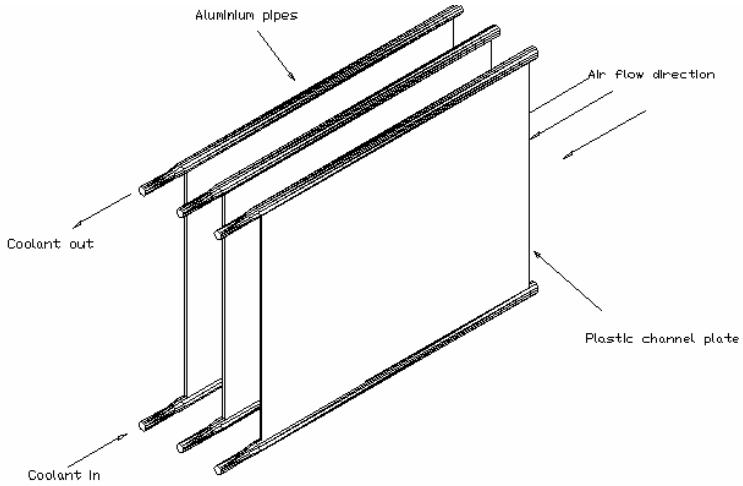

Figure 5.5: Plate channel condenser arrangement

5.3 Results and Discussions

The experimental results with plate channel condenser were obtained for different parameters: the air inlet temperature, humidity and velocity and the coolant (water) temperature and flow rate. Prior to each run the air conditioning unit was set at the conditions required and let run for one hour to achieve a steady state air condition. This is to ensure constant parameters of the air (temperature, humidity and flow rate) during the

experiment. Also, in each run three plate channel condenser modules (see Figure 5.5) were installed side by side at certain spacing and the condensate yield from the middle unit is reported as it has identical (symmetric) conditions on both sides. This is to eliminate the effect of the test section side walls. In other words, the middle unit represents an actual unit in a condenser consisting of a bank of these condenser units. Some of the experimental results obtained in this work incorporated a variation of spacing between the condenser units. Also, it must be noted that due to the low air flow rate, and thus low air mean velocities, facilitated by the air conditioning unit a blockage made of polystyrene material was installed on the sides of the test section to increase the average air velocity in the two channels formed by the three condenser units.

Figures 5.6 and 5.7 present the effect of air inlet dry bulb temperature, relative humidity, coolant temperature and coolant flow rate on condensate yield at constant air velocity of 0.2 m/s. It is seen that the higher the air dry bulb temperature (T_{db}) and humidity the higher the condensation rate (compare the curves for a 100% relative humidity at 44 and 36 ^{o}C dry bulb temperatures). The test at 55^{o}C produces more condensate yield than the one at 44^{o}C despite the higher relative humidity for the latter. This is because the former has a higher difference between the air and coolant temperatures (11^{o}C higher). The same behaviour can be seen in Figure 5.7 where the coolant temperature was set at 20^{o}C while under the same air conditions as those of Figure 5.6.

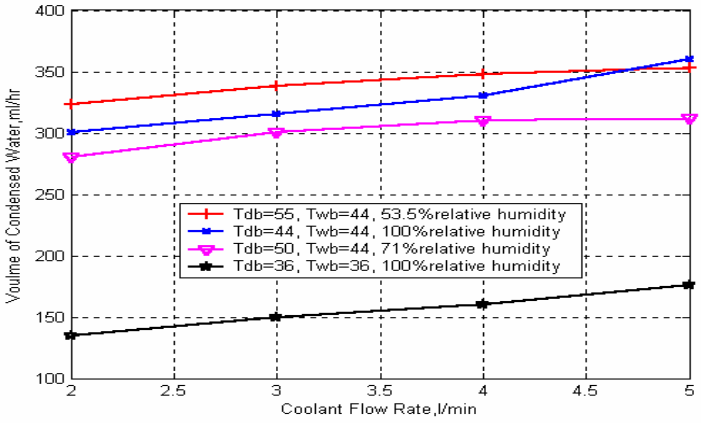

Figure 5.6: Water condensate production at constant coolant temperature of 15 ^{o}C and constant air velocity of 0.2 m/s

This result is quite motivating for introducing design improvements on the greenhouse, a matter that has been recommended by Dawoud et al. (2006). That is, a secondary channel in the greenhouse roof serves as a heater for a portion of the air flowing into the greenhouse. At the exit from the green house, mixing of hot air exiting the secondary channel with that flowing bellow through the greenhouse results in hotter exit air temperature before entering the second evaporator. The net effect is a higher temperature of an almost saturated air at the inlet to the condenser, yielding higher rate of water condensate.

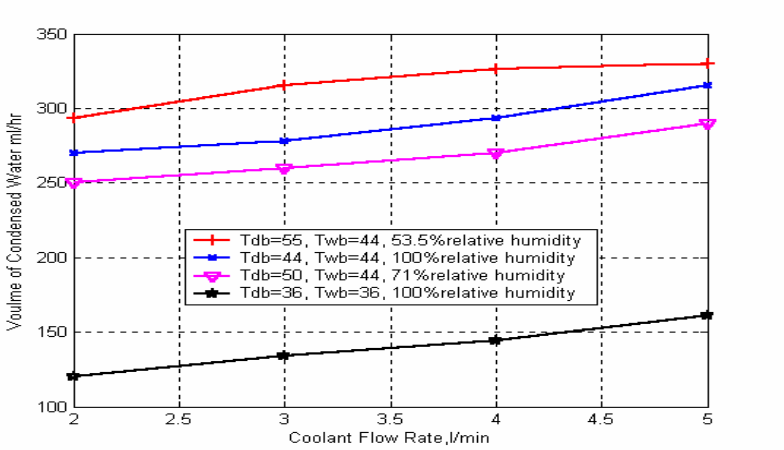

Figure 5.7: Water condensate yield at constant coolant temperature of 20°C and constant air velocity of 0.2 m/s

The above results are consistent with the condensation theory. That is, one of the major factors affecting the condensation process is the temperature difference between the bulk air-vapour mixture and the cooling surface temperature. While the surface temperature was not measured (a very thin plastic plate of 50 micron thickness) it is assumed that the surface temperature is very close to the coolant temperature, i.e., 15 °C in Figure 5.6. By looking at the temperature difference we can see that the curves for the dry bulb temperatures of 44 °C and 36 °C have temperature differences (T_{db}-$T_{coolant}$) of 24 and 16 °C, respectively. By increasing the coolant flow rate, more heat can be extracted by the coolant resulting in higher condensation rate.

Figures 5.8 and 5.9 show the effect of coolant temperature on condensation rate at different air inlet conditions. The general trend is that for all coolant temperatures and flow rates the lower the coolant temperature the higher the condensation rate. However, the variation trend with coolant flow rate varies especially at low coolant temperature. That is, in Figure 5.8 the curves for coolant temperatures of 15 °C and 20 °C level off contrary to the case shown in Figure 5.9. In an attempt to explain this behavior it was initially thought that experimental errors are responsible. However, the pattern persisted despite the repetition of the experiments. The only thing noticeable here is that for the case of Figure 5.9 the air is fully saturated.

To study the effect of air velocity on the condensation with noncondensable gas two cases were tested at two different velocities and two different coolant temperatures. Figure 5.10 for a coolant temperature of 15 °C shows that the effect of velocity is to increase the condensation rate. This could be attributed to two factors: an increase in condensation heat transfer coefficient and the increase level of turbulence which is more effective in counteracting the adverse effect of noncondensable gas. The increase reaches as high as 140 ml/h (or 45%). Similar results have been arrived at for the second case tested (Figure 5.11). That is, for the coolant temperature of 25 °C the behaviour is quantitatively similar (i.e., 140 ml/h) but with higher percentage increase, i.e., 65%.

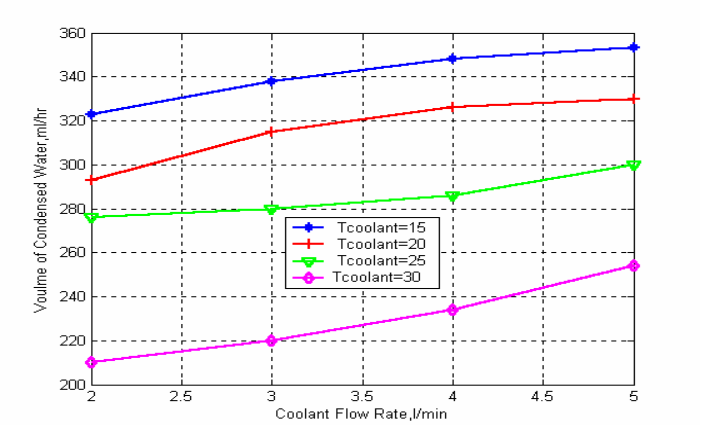

Figure 5.8: Effect of coolant temperature on condensate yield at air inlet conditions of T_{db}=55 ^{o}C, 53% relative humidity at constant air velocity 0.2 m/s

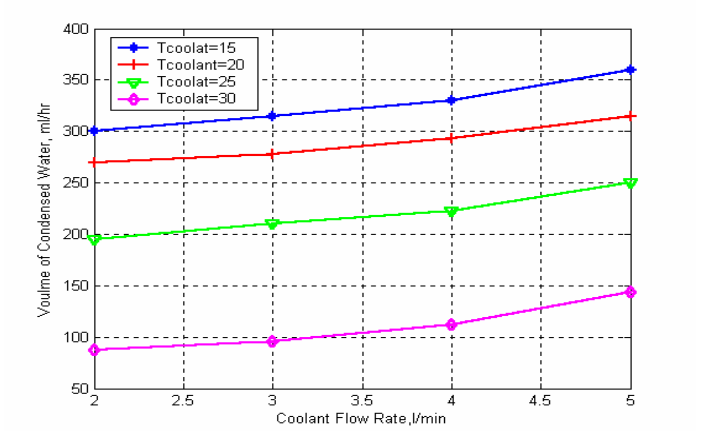

Figure 5.9: Effect of coolant temperature on condensate yield at air inlet conditions of T_{db}=44 ^{o}C, 100% relative humidity at constant air velocity 0.2 m/s

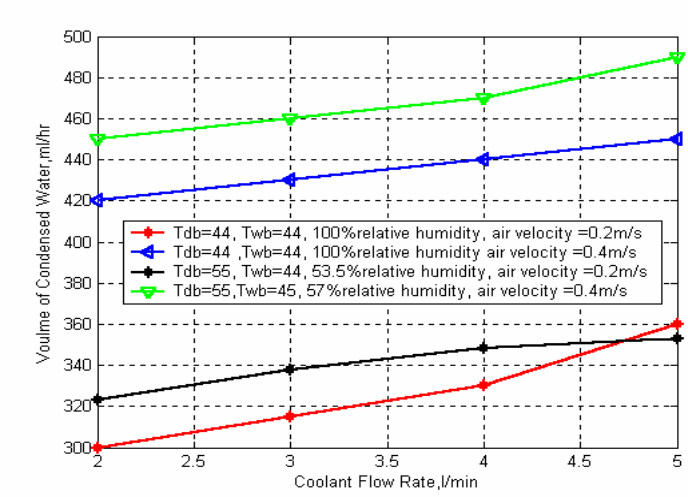

Figure 5.10: Variation of water condensate by varying the air speed at constant coolant temperature of 15 ^{o}C

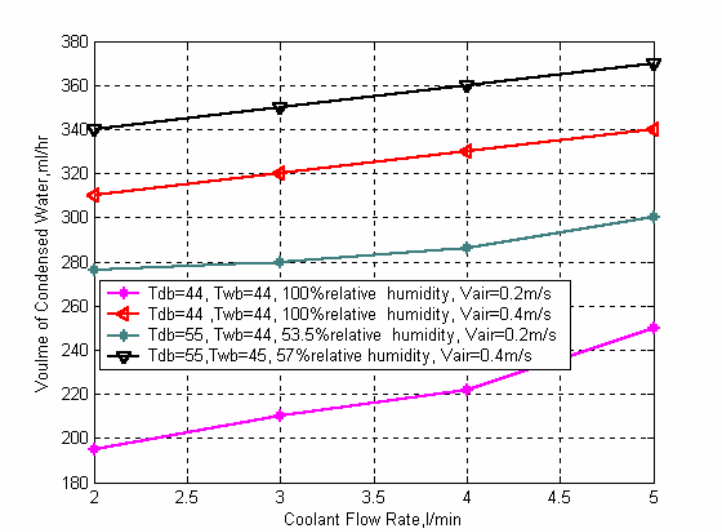

Figure 5.11: Variation of water condensate for two different air velocities at constant cooling temperature of 25 ^{o}C

To study the effect of spacing between the three condenser units experiments were conducted at two different spacings, each at two different velocities. Results are presented in Table 5.1, which also show high repeatability in the experimental results. Note that each run had been made three times at the same conditions to make sure of repeatability of data.

Table 5.1: Effect of air velocity on water condensate yield

Test #	Water condensate (ml/hr) at air speed of 0.2m/s 5 cm spacing	Water condensate (ml/hr) at air speed of 0.2m/s 10 cm spacing	Water condensate (ml/hr) at air speed of 0.4m/s 5 cm spacing	Water condensate (ml/hr) at air speed of 0.4m/s 10 cm spacing
1	80	86	112	126
2	80	84	112	128
3	82	86	114	126
Avg.	81.0	85.0	113.0	127.0

By looking at Table 5.1, it is seen that although small, the effect of spacing is to increase the condensation rate. This slight increase could be attributed to the increase in the volume of air and thus the amount of vapour that is brought into contact with the condenser surface. That is, at constant air velocity more humid air passes through the channel between the condenser units. As a result, it may be stated that the slight increase seen in the foregoing is bought at the expense of compactness which is much more effective in boosting the condensate yield of the condenser in question.

5.4 Heat Transfer Enhancement

In order to boost the condensation rate it was thought that promoting turbulence and mixing of bulk stream will reduce the concentration of the noncondensable gas near the cooled surface. Hence, two kinds of fins (0.5-cm and 1-cm high fins) were mounted on the condenser wall surface (see Figure 5.12). Table 5.2 gives the results for the case considered. It is shown that with the addition of fins there is a slight increase in water condensate. This increase is not significant to warrant a concrete conclusion. Higher fins or different fin arrangements may lead to more conclusive evidence. This is recommended for future works.

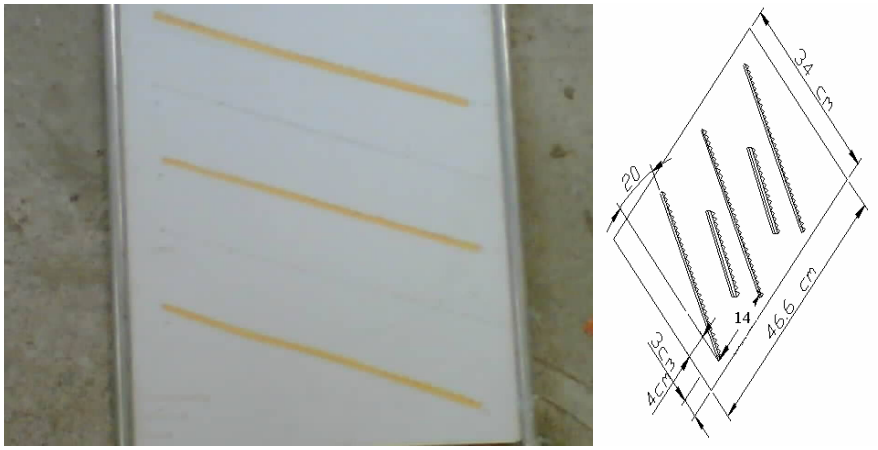

Figure 5.12: Fin distribution on condenser surface

Table 5.2 Effect of fins on water condensate (ml/hr)

Air velocity	5cm spacing without fins	5cm spacing, with three 0.5cm fins	5cm spacing, with three 0.5cm and two 1cm fins	10cm spacing, without fins	10cm spacing with three 0.5cm and two 1cm fins
0.4 m/s	112	116	124	126	132

5.5 Conclusions

In this section desalination based on humidification-dehumidification principles has been experimentally studied in relation to greenhouse desalination. The objective of this study was to develop a condenser design for greenhouse desalination. One design has been developed and laboratory-tested; the plastic plate channel condenser (plane and finned surface). The experimental tests covered a wide range of parameter space; inlet air temperature, humidity, and flow rate and coolant water temperature and flow rate. The results in terms of condensate production rate per unit area were compared with

conventional vertical tube bank condenser (termed a water maker) used by Davies and Paton (2004). The comparison showed that higher rate of condensate production is achieved using the plate channel condenser which is simpler and less expensive than the more elaborate tube bank design used by Davies and Paton (2004). An increase in fresh water production rate of 16.5% is achieved using the plate channel condenser developed in this work compared with water maker condenser used by Davies and Paton (2004). The air temperature and humidity have significant effect on the condenser condensate yield. Higher temperature and humidity produce more condensate for the same flow rate and coolant temperature. The results presented in this work support the proposed by Dawoud et al. (2006) modification to greenhouse design. The tests also showed that the effect of air velocity is significant (increase the water condensate) while the spacing between the condenser modules has a marginal effect. Condensation enhancement using fins mounted on the surface of the condenser has been attempted. Although the results show a marginal enhancement they may be considered preliminary.

6. CFD MATHEMATICAL MODEL OF GREENHOUSE DESALINATION

6.1 Greenhouse physical model

In general, greenhouse microenvironment is highly inhomogeneous. Spatial and temporal variations in air speed, temperature, humidity, and gas concentration are quite strong. Proper prediction of these spatial variations is essential for proper desalination greenhouse design. CFD has become a powerful tool in resolving the fine details of the flow, temperature, and mass concentration fields in many engineering applications. In this section a general CFD mathematical model is developed. In accord with the scope of the project a preliminary CFD simulations have been conducted using the well-known commercial CFD software CFX5.5 and results are presented.

The greenhouse physical model is shown in Figure 6.1. This model has been used to simulate the hydrodynamics of air flow inside the greenhouse.

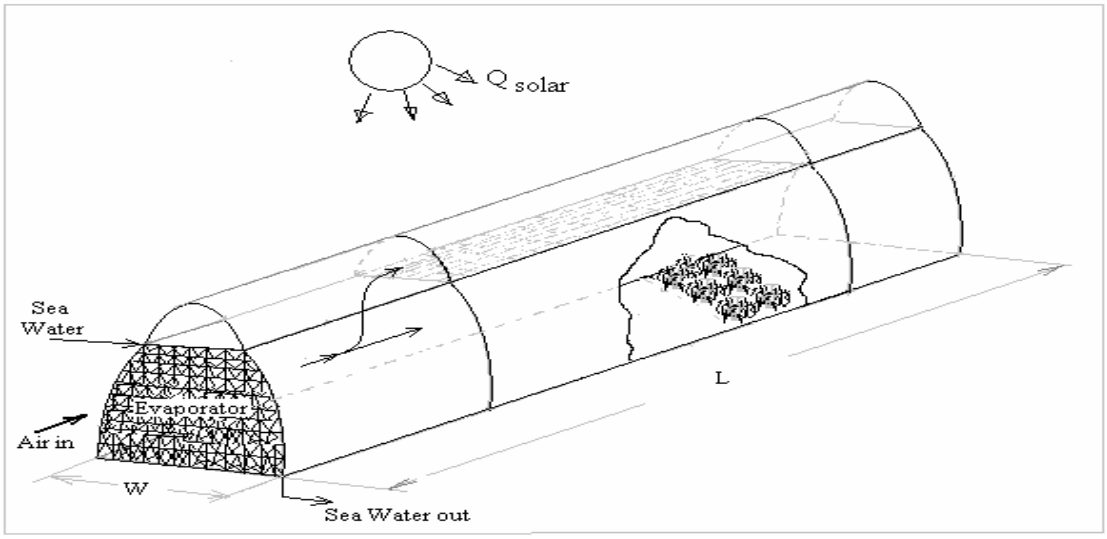

Figure 6.1: Schematic of the desalination greenhouse

6.2 Greenhouse CFD mathematical model

The governing differential equations describing the flow, energy, and mass transport processes may be described by the familiar general transport equation:

$$\frac{\partial \phi}{\partial t} + (\nabla \bullet \rho \vec{V})\phi = \Gamma . \nabla^2 \phi + S_\phi \qquad (6.1)$$

where ϕ stands for the flux components (velocity, temperature, and scalar), Γ is the diffusion coefficient and $\vec{V}$ is the velocity vector.

Because of the large scale of the physical model the flow is expected to be well into the turbulent flow regime. Therefore, a suitable turbulence model must be selected to model the turbulent transport. In this preliminary study the well-known $k-\varepsilon$ turbulence model has been employed.

6.2.1. The Crop Resistance Model

The crop resistance to the flow may be modeled by introducing the drag into the source term S_ϕ as follows (Boulard and Wang, 2002):

$$S_\phi = -LC_D v^2 \tag{6.2}$$

where L is the leaf area density, C_D is the drag coefficient, and v is the local velocity. Equation (6.2) was derived by Boulard and Wang (2002) as follows:

Considering the crop cover as a porous medium where Darcy's law applies and the governing source term in the general transport equation becomes:

$$S_\phi = -\left(\frac{\mu}{K}\right)v - \left(\frac{C_F}{K^{0.5}}\right)v^2 \tag{6.3}$$

Where μ is the fluid (air) dynamic viscosity, K is the porous medium permeability determined experimentally. C_F is the non-linear momentum loss coefficient. The first term in Equation (6.3) is neglected in comparison with the second term which is proportional to v^2. That is,

$$S_\phi = -\left(\frac{C_F}{K^{0.5}}\right)v^2 \tag{6.4}$$

In general, the porous medium resistance may be expressed as:

$$S_\phi = -LC_D v^2 \tag{6.5}$$

Then it follows that:

$$LC_D = C_F / \sqrt{K} \tag{6.6}$$

Equation (6.5) gives a relation by which the ratio $C_F / \sqrt{K}$ can be evaluated experimentally through the measurement of drag coefficient C_D and leaf area density, L.

The drag coefficient for different crops can be found from the literature (for example, for tomato $C_D = 0.32$).

6.2.2 Crop Transpiration Model

In general, transpiration is a form of natural thermal control wherein the plants' leaves give off water vapor resulting in heat loss similar to the cooling of human body by sweating and breathing. To account for both the latent and sensible heat exchanges between the air and the plants energy and mass balance equations need to be developed. In this context, the greenhouse crop is modeled as a porous solid (see Figure 6.2) having a given surface temperature, T_s, and exchanging heat and mass with inside air at $T_{a,i}$ and absorbing a net solar heat flux R_n (Boulard and Wang, 2002). Thus,

$$\dot{q}_n - \dot{q}_{sensible} - \dot{q}_l = 0 \tag{6.7}$$

$$\dot{q}_n - \frac{\rho C_p L_{ai}(T_s - T_{a,i})}{r_a} - L_{ai}\rho\lambda\frac{w_f - w_a}{r_a + r_s} = 0 \tag{6.8}$$

Where Cp is the air specific heat at constant pressure, L_{ai} is leaf area index, w_f and w_a are the specific humidity of the air at leaf and at inside air temperatures respectively (T_s and $T_{a,i}$, respectively), ρ is the air density and λ is the water latent heat of vaporization at T_s. r_a and r_s are, respectively, the aerodynamic and stomatal resistances of the leaf and are given by Campbell (1977) for air velocity less than 0.1 m/s by:

$$r_a = 840\left(\frac{d}{|T_s - T_a|}\right)^{0.25} \tag{6.9}$$

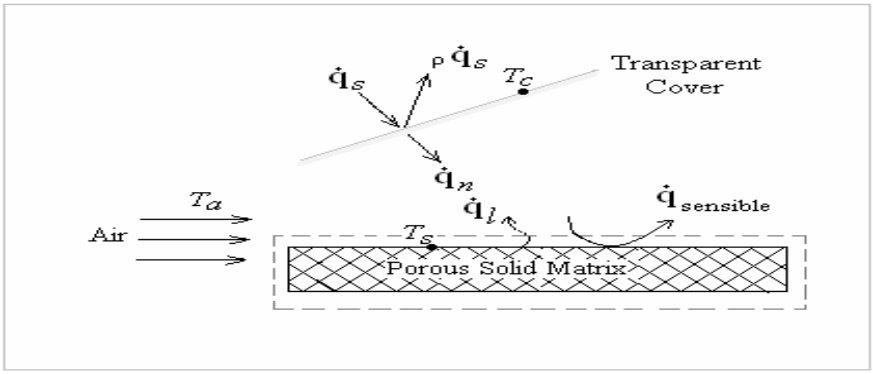

Figure 6.2: Schematic of energy balance on plant canopy

For air velocity greater than 0.1 m/s r_a is given by:

$$r_a = 220\frac{d^{0.2}}{v^{0.8}} \tag{6.10}$$

where d is the characteristic length of the leaf and v is the local air speed. The stomatal resistance is given by Pollet et al. (1999) as:

$$r_s = \frac{200(31 + S_g)\left(1.0 + 0.016(T_a - 16.4)^2\right)}{(6.7 + S_g)} \tag{6.11}$$

where S_g is the local global solar radiation flux (W/m^2).

The photosynthesis mechanism is depicted in Figure 6.3.

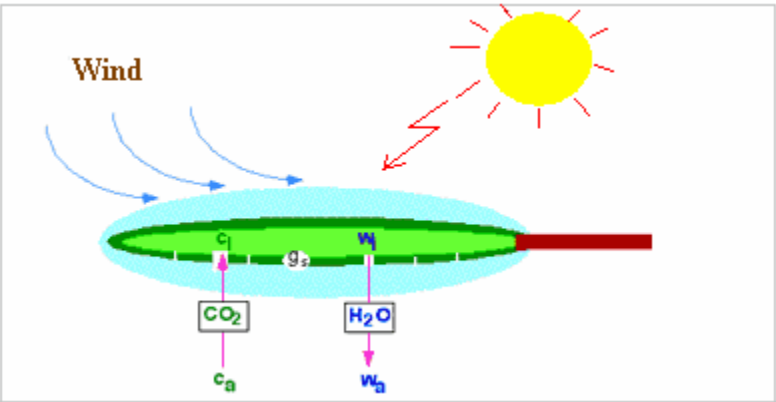

Figure 6.3: Photosynthesis mechanism

The photosynthesis denoted by FS is given by:

$$FS = \frac{g}{1.6}(c_a - c_i) \tag{6.12}$$

where g is the stomatal conductance, the constant 1.6 is the ratio of the diffusivities of water vapor and carbon dioxide in air, c_a and c_i are the leaf intercellular and ambient carbon dioxide concentrations, respectively. The transpiration rate is given by:

$$E = g\,(w_i - w_a) \tag{6.13}$$

where w_i and w_a are the leaf intercellular and ambient water vapor concentration, respectively. The water use efficiency (WUE) is given in terms of FS and E as:

$$WUE = \frac{FS}{E} = \frac{(c_a - c_i)}{1.6(w_a - w_i)} \tag{6.14}$$

c_i is determined by the plant metabolism while c_a, w_a and w_i are externally controlled variables.

6.2.3. Effective Sky Temperature

Thermal radiation exchange between sky and ground objects is normally calculated based on effective sky temperature T_{sky} (or the equivalent temperature of the sky). In general, sky temperature is a function of the ambient temperature, dew point temperature, the pressure, the concentration of CO_2 in the atmosphere, the fraction of opaque cloud cover, and the emissivity of the clouds. Frequently, the sky temperature is expressed as a function of a single variable; the ambient temperature, T_a. Examples include (Duffie and Beckman, 1982):

$$T_s = 0.0552 T_a^{1.5} \tag{6.15}$$

and

$$T_s = T_a - 6.0 \tag{6.16}$$

6.2.4. Ventilation/Insect-Proof Screen Model

The ventilation/insect-proof screens may be modeled as a porous medium using the relation (Fatnassi et al., 2003):

$$S_\phi = -\frac{C_f}{\sqrt{K}} V^2 \tag{6.17}$$

K and C_f in the above equation are given in terms of the screen mesh thread α as:

$$K = 3.44 \times 10^{-9} \alpha^{1.6} \tag{6.18}$$

$$C_f = \frac{4.3 \times 10^{-2}}{\alpha^{2.13}} \tag{6.19}$$

The screen mesh thread α is given by:

$$\alpha = \frac{(L-d)^2}{L^2} \tag{6.20}$$

where L is the size of the mesh and d are the diameter of the thread.

Wire screens are used in many engineering applications. The pressure drop through wire screens has been expressed (Teitel and Shklyar, 1998) as:

$$\Delta p = C \frac{1}{2} \rho V^2 \tag{6.21}$$

where C is given in terms of flow passage and wire screen geometry. For the greenhouse the constant C is deduced from Teitel and Shklyar (1998) as a function of the free surface area, *n* (see Figure 6.4). The data may be curve-fitted by the equation:

$$C = 99.148\,n^4 - 303.92\,n^3 + 348.11\,n^2 - 179.38n + 36.06 \qquad (6.22)$$

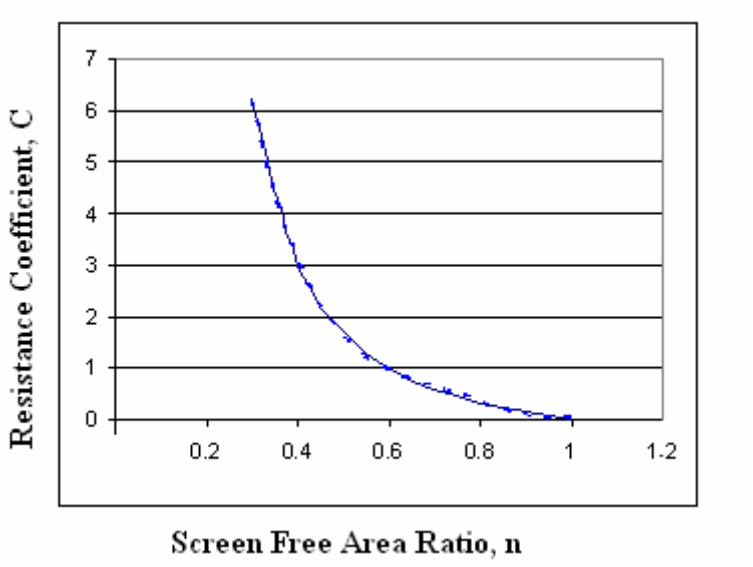

Figure 6.4: Variation of wire screen resistance coefficient with free area ratio

6.2.5 Evaporator Resistance Model

The pressure drop across the media type evaporative cooling pads system ranges between 60 to 150 Pa including the droplet arrestor (Beshkani and Hosseini, 2006).

6.2.6 Hydrodynamics in Greenhouse: A Simple Demonstration

Assuming adiabatic conditions the flow pattern and the percentage of air flowing in the upper channel (see Figure 6.5) are calculated. The inlet is restricted to the evaporator section only and the flow branches out to the upper channel and then joins the main flow in the greenhouse at the end space and exits the greenhouse. The inlet velocity out of the evaporator is assumed to be 0.5 m/s.

Although the actual problem is far more complex than this one the purpose is to simply show the potential of CFD approach to greenhouse desalination simulations. Figures 6.6 to 6.9 show the results using CFX commercial software version 5.5. The results represent the velocity profile across the greenhouse, the velocity vector plots, the grid system and the pressure contours.

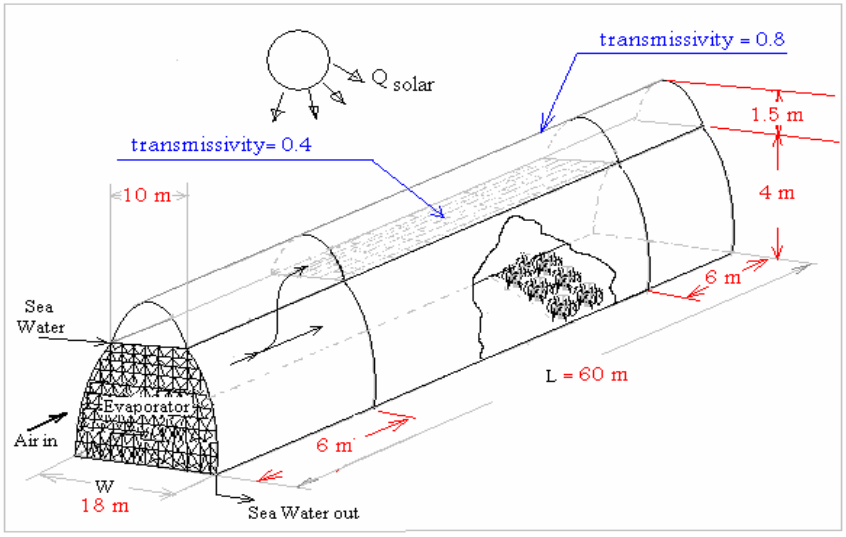

Figure 6.5: Variation of wire screen resistance coefficient with free area ratio

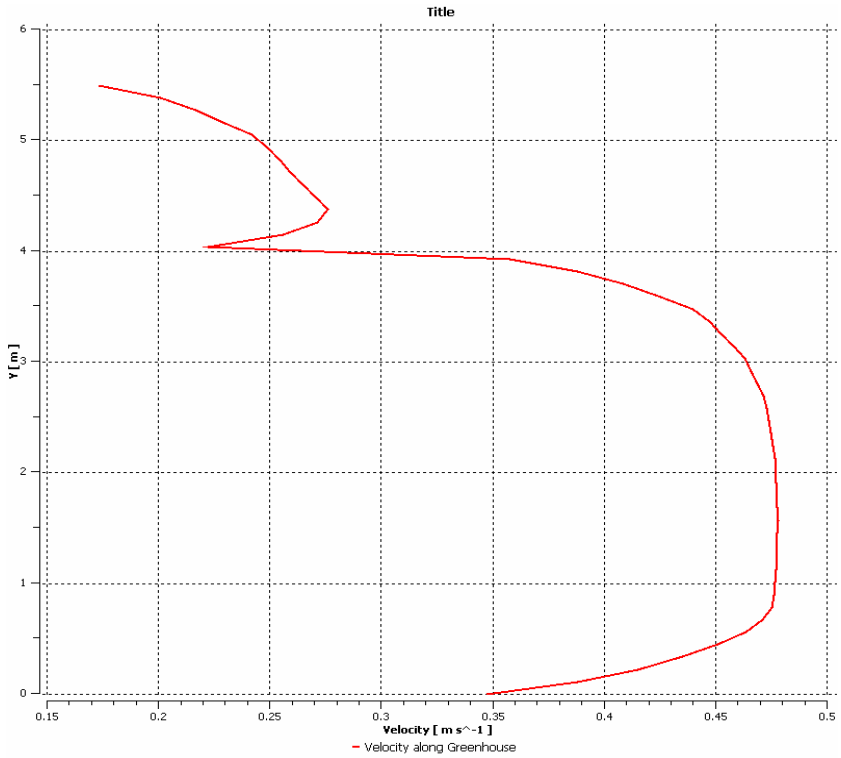

Figure 6.6: Velocity profile across the greenhouse

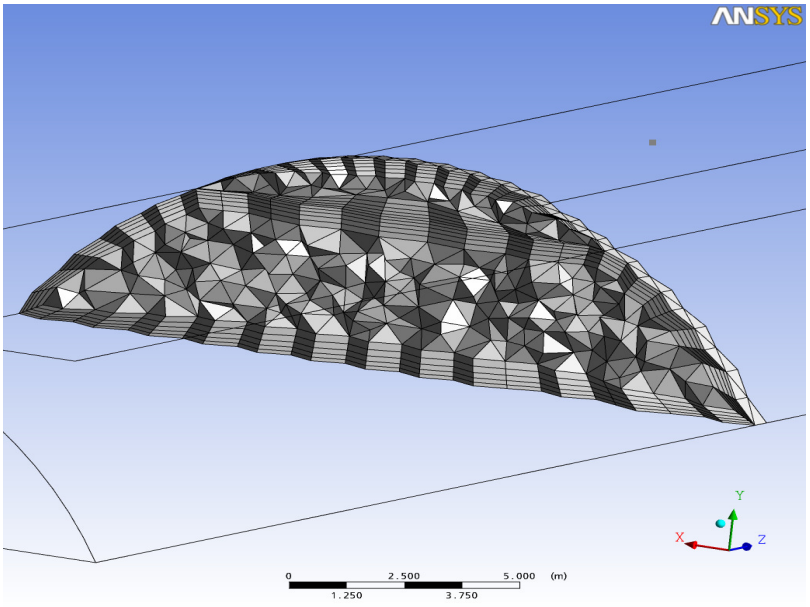

Figure 6.7: The grid system

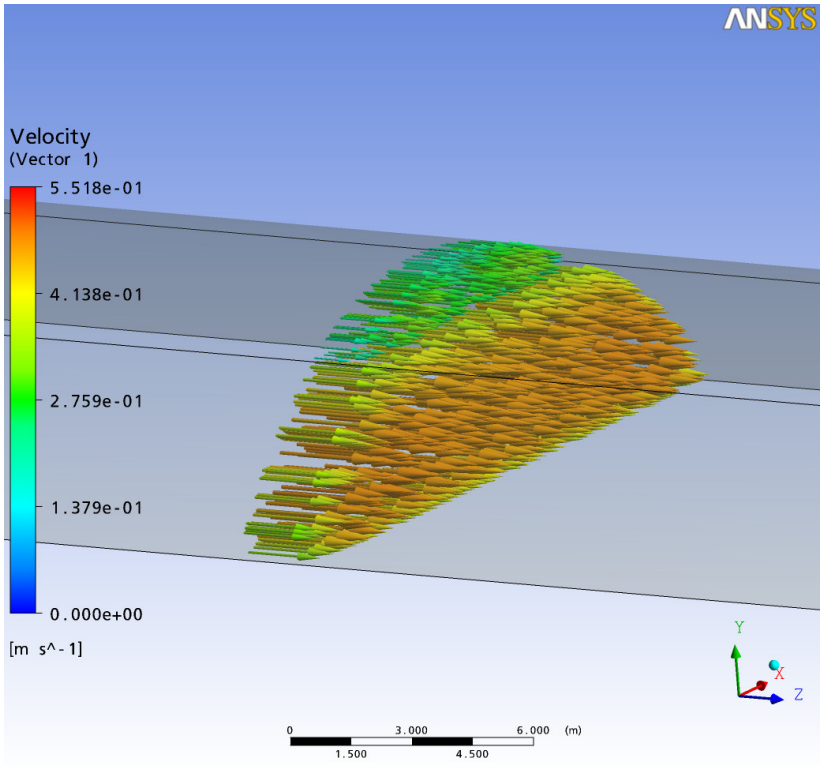

Figure 6.8: Velocity vectors

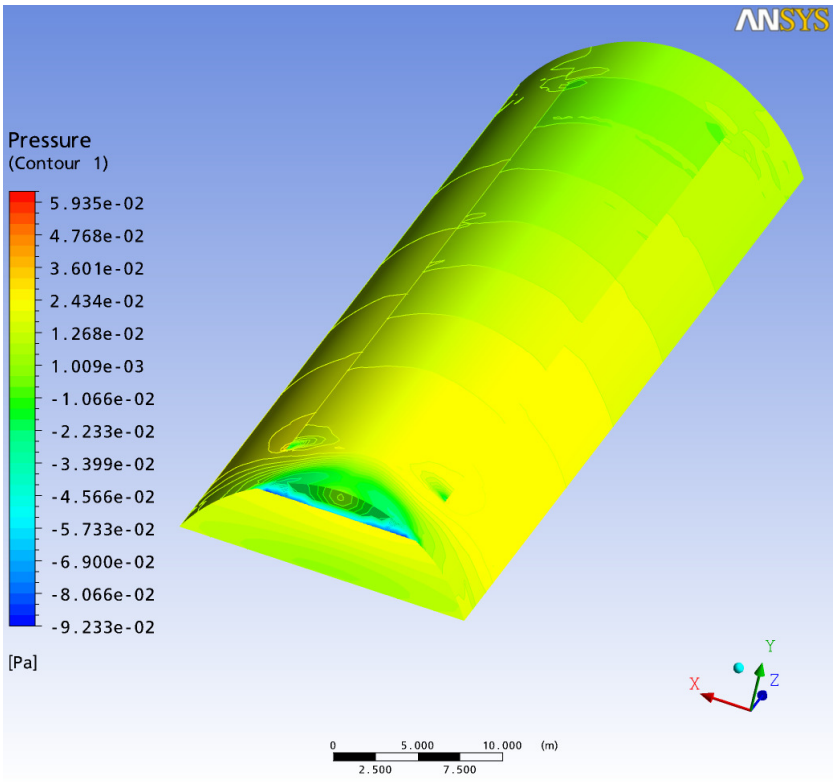

Figure 6.9: Pressure contours

6.3 Summary and conclusions

In this section the CFD modeling of greenhouse was discussed. It is shown that greenhouse microenvironment is highly inhomogeneous. Spatial variations in air speed, temperature, humidity, and gas concentration are quite strong. Proper prediction of these spatial variations is essential for proper desalination greenhouse design. CFD is a powerful computational tool in resolving the fine details of the flow, temperature, and mass concentration fields in many engineering applications. In this report a review of CFD studies on greenhouse microclimate has been conducted and the basic important relations governing the physical processes inside the greenhouse have been identified. CFD model has been developed and preliminary simulations using CFX-5.5 CFD software have been conducted to study the greenhouse microenvironment. The model is based on the governing momentum, heat and mass transfer equations. It is demonstrated that CFD modelling can capture the details of the microclimate inside the greenhouse. Based on the results presented it may be stated that proper design of greenhouse desalination should rely on detailed analysis facilitated by CFD commercial software. Future work in this aspect is recommended.

7. CLOSURE

In this work, the greenhouse desalination was reviewed and the physical processes in this fairly new technology were identified. Based on the work done in this project it was found that the amount of water evaporated at the evaporator (see Fig. 2.2) is quite significant if it can be condensed back into liquid water. Thus, the potential of greenhouse desalination is seen to rely heavily on the condenser performance. However, the performance of the condenser for this application is highly affected by the presence of non-condensable gas. This problem has been reviewed and condenser configurations were identified. A plate channel type condenser was developed and tested. The condenser developed in this work is shown to perform better than the more conventional and expensive fin-tube bank condenser developed by other investigators.

The methods for cooling the condenser coolant were investigated in this work and the feasibility of different techniques was studied. One such technique is the evaporative cooling of surface seawater as a condenser coolant. It was found that while this technique is the most convenient, it is limited by the ambient air conditions (see Table 3.1). It works subject to the conditions that ambient relative humidity be between 54 and 40% for corresponding ambient air dry bulb temperatures between 45 and 25^{o}C. Of course, fouling will be a problem that may prove to be costly. A measure to permit applying evaporative cooling for a wider range of ambient relative humidities is to increase the temperature of air entering the condenser. A modification on seawater greenhouse (SWGH) design in order to realize this option has been recommended. The roof zone of the greenhouse has to be sealed and an air collector or a hybrid (air-water) collector has to be integrated into it. After the canopy, an additional zone has to be constructed for mixing the so heated air in the roof zone with the air leaving the planting zone. The heated seawater in such a hybrid collector will then be used to humidify the mixed air before entering the 1st condenser. Moreover, the mixing zone can be designed as a hybrid collector in order to further enhance the freshwater production rate of SWGHs.

Cooling the condenser coolant via cooling machines and deep seawater was also considered. A cooling capacity in the order of 1 MW is required for an air flow rate of 15 m^3/s entering the SWGH. A deep seawater flow rate of about 100 tons/h will be sufficient to remove the same cooling capacity, despite the fouling problem, which will be encountered. Both cooling capacity and the corresponding deep seawater flow rate are directly proportional to the air volume flow rate. A life-cycle cost analysis seems a must in the last two cases. Moreover, alternative solutions for hot and humid climates have to be worked out with, for example, applying rotating desiccant wheels or liquid desiccant systems to dehumidify the entering air to the greenhouse. The heat of sorption, which has then to be removed, can be utilized to heat the air stream before it flows into the 2nd evaporator. These ideas are in phase with our recommendation to apply an air or a hybrid collector in the roof zone; namely to increase the temperature of air entering the condenser to enhance the freshwater production of seawater greenhouses.

Based on the condenser cooling water requirements (in the form of deep seawater) calculations show that large amounts of cooling water is required which may render the greenhouse desalination impractical. While this statement represents one aspect of the greenhouse desalination, concrete statement should be based on economic study which is recommended for future work. A condenser with plastic cover was proposed (see Fig. 2.9) and a preliminary testing was carried out (Al-Khalidi, 2006). While its performance is not competitive with plate channel condenser, future work on this condenser is recommended. Also, future work should focus on direct contact condensers as they have much higher condensation rates and are simpler in design. The condenser proposed in this work may prove suitable for this function (see Fig. 2.9) once the plastic cover is removed. It is also recommended that overall greenhouse system simulations be conducted based on the mathematical models (including CFD model) developed in this work.

It should be mentioned that more than one SWGH have been built; two of them in the gulf region, namely in UAE and Oman. It is essential that performance data on the performance of these greenhouses be made public for the benefit of researchers in this seemingly promising area of desalination.

8. REFERENCES

Al-Diwany H.K.and Rose, J.W., (1973), “Free convection film condensation of steam in the presence of non-condensing gases”, Int. J. Heat Mass Transfer, 1359–1369

Al-Kasabi, T.O., Abdel-Khalik, S.I., Dix, T.E., Hagenson, R., Husseiny, A.A., McLagan, G.P., Laporta, C. and Matthews, J., (1981), "Design of a commercial solar-powered greenhouse", Desalination, 39, 53-62

Al-Khalidi, A., (2006), "Improved design of the condenser for efficient greenhouse desalination technology", MSc Thesis, Mechanical Engineering Department, The University of Jordan, Amman-Jordan

Avissar, R. and Mahrer, Y., (1982), "Verification study of a numerical greenhouse microclimate model", Trans. ASAE, 25, 1711-1720

Baehr, H.D., (1961), "Mollier-i-x-Diagramme für feuchte Luft", Springer Verlag, Berlin, Germany

Bartzanas, T., Boulard, T. and Kittas, C., (2004), "Effect of Vent Arrangement on Windward Ventilation of a Tunnel Greenhouse", Biosystems Engineering, 88(4), 479-490

Bartzanas, T., Boulard, T. and Kittas, C., (2002), "Numerical Simulation of the Airflow and Temperature Distribution in a Tunnel Greenhouse Equipped with Insect-Proof Screen in the Openings", Computers and Electronics in Agriculture, 34**,** 207-221

Bell, K.J. and Ghaly, M.A., (1973), "An approximate generalized design method for multi-component/ partial condenser", Industrial Eng. Chem., 69, 6-13

Berliner P., (1975), "Kühltürme: Grundlagen der Berechnung und Konstruktion", Springer Verlag, Berlin, Heidelberg, New York

Beshkani, A. and Hosseini, R., (2006), "Numerical modeling of rigid media evaporative cooler", Applied Thermal Engineering, vol. 26, no. 5-6, 636-643

Bot, G.P.A., (1983), "Greenhouse climate: From physical processes to a dynamic model", PhD Thesis, Wageningen, the Netherlands: Agricultaral Highschool of Wageningen

Boulard, T. and Wang, S., (2002), "Experimental and Numerical Studies on the Heterogeneity of Crop Transpiration in a Plastic Tunnel", Computers and electronics in agriculture, 34(1-3), 173-190

Campbell, G.S., (1977), "An Introduction to Environmental Biophysics", Springer-Verlag, New York

Chaibi M.T., (2003), "Greenhouse Systems with Integrated Water Desalination for Arid Areas Based on Solar Energy", Doctoral Thesis, Swedish University of Agricultural Sciences, Alnarp

Davies, P., K. Turner and C. Paton, (2004), "Potential of the seawater greenhouse in middle eastern climates", Proc. of the Int. Engineering Conf. (IEC), Mutah University, Jordan, April 26-28, 523-540

Davies P. and C. Paton, (2004), "The seawater greenhouse and the watermaker condenser", Proceedings of the HPC2004-3rd International conference on Heat Powered Cycles, Larnaca, Cyprus, October

Dawoud, B., Zurigat, Y.H., Klitzing, B. Aldoss, T. and Theodoridis, G., (2006), "On the possible techniques to cool the condenser of seawater greenhouses", Desalination, 195, 119-140

De Vuono, A.C., (1983), "Pressure effects on the film condensation of steam-air mixtures with applications to nuclear systems", PhD. Thesis, Ohio State University

Dilip, J. and Gopal, N.T., (2002), "Modeling and optimal design of evaporative cooling system in controlled environment greenhouse", Energy Conversion and Management, 43, 2235-2250

Duffie, J.A. and Beckman, W.A., (1982), "Solar Engineering of Thermal Processes", John Wiley & Sons, NY

Fatnassi, H., Boulard, T. and Bouirden, L., (2003), "Simulation of Climatic Conditions in Full-Scale Greenhouse Fitted with Insect-Proof Screens", Journal of Agricultural and Forest Meteorology, 118 (1), 97-111

Finlay, I.C and D. Harris, (1984), "Evaporative cooling of tube banks", International Journal of Refrigeration, 7(4), 214-224

Gale, S. and Zeroni, M. (1984), "Cultivation of plants in brackish water in controlled environment agriculture". In R.C. Staples and G.H. Toenniessen ed., "Salinity tolerance in plants, strategies for crop improvement", John Willey and Sons, New York, 363-380

Hasan A. and K. Siren, (2003), "Performance investigation of plain and finned tube evaporatively cooled heat exchangers", Applied Thermal Engineering, 23, 325-340

Hassan, M.S., Toyoma, S., Murase, K. and Wahhab, M.A., (1989), "Multi-effect solar still for agricultural purposes in hot climate", Desalination, 71, 347 -353

Heldt H.-D. und H. G. Schnell, (2000), "Kühlwasser: Verfahren und Systeme der Aufbereitung, Behandlung und Kühlung von Süßwasser – Brackwasser – Meerwasser zur Industriellen Nutzung", 5. Auflage, Vulkan-Verlag, Essen, Germany

Hetsroni, G. (1982), "Handbook of Multiphase Systems", McGraw Hill Book Company

Hoxey, H.J. and Moran, M.M., (1991), "Full scale wind pressure and load experiments—Multispan 167×111 m glasshouse (Venlo)", Divisional note 1594, AFRC Institute of Engineering Research, Wrest Park, Silsoe, Bedford

Jones, W.P., (1994), "Air Conditioning Engineering", 4th Edition, Arnold, pp. 14-27

Jurgen, K. and Dietmar, H., (1999), "Effect of spontaneous condensation on condensation heat transfer in the presence of non condensable gases", Paper No. AJTE99-6118, Proceedings of the 5th ASME/JSME Joint Thermal Engineering Conference, March 15-19, San Diego, California

Kindelan, M., (1980), "Dynamic modeling of greenhouse environment", Transactions of the ASAE, 1232-1238

Landsberg, J.T., White B.T., (1979), "Comparative analysis of efficiency of evaporative cooling for a glasshouse in high energy environment", J. Agric Eng Res, 24, 29-39

Lee, I., Kang, C., Yun, J., Jeun, J. and Kim, G., (2003), "A study of Aerodynamics in Agriculture – Modern Technologies", Agricultural Engineering International: The CIGR Journal of Scientific Research and Development, Vol V, Invited Overview Paper, Presented at the Forum on Bioproduction in East Asia: Technology Development and Opportunities. ASAE Annual meeting, Las Vegas, 27 July 2003

Lee, I., Sase, S., Okushima, L., Ikeguchi, A. and Parl, W., (2002), "The Accuracy of Computational Simulation for Naturally Ventilated Multi-Span Greenhouse", ASAE Annual International Meeting / CIGR XVth World Congress, Chicago, Illinois, USA, 28-31 July 2002

Leidenfrost, W and B. Korenic, (1986), "Principles of evaporative cooling and heat transfer augmentation", in: N.P. Cheremisinoff (ed.), Handbook of Heat and Mass Transfer, vol. 1, Gulf Publishing, Houston, 1025-1063

Lucas, K., (2003), "Thermodynamik, Die Grundgesetze der Energie- und Stoffumwandlungen", Vierte Auflage, Springer Verlag, Berlin-Heidelberg, Germany

Maalej, A.Y., (1991), "Solar still performance", Desalination, 82, 207-219

Malik, M.A.S., Tiwari, G.N., Kumar, A. and Sodha, M.S., (1996), "Solar distillation: A practical study of a wide range of stills and their optimum design, construction and performance", First edition. Pergamon Press Ltd. Oxford, England

Merkel, F., (1925), "Verdunstungskühlung, Habilitationsschrift", VDI Verlag GmbH, Berlin, Germany

Mikheyev, M., (1977), "Fundamental of Heat Transfer", Mir Publishers, Moscow, p. 145

Mistriotis, A., Bot, G.P.A., Picuno, P. and Scarascia-Mugnozza, G., (1997), "Analysis of the Efficiency of Greenhouse Ventilation Using Computational Fluid Dynamics", Journal of Agricultural and Forest Meteorology, 85, 217-228

Morris, L.G., (1956), "Some aspects of control of plant environment", J. Agric. Eng Res., 1,156-66

Müller-Holst, H., (2001), "Small scale thermal water desalination system using solar energy or waste heat", Final Report, MEDRC Project number 098-AS-024b

Nawayseh, N.K., Farid, M.M., Omar, A.Z., Al-Hallaj, S. and Tamimi, A.R., (1997), "A simulation study to improve the performance of a desalination unit constructed in Jordan", Desalination, 109: 277-284

Oztoker, U. and Selsuk, M.K., (1971), "Theoretical analysis of system combining a solar still with a controlled environment greenhouse", ASM N°71/WA/SOL-9, 3-11

Paton, A.C. and Davies, (1996), "The seawater greenhouse for arid lands", Proceedings of Mediterranian Conference on Renewable Energy Sources for Water Production, Santorini, 10-12 June

Paton, A.C., (2001), "Seawater greenhouse development for Oman: thermodynamic modeling and economic analysis", MEDRC Project 97-AS-005b

Paton, A.C., (2004), (personal communications)

Peterson, P.F., (2000), "Diffusion layer modeling for condensation with multi-component non-condensable gases", ASME J. Heat Transfer, vol. 122, pp. 716-720

Pieters, J.G., Deltour, J.M., Debruyckere, M.J., (1996), "Condensation and dynamic heat transfer in greenhouses, Part I: Theoretical model", Agricultural Engineering Journal, 5:119-133

Pita E.G. and J.E.A. John, (1970), "The effect of forced convection on evaporative cooling of sprays in air", Proceedings of the 4th International Heat Transfer Conference, Paris-Versailles, 7: Paper CT3.12

Pollet, S. (1999), "Application of the Penman–Monteith model to calculate the evapotranspiration of head lettuce *Lactuca sativa* L. var capitata in glasshouse conditions", *Acta Horticulturae,* **519**, pp. 151–161

Poppe M. und H. Rögener, (1991), "Berechnung von Rückkühlwerken", VDI-Wärmeatlas, 6. Auflage, VDI Verlag GmbH, Berlin, Germany

Reichrath, S. and Davies, T.W. (2001), "Computational Fluid Dynamics Simulations and Validation of the Pressure Distribution on the Roof of a Commercial Multi-Span Venlo-

Type Glasshouse", Journal of Wind Engineering and Industrial Aerodynamics, 90, 139-149

Sablani, S.S., Goosen, M.F.A., Paton, A.C., Shayya, W.H. and Al-Hinai, H., (2002), "Simulation of fresh water production using a humidification-dehumidification seawater greenhouse", World Renewable Energy Congress VII, 29 June-5 July, Cologne, Germany

Sablania, M.F.A., Goosen, T., Paton, C., Shayyac, W.H., Al-Hinai, H. (2003), "Simulation of fresh water production using a humidification–dehumidification seawater greenhouse", Desalination, 159, 283–288

Shklyar A. and Arbel A., (2004), "Numerical Model of the Three-Dimensional Isothermal Flow Patterns and Mass Fluxes in a Pitched-Roof Greenhouse", Journal of Wind Engineering and Industrial Aerodynamics, **92,** 1039-1059

Sodha, M.S., Kumar, A., Srivastava, A. and Tiwari, G.N., (1980), "Thermal performance of solar still on roof system, Energy Conversion and Management", 20/3,181-184

Sparrow, E.M. and Eckert, E.R.G., (1961), "Effect of superheated vapor and non-condensable gases on laminar film condensation", AIChE J., 7, 474–477

Sparrow, E.M. and Lin, S.H., (1964), "Condensation Heat Transfer in the Presence of a Noncondensable Gas", J Heat Transfer, 86, 430-436

Stoecker, W.F, Jones J.W., (1982), "Refrigeration and Air Conditioning", 2nd ed. Singapore: McGraw Hill, 418-9

Takakura, T., Jordan, K.A. and Boyd, L.L., (1971), "Dynamic simulation of plant growth and the environment in the greenhouse", Transactions of the ASAE, vol. 14, pp. 964-971

Teitel, M and Shklyar, A., (1998), Pressure drop across insect proof screens, ASAE vol 41, no. 6, 1829-1834

Tiwari, G.N., Sharma, P.K., Goyal, R.K., Sutar, R.F., (1998), "Energy and Buildings", vol. 28, pp. 241-250

Uchida, H., Oyama, A. and Togo, Y., (1965), "Evaluation of Post-Accident Cooling Systems of LWR's", Proc Int Conf Peaceful Uses of Atomic Energy, 13, pp 93-102

Wagner, W. and Pruss, A., (1993), "International Equations for the Saturation Properties of Ordinary Water Substance", Revised According to the International Temperature Scale of 1990, Journal of Phys. Chem. Ref. Data, 22(3), 783-787

Zhu S.A., J. Deltour, B., Wang S., (1998), "Modeling the Thermal Characteristics of Greenhouse Pond Systems", Aquacultural Engineering, 18/3, 201-217

Zurigat, Y.H., Sawaqed, N.M., Al-Hinai, H. and Jubran, B.A., (2003), "Development of typical meteorological years for different locations in Oman", Final Report, Petroleum Development of Oman, Oman

Zurigat, Y.H., Dawoud, B., Bortmany, J. and Al-Shiahabi, S., (2004), "Technical and economical feasibility of gas turbine inlet cooling using evaporative fogging system in two different locations in Sultanate of Oman", ASME Paper GT2004-53122, ASME Turbo Expo, 14-17 June, Vienna, Austria

Zurigat, Y.H., Sawaqed, N.M., Al-Hinai, H. and Jubran, B.A., (2007), "Analysis of Typical Meteorological Year for Seeb/Muscat", The International Journal of Low Carbon Technologies, vol. 2, no. 4, 323-338